A FUNCTIONAL AND ONTOGENETIC SKULL ANALYSIS OF THE EXTANT RHINOCEROSES AND *TELEOCERAS MAJOR*, AN EXTINCT MIOCENE NORTH AMERICAN RHINOCEROS

A Thesis

Submitted to the Graduate Faculty of the
Louisiana State University and
Agricultural and Mechanical College
in partial fulfillment of the
requirements for the degree of
Master of Science

in

The Department of Geology & Geophysics

by
Mark Daniel Hagge
B.S., University of Wisconsin-Madison, 2004
May 2010

ACKNOWLEDGMENTS

I would like to thank Judith Schiebout for the utmost patience and encouragement in helping me complete this thesis. She has always been a true advisor to me, helping me brainstorm ideas and guide them to an attainable goal. I would like to thank the rest of my committee for excellent advice and support, which without, this thesis would not have been possible. Dominique Homberger taught me the importance of thorough thinking in scientific research, enabling me to develop this project. Dominique Homberger also spent numerous hours helping develop this experiment, and with the aid of Michelle Osborn, they helped me learn orthographic projection techniques. Barbara Dutrow gave wonderfully positive guidance for my project endeavors. Laurie Anderson provided a much-appreciated expertise in paleontological analytical methods. I would also like to thank the Louisiana State University Department of Geology & Geophysics and the Field Museum of Natural History for the funding that provided me with the means to visit the museums for this project. I am grateful for the amazing assistance I received in accessing the specimens, most notably Eileen Westwig of the American Museum of Natural History, Michi Schulenberg and Bill Simpson of the Field Museum of Natural History, George Corner and Shane Tucker of the University of Nebraska State Museum, and Linda Gordon and Helen Kafka of the Smithsonian Institution National Museum of Natural History. I would like to thank the team of researchers and volunteers, especially Suyin Ting, Kathleen MacDonald, Mike Williams, John Wrenn, Bill Lee, and Julie Hill who discovered and uncovered the Tunica Hills/Kerry fossil site, which opened my eyes to the possibility of researching *Teleoceras*. Thank you all.

TABLE OF CONTENTS

LIST OF TABLES

LIST OF FIGURES

ABSTRACT

Functional and ontogenetic skull differences among extant rhinoceroses and the extinct North American rhinoceros *Teleoceras major* were investigated to assess the unknown feeding ecology of *Teleoceras*. Ontogenetic skull sequences of the extant Indian rhino (*Rhinoceros unicornis*), Sumatran rhino (*Dicerorhinus sumatrensis*), white rhino (*Ceratotherium simum*), and black rhino (*Diceros bicornis*), and the extinct Miocene North American rhino *T. major* were gathered for both qualitative and quantitative assessments. Eleven functional characters related to specific feeding ecologies in extant perissodactyls were morphologically described, and each species' skull development was described in detail. Nineteen linear skull measurements were taken across all specimens of all ages to statistically investigate functional and developmental differences among the species. Specimens were also photographically documented for geometric morphometric analyses of ontogenetic shape transformations. Functional character results indicated that *T. major* was likely a grazer based on its high number of grazing characters, such as its large posterior maxilla, broad jugal, and strong mandibular angle. *Teleoceras major* and the extant grazer *C. simum* also shared grazing character states, such as an anterior jugal extension, a low occiput, and a deep mandibular body. Ontogenetic comparisons revealed both shared and distinct patterns among the species. The rhino species all shared early cranial lengthening, similar timing in horn and tusks development, and strong adult development of the masseter and temporalis attachment areas. Distinctions in the species' ontogenies are in the occiput, zygomatic arch, mandibular angle, and mandibular body, which are all characters related to feeding ecology. Early development of masseter attachment areas in *T. major* and the temporalis attachment areas in *C. simum* are understood as differing adaptations to grazing feeding ecologies.

CHAPTER 1. INTRODUCTION

The living rhinoceroses are represented by five threatened and endangered species with about 24,600 total individuals currently existing in the wild, according to the International Rhino Foundation (www.rhinos-irf.org). The white rhino and black rhino inhabit small areas within south and east Africa, and the Indian rhino, Sumatran rhino, and Javan rhino have been reduced to a few scattered pockets within Southeast Asia. The extant rhinos are all large-bodied herbivores, varying in size between 800-2000 kg with differing feeding ecologies as browsers, a mixed feeder, and a grazer (Owen-Smith 1988). Features used for fighting and defense are represented by different combinations of a nasal horn, a frontal horn, and tusks.

The earliest rhino fossil records date to the Oligocene, approximately 47 million years ago (Prothero 2005). Rhino lineages existed across Africa, Asia, North America, and Europe, with species disappearing from North America in the Pliocene and from Europe in the Pleistocene (Groves 1983, Prothero 2005). The numerous extinct lineages were more diverse compared to the extant rhinos, with greater variations in body size, skull morphology, and weapon combinations. Although similar morphologies are not necessarily present in the extant rhinos, extinct rhino species must be compared with the extant rhinos for meaningful paleoecological inferences.

The extinct rhino in this study is *Teleoceras*, a North American rhino genus from the Miocene, which existed between 19.0 - 4.5 million years ago (Prothero 2005). Among the extinct North American rhino genera such as *Aphelops*, *Menoceras*, and *Teleoceras*, *Teleoceras* has the most numerous fossil specimens, the widest geographic range, and perhaps the most distinct morphology (Prothero 2005). *Teleoceras* has a shortened skull, high-crowned dentition, and shortened limbs, which have invited comparisons to hippos and led to an assumed similar

semi-aquatic, soft-grass grazing, herd-forming ecology (Osborn 1898, Voorhies 1985, Mead 2000, Prothero 2005). Mihlbachler (2001) challenged the hippo-morph hypothesis for *Teleoceras* by demonstrating that its shortened limbs are not a likely adaptation for a semi-aquatic lifestyle. Instead, Mihlbachler (2001) argued that a shortened skull and shortened limbs are more likely related to short-grass grazing. Mihlbachler (2001, 2003) also found no evidence for herd forming in *Teleoceras* based on bone bed accumulations comparable with extant rhinos. A study by MacFadden (1998) brought the feeding ecology of *Teleoceras* into question. MacFadden (1998) assessed carbon isotopes in the teeth of *T. proterum*, finding isotopic signatures suggestive of a mixed feeding ecology of consuming both browse and grass, contrary to the traditional grazing assumptions of primarily feeding on grass.

Mihlbachler (2001) stated and demonstrated the importance of drawing comparisons with extant rhinos before making ecological inferences for extinct rhinos. This study addresses functional morphology of feeding in *Teleoceras* by comparing extant rhinos, whose ecologies are already known, with an extinct rhino. By assessing functional skull characters, the feeding ecology of *Teleoceras* can be elucidated.

An ontogenetic assessment of skull morphology in extant rhinos and *Teleoceras* with emphasis on functional skull characters can provide evidence for feeding adaptations in the rhinos. An exceptional *T. major* fossil assemblage in Nebraska makes this analysis possible. A population of over 100 *T. major* individuals, representing all ages with complete and articulated skulls and skeletons, is preserved in ash from approximately 12 million years ago (Voorhies 1985, Mead 2000). By comparing the ontogenies in extant rhinos and *Teleoceras*, shared and distinct growth patterns can elucidate morphological development related to specific feeding ecologies.

CHAPTER 2. BACKGROUND

2.1 EXTANT RHINOS

Ecological and morphological attributes for the four extant rhinos investigated in this study are summarized below and in Table 2-1. Each species' previous and current geographical range, recognized subspecies, characteristic skull and dental morphology, size, habitat preference, and feeding ecology are described below.

Rhinoceros unicornis

The current range of *Rhinoceros unicornis*, the Indian rhino, is confined to protected areas in two regions, southern Nepal (Chitwan) and northeastern India (Kaziranga) (Zschokke and Baur 2002). The previous range was more expansive throughout India and adjacent areas (Owen-Smith 1988). In the Pleistocene, *R. unicornis* inhabited a wide region, with fossil occurrences spanning across India to Pakistan and Sri Lanka, and from Java into Indochina and China (Laurie et al. 1983). No subspecies of *R. unicornis* are recognized (Laurie et al. 1983).

Several skull and dental features characterize *R. unicornis* (Figure 2-1). The skull is short and wide with a very high, steep, and anteriorly inclined occiput (Laurie et al. 1983). Nasals are long and ventrally curved at the tip with a large and rugose horn boss. The horn is moderate in length, usually 150-450 mm. The longest recorded nasal horn was over 600 mm (Laurie 1982). Teeth are moderately high-crowned (sub-hypsodont). The i2 are enlarged as tusks, and the I1 serve as upper honing mechanisms. A prehensile upper lip is used to grab and crop grasses and brush.

Rhinoceros unicornis is a large species that is sexually dimorphic in body size, with adult females and males reaching 1600 kg and 2100 kg, respectively (Owen-Smith 1988, Dinerstein

1991). *Rhinoceros unicornis* is also tall, with adult females and males approximately 1600 mm and 1860 mm at the shoulder, respectively (Laurie et al. 1983).

The habitat preferences of *R. unicornis* are alluvial plain tall grasslands and forests in a monsoonal climate (Laurie 1982, Owen-Smith 1988). *Rhinoceros unicornis* is considered a mixed feeder, with 70-89% of its diet being short and tall grass, depending on the season (Laurie et al. 1983). It also consumes a wide range of vegetation, such as browse, fruits, ferns, and aquatic plants.

The extant congeneric member with *Rhinoceros unicornis* is *Rhinoceros sondaicus,* the Javan rhino. *Rhinoceros sondaicus* is the most endangered rhino species, and due to its paucity in North American museums, *R. sondaicus* is not included in this study.

Dicerorhinus sumatrensis

The former range of *Dicerorhinus sumatrensis,* the Sumatran rhino, was throughout Southeast Asia, spanning from Borneo and Sumatra up through Vietnam, India, and Pakistan (Groves 1967, Owen-Smith 1988). *Dicerorhinus sumatrensis* currently is restricted in small pockets in the southern part of its former range in Burma, Thailand, mainland Malaysia, Borneo, and Sumatra (Owen-Smith 1988). Three extant subspecies that are geographically disjunct are recognized. *Dicerorhinus sumatrensis harrissoni* inhabits Borneo, *D. s. sumatrensis* inhabits Sumatra and peninsular Burma, Thailand, and Malaysia, and *D. s. lasiotis* inhabits mainland Burma (Groves and Kurt 1972).

The skull of *D. sumatrensis* has a low occiput with a vertical occipital slope and a gentle parietal slope (Figure 2-1). Anterior of the orbit, the skull is lengthened and the nasals are thin (Groves and Kurt 1972). A short nasal horn and frontal horn are roughly 250 mm and 100 mm in length, respectively (Laurie 1982). The maximum nasal horn length is close to 400 mm

(Groves and Kurt 1972). The teeth of *D. sumatrensis* are low-crowned (brachydont) (Owen-Smith 1988). The i2 are enlarged as tusks, and the I1 serve as upper honing mechanisms. The premaxillae are long, and a prehensile upper lip aids in feeding.

Dicerorhinus sumatrensis is the smallest extant rhino species, with adults at approximately 800 kg and a maximum of 1450 mm at the shoulder (Groves and Kurt 1972, Owen-Smith 1988). The species is not known to be sexually dimorphic in body size.

Dicerorhinus sumatrensis lives in highland and lowland zones of tropical rain forests (Groves 1967, Owen-Smith 1988). *Dicerorhinus sumatrensis* is a browser with a diet including leaves, twigs, and shrubs, and fruit (Groves and Kurt 1972).

Ceratotherium simum

Ceratotherium simum, the white rhino, has two extant subspecies that were historically separated by more than 2000 km between southern and central Africa. The southern subspecies (*C. s. simum*) ranged from South Africa to Namibia and Angola. The northern subspecies (*C. s. cottoni*) ranged from Uganda to Sudan and the Central African Republic (Owen-Smith 1988). Currently, *C. s. simum* is scattered across its former range, while *C. s. cottoni* is nearly extinct, residing in a single reserve in Zaire (Owen-Smith 1988).

The skull of *C. simum* is long with a posteriorly elongated occiput (Figure 2-1) (Groves 1972). The nasals, premaxillae, and mandible are anteriorly shortened and widened. *Ceratotherium simum* has a nasal and frontal horn, both often exceeding 1000mm (Laurie 1982). The teeth of *C. simum* are high-crowned (hypsodont), the anterior dentition is lost, and the mouth is wide with broad lips (Groves 1972, Owen-Smith 1988).

Ceratotherium simum is the largest extant rhino, and it is sexually dimorphic in body size, with female and male body mass between 1600-1800 kg and 2000-2300 kg, respectively (Laurie 1982, Owen-Smith 1988). Adult height at the shoulder is 1700-1850 mm (Groves 1972).

Ceratotherium simum lives in dry savannas and open forests (Groves 1972). It is a grazer that feeds on tall and short grasses, depending on the season. Browse is only consumed occasionally when feeding on grass (Owen-Smith 1988).

Diceros bicornis

Diceros bicornis, the black rhino, originally occurred across southern, eastern, and central Africa (Owen-Smith 1988). Seven recognized subspecies existed in scattered populations across this area, as far west as Cameroon, east into Kenya, and south into South Africa (Owen-Smith 1988, Hillman-Smith and Groves 1994). Only three of the subspecies (*D. b. michaeli*, *D. b. bicornis*, *D. b. minor*) currently exist in the wild (International Rhino Foundation, 2009).

The skull of *D. bicornis* is long with a high, posteriorly oriented occiput (Figure 2-1). The nasals, premaxillae, and mandible are anteriorly shortened and constricted, forming a narrow mouth. *Diceros bicornis* has a nasal and frontal horn, both of which are long and slender with maximum lengths around 1300 mm and 800 mm, respectively (Hillman-Smith and Groves 1994). Its teeth are brachydont and anterior dentition is lost in adults, although rudimentary incisors are often present in juveniles. A narrow, pointed, prehensile upper lip works with an extending lower lip in feeding (Hillman-Smith and Groves 1994).

Diceros bicornis is medium in size for extant rhino species, with adult body mass up to 1100 kg, and adult body height between 1320-1800 mm. *Diceros bicornis* is not sexually dimorphic in body size (Owen-Smith 1988).

Diceros bicornis lives in a wide range of closed arid habitats, such as mountain and savanna forests, shrub steppes, grasslands, and semi-deserts (Hillman-Smith and Groves 1994, Owen-Smith 1988). *Diceros bicornis* is a browser of leaves, twigs, shrubs, herbs, and occasional grasses (Hillman-Smith and Groves 1994).

Figure 2-1. Skull images of extant rhino species. From top left, clockwise: *R. unicornis* (AMNH 54454), *D. sumatrensis* (AMNH 81892), *C. simum* (AMNH 51856), and *D. bicornis* (FMNH 127849).

2.2 *TELEOCERAS*

Evolutionary History

The genus *Teleoceras* contains nine species that existed in the Miocene and earliest Pliocene of North America (e.g. Prothero 2005). *Teleoceras* is placed in the extinct tribe

Table 2.1. Ecological and morphological attributes of the four extant rhino species. Sources: 1. Owen-Smith (1988), 2. Groves (1972), 3. Groves and Kurt (1972), 4. Laurie et al. (1983), 5. Groves (1982), 6. Dinerstein (1991), 7. Hillman-Smith and Groves (1994), 8. Laurie (1982), 9. Groves (1967), 10. Zschokke and Baur (2002), 11. International Rhino Foundation (2009)

Attribute / Species	***R. unicornis***	***D. sumatrensis***	***C. simum***	***D. bicornis***
Common name	Indian rhino	Sumatran rhino	White rhino	Black rhino
Adult Body Mass	1600 kg (female) 2100 kg (male)[1]	800 kg[1]	1600-1800 kg (female) 2000-2300 kg (male)[1]	800-1100 kg[1]
Height at shoulders	1600 mm (female) 1860 mm (male)[4]	1450 mm[3]	1710-1850 mm[2]	1800 mm[1]
Weapons	Large tusks, moderate nasal horn[4,8]	Large tusks, small nasal and frontal horns[3]	Large nasal and frontal horns[1,2]	Large nasal and frontal horns[7]
Sexual Dimorphism	Body size, tusks, horn, neck[5,6]	Skull size, horn[5]	Body size, horn[1,2]	None[1,7]
Habitat	Alluvial plain grasslands and forests[1,8]	Tropical rain forest[1,9]	Savanna grass plains and open forests[2]	Forests, savannas, semi-deserts[1,7]
Feeding niche	Mixed feeder[1,4]	Browser[1,3]	Grazer[1,2]	Browser[1,7]
Region	Southeast Asia[1,4,10]	Southeast Asia[1,3,9]	central and southern Africa[1,2]	central, southern, and eastern Africa[1,7]
Dentition	Sub-hypsodont[1]	Brachydont[1]	Hypsodont[1,2]	Brachydont[7]
Total Population[11]	2700	200	17500	4200

Teleoceratini, which also contains several Old World genera (Heissig 1999). *Teleoceras* was the sole teleoceratin representative in North America, and no *Teleoceras* remains have been found outside of North America (Prothero 2005).

Teleoceras is first found in North America approximately 19 Ma in the Early Hemingfordian North American Land Mammal Age (NALMA) (Prothero 2005). Eight species succeeded the first, *T. americanum*; the temporal and geographic ranges of *Teleoceras* are summarized in Table 2-2. *Teleoceras* species in the Hemingfordian and Barstovian NALMA (19-16 Ma and 16-11 Ma, respectively) have been found in western and central plains regions of the U.S. (Prothero 2005). *Teleoceras brachyrhinum* was an endemic species found only in New Mexico, while *T. americanum*, *T. medicornutum*, and *T. meridianum* had more expansive geographic ranges (Prothero 2005).

In the Clarendonian and Hemphillian NALMA (11-9 Ma and 9-4.5 Ma, respectively), *Teleoceras* expanded into the southeastern U.S. *Teleoceras proterum* was an endemic species in Florida, and four other species (*T. major*, *T. fossiger*, *T. hicksi*, and *T. guymonense*) were widespread across the western and central U.S. (Prothero 2005).

Morphology

Several cranial, dental, and postcranial characters define the tribe Teleoceratini (Prothero (2005). The skull is short and wide with a prominent occipital crest and robust zygomatic arches. The nasal incision is above the anterior of P3, and a small, terminal nasal horn rugosity is sometimes present. Lateral nasals are angled sharply ventrally. Limbs are shortened, especially the distal segments. Carpals, tarsals, and metapodials are flat and robust, and the calcaneal tuber is long. The lower tusks are exaggerated and the honing upper incisors are large (Heissig 1989, 1999).

Table 2-2. Temporal ranges (above) and geographic ranges (below) of the nine *Teleoceras* species. Dates and states from Prothero (2005). Abbreviations refer to U.S. states.

19.2. – 16.0 Ma			16.0 – 11.0 Ma			11.0 – 8.8 Ma			8.8 – 4.5 Ma		
Hemingfordian			Barstovian			Clarendonian			Hemphillian		
Early	Middle	Late	Early	Middle	Late	Early	Middle	Late	Early	Middle	Late
----------*T. americanum*-----											
			--------*T. medicornutum*--------								
			--------*T. meridianum*----------								
			------------------------------*T. brachyrhinum*----------								
						----------*T. major*----------					
								-*T. proterum*-			
									-*T. fossiger*--		
											----------*T. hicksi*--------
											-*T. guymonense*-

T. americanum	*T. medicornutum*	*T. meridianum*	*T. brachyrhinum*	*T. major*
NV, CO, NE	NV, CO, TX, NE	TX, NE	NM	NV, TX, NE, SD, KS

T. proterum	*T. fossiger*	*T. hicksi*	*T. guymonense*
FL	NV, TX, OK, NE, SD, KS	Mexico, AZ, NM, NV, TX, CO, NE, KS, FL	NM, TX, OK, KS

Teleoceras is distinguished within the Teleoceratini by several cranial and dental characters (Figure 2-2) (Prothero 2005). Zygomatic arches are especially wide and robust. Nasals are narrow and fused with a small terminal horn. Tusks are long, sharp, curved anteriorly-dorsally, and teardrop-shaped in cross-section. Teeth are hypsodont, P1/p1 are lost, and P2/p2 are occasionally lost. Heissig (1989) noted that limbs of *Teleoceras* are further shortened compared to other teleoceratins.

In the *Teleoceras* lineage, some morphological traits gradually changed from the Hemingfordian through the Hemphillian, as discussed by Prothero (2005). For example, the teeth became more hypsodont, and limbs became shorter and more robust. Overall size, as estimated by the length of lower molars 1-3 (m1-3), increased up to the Early Hemphillian and decreased through the Late Hemphillian. Differing morphological characters, some of which also gradually changed through time, distinguish *Teleoceras* species. For example, *T. major* is distinguished from its predecessor *T. medicornutum* by having a shorter and wider skull, shorter nasals, and shorter and more robust limbs (Prothero 2005). Species also are distinguished by distinct differences in adult size. Both *T. meridianum* and *T. guymonense* were approximately 20% smaller than respective coexisting species, *T. medicornutum* and *T. hicksi* (Prothero 2005).

Teleoceras had different body dimensions than extant rhinos. Osborn (1898) compared a complete *T. fossiger* skeleton to an *R. unicornis* skeleton, noting similarities in length (3.1 m) but differences in height at the shoulders (1.21 m in *T. fossiger* and 1.69 m in *R. unicornis*). Osborn (1898) also described the *T. fossiger* skeleton as having shorter limbs and a wider rib cage than *R. unicornis*, and he indicated that *Teleoceras* was shorter and closer to the ground, resembling the body shape of a hippo more than a rhino.

Figure 2-2. Skull image of *Teleoceras major* (UNSM 52288).

Paleoecology

Due to its hypsodont dentition, a grazing niche has been historically suggested for *Teleoceras* (Osborn 1898, Matthew 1932), and two studies support this feeding ecology suggestion. Voorhies and Thomasson (1979) found fossilized grass remnants from sediments where throats and rib cages would be in several *T. major* skeletons from Ashfall Fossil Beds in Nebraska. The grass remains were viewed as a paleodiet indicator for *Teleoceras*. Mihlbachler (2001) and Mihlbachler et al. (2004) presented a morphological argument for a grazing lifestyle in *Teleoceras* based on comparisons with extant and extinct rhinos. Both *Teleoceras* and *Chilotherium*, a Eurasian Miocene rhino, had short skulls, horizontal head orientations, hypsodont teeth, large tusks, and shortened limbs (Mihlbachler 2001, Mihlbachler et al. 2004). Heissig (1999) previously proposed that *Chilotherium* needed a horizontal head orientation for tusk fighting. Heissig (1999) also believed that shortened limbs were a solution to be close to the ground for grazing, which would not be possible with a short, horizontally oriented skull and long limbs. Mihlbachler (2001, et al. 2004) used the same explanation for *Teleoceras*, suggesting the shortened limbs of *Teleoceras* were an adaptation for short-grass grazing.

An investigation by MacFadden (1998) indicated that the feeding ecology of *Teleoceras* might not be as simple as previously supposed. To examine the diet of *Teleoceras*, MacFadden (1998) analyzed stable carbon isotopes of *T. proterum* teeth from Florida localities. From 9.5-7.0 Ma, *T. proterum* had $\delta^{13}C$ values suggesting a diet of C_3 grasses and browse. From 7.0-4.5 Ma, *T. proterum* had $\delta^{13}C$ values suggesting a diet of primarily C_4 grasses. MacFadden (1998) hypothesized that *Teleoceras* was a mixed feeder, and the change in delta ^{13}C values reflected an increase in grass intake related to the spread of C_4 grasses at the end of the Miocene.

In addition to its feeding niche, the combative behavior of *Teleoceras* has been investigated. Webb (1969) discussed the presence of nasal bone wounds healed-over on a male *Teleoceras* skull. Although the nasal rugosity of *Teleoceras* is small compared to extant rhinos, this evidence suggests that *Teleoceras* also aggressively used its horn for combat, possibly in a male butting contest as Webb (1969) suggested.

2.3 RHINOCEROTIDAE

Tusks and Horns

All extant and extinct rhinos are members of the Family Rhinocerotidae, which was defined by Radinsky (1966) as the perissodactyl group ancestrally sharing a shearing mechanism between the I1 and i2. The I1 are extended ventrally as chisels that shear against the anteriorly elongated and pointed i2. In the early Oligocene, European *Epiaceratherium* and North American *Trigonias* are the first genera to display this unique mechanism (Radinsky 1966). Descendants that may have lost the I1-i2 shearing function, such as extant *C. simum* and *D. bicornis*, also are included as members of the Rhinocerotidae.

Extant and extinct rhinos all share a combination of tusks and/or horns used as weapons (Figure 2-1), although horns are not synapomorphies for the Rhinocerotidae (Prothero et al.

1986). In extant rhinos, three combinations of tusks and horns are present. *Rhinoceros unicornis* and *D. sumatrensis* have a small nasal horn and enlarged lower incisor tusks; *Dicerorhinus sumatrensis* also has a small frontal horn (Owen-Smith 1988). *Rhinoceros unicornis* males primarily spar using tusks, while the horns are used secondarily (Dinerstein 1991). Conversely, *C. simum* and *D. bicornis* have large nasal and frontal horns with no anterior dentition; the horns are used in combat and defense (Berger 1994). *Teleoceras* has a weapon combination similar to *R. unicornis*, with tusks and a nasal horn, but some extinct rhinos displayed a further diversity of weapon combinations. For example, the North American rhino genus *Aphelops* had a large i2 tusk with no shearing I1 or horns, and the North American rhino genus *Menoceras* had the I1-i2 shearing mechanism as well as laterally paired nasal horns (Prothero 2005).

Evolutionary History

In the Rhinocerotidae, several tribes within four subfamilies (Diceratheriinae, Menoceratinae, Aceratheriinae, and Rhinocerotinae) represent different evolutionary lineages (Prothero et al. 1986). Extant rhinos are separated within the subfamily Rhinocerotinae into two different tribes, the Rhinocerotini (*Rhinoceros* and *Dicerorhinus*) and the Dicerotini (*Ceratotherium* and *Diceros*) (Groves 1983). Although they never expanded into North America, both groups had a wide geographic range in Europe, Asia, and Africa. The Rhinocerotini primarily existed in Asia while the Dicerotini mostly inhabited Africa (Owen-Smith 1988, Heissig 1989).

Rhinocerotini are first found in the late Oligocene with *Dicerorhinus* in Europe and Asia (Owen-Smith 1988, Heissig 1989). Based on fossil records, the extant species *D. sumatrensis* originated in the middle Miocene in Southeast Asia (Heissig 1989). *Rhinoceros* is found in the

late Miocene in Africa and early Pliocene in Asia (McKenna and Bell 1997). *Rhinoceros unicornis* remains date back to the Pleistocene (Laurie et al. 1983).

Dicerotini originated in the middle Miocene in Africa with *Ceratotherium neumayri* the earliest representative of the genus (Geraads 2005). *Diceros* arose in the early Pliocene, and specimens identified as belonging to extant *D. bicornis* and *C. simum* are first found in the early Pleistocene (Geraads 2005). *Ceratotherium neumayri* exhibits an intermediate set of skull characters between that of *C. simum* and *D. bicornis*, which Geraads (2005) interpreted as an indicator of a mixed feeding diet. *Ceratotherium simum* and *D. bicornis* lineages likely diverged towards grazing and browsing diets in the early Pliocene (Geraads 2005).

The tribe Teleoceratini includes *Teleoceras* and Eurasian *Aprotodon*, *Brachydiceratherium*, *Diaceratherium*, *Prosantorhinus*, and *Brachypotherium* (Heissig 1989, Prothero 2005). *Brachydiceratherium* is the earliest known teleoceratin, first found in the Late Oligocene of France (Heissig 1989, 1999). Phylogenetic affinities of the teleoceratins are disputed, with the tribe placed in the Aceratheriinae (Heissig 1989, Cerdeño 1995) or Rhinocerotinae (Prothero et al. 1986).

2.4 ECOLOGY

Grazers, Browsers, and Mixed Feeders

Extant rhinos are all exclusively herbivores, which consume two basic types of vegetation: dicotyledonous material and grass. Commonly called browse, dicotyledonous material consists of leaves, stems, and fruits from woody and herbaceous plants. Compared to grasses, dicotyledonous material is generally softer with a higher nutritional value. Grasses have more silica, fiber, and grit, making them more difficult to digest than dicotyledonous material (Owen-Smith 1988, Sanson 2006).

Herbivorous ungulates are generally classified into three feeding categories determined by the percentage of grass and dicotyledonous material in the diet. Hofmann and Stewart (1972) defined these categories as grazer, browser, and mixed feeder. A grazer consumes more than 90% grass, a browser consumes more than 90% dicotyledonous, and a mixed feeder consumes both grass and browse with neither amounting to more than 90% of the diet. Hofmann (1973) discussed these three feeding categories as ecologically significant groupings by associating them with stomach anatomy.

Several investigations have correlated these feeding categories with skull morphology and dentition in perissodactyls and artiodactyls. Perhaps the most accurate predictor of feeding preference is molar crown height (Janis 1995). Due to the abrasive nature of grasses, grazers generally have hypsodont molars to process grass over a lifetime. Consuming softer and less abrasive vegetation, browsers have brachydont molars. With an intermediate diet, mixed feeders typically have intermediate crowned (mesodont) molars (Janis 1995).

Janis and Ehrhardt (1988) quantitatively correlated muzzle shape with feeding categories in herbivorous ungulates. Using the ratio of palate width to premaxilla width, Janis and Ehrhardt (1988) found that grazers have broad muzzles, browsers have narrow muzzles, and mixed feeders have intermediate muzzle widths. These findings supported the hypothesis that broad muzzles aid in consuming large quantities of less nutritional grasses, while narrow muzzles help in selecting edible parts of nutritious dicotyledonous plants.

The primary mastication muscles also have been used to understand feeding ecology in herbivorous ungulates. In the mammalian skull, the two primary external adductor muscles are the masseter and temporalis, which provide most of the jaw movement forces during mastication (Figure 2-3) (Smith 1993). The temporalis, which primarily controls closing movements of the

jaw, originates on the parietal and occipital crests of the skull and inserts on the coronoid process of the mandible (Homberger and Walker 2004). The masseter, which provides mediolateral jaw movements, has deep and superficial portions (Smith 1993, Homberger and Walker 2004). The deep masseter originates on the posterior maxilla and the medial surface of the posterior jugal, and the superficial masseter originates on the anterior jugal. The deep masseter inserts in the masseteric fossa of the mandibular angle and ramus, and the superficial masseter inserts along the edge of the mandibular angle (Homberger and Walker 2004).

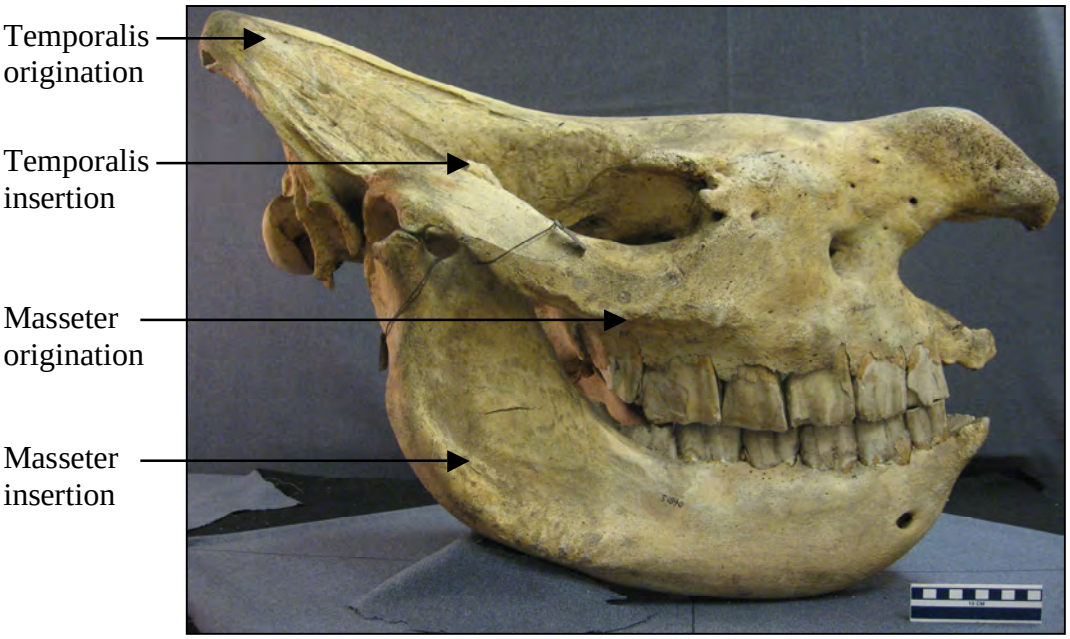

Figure 2-3. Masseter muscle and temporalis muscle originations and insertions. Depicted on a *C. simum* specimen, AMNH 51890.

Relative sizes of the temporalis and masseter have been related to feeding categories in herbivorous ungulates. In grazers, the size and force of the masseter are expected to be larger because medial-lateral jaw movements need to be more powerful for grinding coarse vegetation (Smith 1993, Janis 1995). In browsers, the temporalis muscle is thought to be larger for stronger opening and closing motions of the jaw to snip dicotyledonous material (Mead and Wall 1998a).

A suite of morphological characters has been associated with grazers and browsers. Janis (1995) summarized two studies, Solounias and Dawson-Saunders (1988) and Janis (1990), that described cranial, mandibular, and dental differences between grazers and browsers, with mixed feeders often having intermediate states. Mendoza et al. (2002) provided a few more character differences between grazers and browsers. From Janis (1990) and Mendoza et al. (2002), 12 character differences between grazers and browsers are described below, summarized in Table 2-3, and depicted in Figure 2-4.

Characters 1-2 relate to the facial region of the skull. Premaxilla width to palate width ratio describes muzzle shape. A low ratio indicates a narrow mouth opening compared to medial palate width, which is expected for browsers that are selective in choosing highly nutritious dicotyledonous material (Janis and Ehrhardt 1988). A high ratio indicates a wide mouth opening compared to medial palate width, which is expected in grazers that need to consume a large amount of less nutritious grasses (Janis and Ehrhardt 1988). The anterior maxilla above the premolars is the region for lip muscle insertion, and browsers typically have a deeper and larger area for the insertion of enlarged lip muscles for selective browsing (Janis 1995).

Characters 3-4, 8, and 11-12 relate to masseter muscle size, shape, and orientation. A broader posterior maxilla and jugal reflect a greater attachment area for the deep masseter. A further anterior extension of the jugal reflects a greater attachment area for the superficial masseter. Strong curvature of the mandibular angle and a large size of the mandibular ramus reflect a greater attachment area for the deep and superficial masseter (Janis and Ehrhardt 1988). The height of the mandibular condyle above the occlusal plane is an estimation of the moment arm of the masseter (Radinsky 1984, Homberger and Walker 2004). In contrast, characters 6-7 relate to temporalis muscle size, shape, and orientation. Braincase length estimates temporalis

size anterior-posteriorly, and occipital height estimates temporalis size dorsal-ventrally (Pérez-Barbería and Gordon 1999).

Characters 5 and 10 relate to housing space for molars. A deep mandibular body and a posterior orbit location provide room for high-crowned mandibular molars that are common in grazers (Radinsky 1984, Mendoza et al. 2002). Character 9 is also a character related to dentition, a ratio of premolar row length to molar row length. Grazers often have a greater dental surface area for grinding coarse vegetation, and artiodactyls and perissodactyls possess two contrasting solutions (Janis 1995). Artiodactyl grazers tend to have a long molar row and a short premolar row to form a long grinding surface (Janis 1995). Conversely, perissodactyl grazers tend to have a premolar row that is equal to or longer than the molar row (Janis 1995).

Functional Morphology in Rhinos

Zeuner (1936, 1945) assessed the feeding ecologies of the Pleistocene woolly rhino *Coelodonta antiquitatis* and the extant rhinos by comparing head orientations. As Zeuner proposed, the strongly inclined occipital slope of *C. simum* directs the head towards the ground for low-grass grazing in open habitats. *Diceros bicornis* has a slightly inclined occipital slope to orient the head slightly towards the ground for browsing in open habitats. The vertical occipital slope of *R. unicornis* directs the head horizontal with the ground for feeding on high-growing grass and browse in closed habitats. As *C. antiquitatis* and *C. simum* had similar head orientations, Zeuner (1936, 1945) concluded *C. antiquitatis* was likely an open grass grazer.

Heissig (1989) used horns and tusks to explain differences in posterior skull morphology. Heissig (1989) reasoned that the primary use of horns for combat requires the head to be angled towards the ground, while the use of tusks requires the head to be horizontally oriented. The extant rhinos illustrate this reasoning, as the horn-fighting *C. simum* and *D. bicornis* have

Table 2-3. Functional character differences between grazers and browsers. General character states are summarized for 12 functional characters in perissodactyls, as described by Janis (1990) and Mendoza et al. (2002).

Character Name	**Character Number**	**Grazer Character**	**Browser Character**
Premaxilla width / palate width	1	High	Low
Anterior maxilla	2	Shallow	Deep
Posterior maxilla and posterior jugal	3	Large	Small
Anterior jugal extension	4	Anterior	Posterior
Orbit location	5	Posterior	Anterior
Braincase length	6	Short	Long
Occipital height	7	Low	High
Mandibular condyle height above occlusal plane	8	High	Low
Premolar row length / molar row length	9	High	Low
Mandibular body	10	Deep	Shallow
Mandibular angle	11	More convex	Less convex
Mandibular ramus	12	Large	Small

Figure 2-4. Twelve functional characters depicted on a *D. bicornis* specimen (AMNH 51890).

inclined occipital slopes, while the tusk-fighting *R. unicornis* and *D. sumatrensis* have vertical occipital slopes.

Heissig (1989) understood head orientation in rhinos differently than Zeuner (1936, 1945) and recognized other feeding adaptations to low-grass grazing. Horn-fighting rhinos like *C. simum* and *C. antiquitatis* often have lengthened skulls, while tusk-fighting rhinos like *Chilotherium* and *Teleoceras* often have shortened limbs. Both groups, therefore, can maintain fighting position while being able to reach short grasses.

Purpose of Functional Morphological Comparison

Characteristic morphologies for grazers, browsers, and mixed feeders have been documented in herbivorous ungulates with strong empirical evidence and quantitative analyses. Further, skull morphologies in extant and extinct rhinos have previously been assessed, demonstrating both the possibilities and difficulties of interpreting skull morphologies as evidence of ecological adaptations. I hypothesize that comparisons of morphological attributes of the extant rhinos and *Teleoceras* will suggest a grazing feeding niche for *Teleoceras.*

2.5 SKULL DEVELOPMENT

Ontogeny

Through ontogeny, or development, different parts of the mammalian skull undergo various shape changes with growth, termed allometry. Tracing allometric shape changes through ontogeny can provide insight into development of functional roles of the mammalian skull, such as food acquisition, mastication, brain protection, and weapon support (Emerson and Bramble 1993). In light of function, these developmental insights may then be understood as adaptive responses to the environment, involving feeding, competition, defense, and social-interactions.

To functionally assess skull development, an understanding of mammalian skull growth is necessary. The vertebrate skull is generally separated into cerebral and facial components based on differing functions and growth patterns. The primary divisions of the cerebral component are the braincase, basicranium, and optic and auditory capsules. The facial component contains the jaw, adductor musculature, dentition, and facial bones. In vertebrates, especially mammals, the cerebral component develops mostly prenatally, while the facial component develops mostly postnatally (Emerson and Bramble 1993).

Ontogenetic investigations of skull growth in the extant rhinos are relatively sparse. Ontogenetic research has focused primarily on distinguishing between subspecies and uncovering sexually dimorphic characters during growth. Groves (1967, 1975) completed the most comprehensive ontogenetic assessments for *D. sumatrensis* and *C. simum*. Analyzing skulls from complete ontogenetic sequences, Groves (1967, 1975) separated his specimens into six dental stages. He provided cranial dimensions for each stage, distinguishing when adult size is reached as well as when sexual dimorphism appears.

Among extinct rhinos, there is an even greater paucity of ontogenetic skull investigations, primarily because few articulated and well-preserved ontogenetic sequences have been discovered (Prothero 2005). The most descriptive work of an extinct rhino species' ontogeny was of *Chilotherium wimani*, a member of the subfamily Aceratheriinae from the Late Miocene of China. Deng (2001) described cranial changes with growth of nine complete specimens covering infant, subadult, young adult, and old adult age classes.

The extinct rhino species with perhaps the most extensive ontogenetic representation is *T. major* preserved in the Ashfall Fossil Beds of the Late Clarendonian in Nebraska. More than 100 specimens of all ages are fully or partially articulated in 3-dimensional death poses, thought

to represent a catastrophic death assemblage occurring over several days (Voorhies 1985, Mead 2000). Exceptional examples of fossilization include the preservation of grass silicates in mouth and stomach cavities, fetal contents, hyoid apparatuses, healed broken ribs, and mother-calf pairs (Voorhies and Stover 1978, Voorhies 1985). The well-preserved ontogenetic sequence at the Ashfall Fossil Beds provides a rare opportunity to investigate the functional development of *Teleoceras,* as discussed below.

Sexual Dimorphism

Sexual dimorphism in mammals is a result of competition to reproduce, typically displayed in males by increased body size and weaponry for combat and display (e.g. Zschokke and Baur 2002). Dimorphism in body size and weaponry have been previously documented in the extant rhinos. In *R. unicornis* adults, Groves (1982) found dimorphism in various cranial dimensions including cranial length, zygomatic breadth, occipital height, and nasal breadth. Dinerstein (1991) indicated dimorphisms between old adult males and females, including tusk length, horn base circumference, and neck, shoulder, and skull dimensions. Groves (1982) found that the subspecies *D. s. sumatrensis* and *D. s. lasiotis* could both be sexually demarcated by nasal breadth. Furthermore, Groves (1982) stated that *D. s. sumatrensis* males had significantly larger skulls. *Ceratotherium simum* males are significantly larger in body size and horn size, but *D. bicornis* is completely monomorphic (Owen-Smith 1988).

These dimorphisms in extant rhinos are likely related to reproductive competition. *Rhinoceros unicornis* males primarily fight using tusks, so enlarged tusk and body size are likely advantages in combat for breeding rights (Dinerstein 1991). Larger horn base and body size in males are also probable products of selection through reproductive competition, as horn-related fights account for 50% of all *C. simum* adult male deaths in the wild (Owen-Smith 1988).

Sexual dimorphism similar to that of the extant rhinos has also been documented in *Teleoceras*. Osborn (1898) first inferred sexual dimorphism in *Teleoceras*, deducing that *T. fossiger* males had larger and more rugose skulls, more pronounced nasals, and larger tusks. Voorhies and Stover (1978) confirmed tusk dimorphism in *T. major* by finding fetal bones inside an adult with smaller tusks, indicating that smaller-tusked individuals were indeed females.

Two quantitative assessments of sexual dimorphism in *Teleoceras* have expounded Osborn's initial findings. Mead (2000) investigated the Ashfall Fossil Beds *T. major* assemblage and found statistically significant size dimorphisms in the cranium, mandible, postcrania, and tusks. Dimorphic dimensions included cranial length, occipital width, mandibular length, mandibular condyle height, and tusk diameter. Mihlbachler (2005) investigated sexual dimorphism in *T. proterum* of Florida's Love Bone Bed and Mixson's Bone Bed. Disarticulated specimens prevented an investigation of cranial and mandibular dimensions, but statistically significant differences were found in postcrania and tusk size. These dimorphisms in *Teleoceras* suggest that male body size and weaponry were equally important in reproductive competition as in extant rhinos.

In sexually dimorphic species, there are three possible developmental patterns that can result in male morphological enlargements. Males can have faster growth rates, later maturation resulting in prolonged growth, or more resources invested to them in gestation or lactation (Zschokke and Baur 2002). In the extant rhinos, males of dimorphic *R. unicornis* and *C. simum* are known to reach sexual maturity later than females (Owen-Smith 1988), and faster growth rates were found in *C. simum* males by Groves (1973). Also, in a study of captive *R. unicornis* individuals, Zschokke and Baur (2002) found no dimorphic differences in growth rates or infant mass, yet dimorphisms were found in adult body size. Therefore, later maturation and faster

growth rates are probable developmental patterns that result in male morphological enlargement in the extant rhinos.

Later maturation also has been determined as a cause for dimorphisms in *Teleoceras.* Mead (2000) found that *T. major* males had prolonged limb growth and delayed epiphyseal fusion. Mihlbachler (2005) indicated that the tusks of *T. proterum* males erupted later in life and continued to lengthen until old age, while female tusks stopped growing a few years after eruption. These findings suggest that similar developmental patterns are likely responsible for sexual dimorphism in the extant rhinos and *Teleoceras*. Further ontogenetic investigations of extant and extinct rhinos can further clarify morphological developments as adaptations in light of social dynamics.

Captivity

Captivity can have varying effects on morphological development in rhinos, including exaggerations of features and changes in growth rates. Groves (1982) found that captive *R. unicornis* individuals developed higher occiputs and wider zygomatic arches and mastoids; captive adults were also smaller than wild adults. Dinerstein (1991) documented faster than normal growth rates in captive *R. unicornis* males. In an uncompetitive captive environment, four-year old males were often as large as adult females; this was never the case in the wild (Dinerstein 1991). Groves (1982) also reported that *D. sumatrensis* could be variably affected in captivity; instances of enhanced, stunted, and unaffected growth all were described.

Captivity can also result in retarded dental development in rhinos. Goddard (1970) observed that *D. bicornis* captives often displayed retarded dental eruption and wear. For example, a seven-year old had a dental age of five-years, and a 34-year old had a dental age of 25 years. Hillman-Smith et al. (1986) also indicated retarded eruption rates in a *C. simum* calf

reared on an artificial diet. Captive specimens, if included in ontogenetic assessments, need to be assessed for dental and skull development inconsistencies among non-captive specimens of similar ages to ensure accurate ontogenetic portrayals.

Purpose of Ontogenetic Investigation

A comparison of the developmental patterns in extant and extinct rhinos is possible with a full ontogenetic sequence of well-preserved and articulated *Teleoceras* skulls, and an expansive extant rhino skeletal collection in American natural history museums. By comparing the growth of these rhinos, and by placing emphasis on skull shape, muscle attachment sites, and tusk and horn changes, shared and species-specific developmental patterns can be elucidated. I hypothesize that differences skull development will be understood as adaptations related to functional morphology, feeding ecology, and sexual dimorphism.

CHAPTER 3. METHODOLOGY

The following methods were used to investigate functional morphology and development of extant rhinos and *Teleoceras*. Specimens from *Teleoceras* and four extant rhino species across all ages were obtained from museums in the United States. A dental age classification method was used to assign all specimens to comparable age groups. Functional character states for each species' ontogeny were described. Dimensions to describe functional and ontogenetic differences and use for statistical analyses were measured on each specimen. Digital images of each specimen were taken for use in geometric morphometric shape analysis techniques. These methods are described in detail below. Statistical analyses using measurement data were completed using the program PAST (Hammer et al. 2009). Geometric morphometric analyses were completed using PAST and MorphoJ (Klingenberg 2008).

3.1 SPECIMENS

Teleoceras major specimens from Ashfall Fossil Beds are held at the University of Nebraska State Museum (UNSM) in Lincoln, Nebraska. Twenty-seven individuals had articulated crania and mandibles with complete dentition allowing age classification, morphological descriptions, a series of measurements, and photo documentation. Adult males and females were easy to distinguish by sexually dimorphic tusk size. Specimens with erupted tusks were visually sexed based on two noticeable groupings of overall tusk size (Mead 2000). Sex identification for some specimens was not possible because adult tusks were not erupted. Of the 27 specimens, there were two adult males, 13 adult females, and 12 unsexed pre-adults.

The extant rhino samples consisted of specimens from four museums: the American Museum of Natural History (AMNH), in New York City, New York; the Field Museum of Natural History (FMNH), in Chicago, Illinois; the National Museum of Natural History

(USNM), in Washington, DC, and UNSM. A total of 68 specimens had articulated crania and mandibles with complete dentition, allowing for age classification, morphological descriptions, a series of measurements, and photo documentation. In total the species' sample sizes were: *R. unicornis*, n =15; *D. sumatrensis*, n = 7; *C. simum*, n = 20; and *D. bicornis*, n = 26.

The samples contained specimens with documentation of different subspecies, sexes, and environments (wild versus captivity). The specimens' developmental histories might be considerably different, and combining all specimens into one sample could result in inaccurate ontogenetic portrayals and comparisons. Assessments of sample differences in sex, subspecies, and environment are discussed below.

Sex Differences

In the extant rhino sample, the male-female ratio for was mostly even with 21 males and 24 females. However, 23 of the total 68 specimens (34%) were of unreported sex. Specimen sex counts are included in Table 3-1. Upon inspection of extant rhino specimens, no morphological sexual differences were visually apparent. The males, females, and unsexed specimens formed a uniform developmental series, and all individuals were included in ontogenetic descriptions. Morphometric differences among sexes were statistically tested, and the methods are discussed in the Traditional Morphometrics section.

Table 3-1. Specimen counts for male, female, and unknown sex for the five species.

Sex / Species	***T. major***	***R. unicornis***	***D. sumatrensis***	***C. simum***	***D. bicornis***
Male	2	6	2	5	8
Female	13	5	2	10	7
Unknown	12	4	3	5	11

Subspecies Differences

In the extant rhino samples, only *C. simum* specimens were identified to subspecies: *C. s. cottoni* (18) and *C. s. simum* (2). *Ceratotherium simum cottoni* specimens were from Zaire, Sudan, and Uganda, while *C. s. simum* specimens were from South Africa. For *D. sumatrensis,* five specimens were from Burma, Sumatra, Borneo, or Malaysia, and two specimens were from unknown localities. Therefore, based on the geographic ranges of its subspecies, at least two subspecies, *D. s. harrissoni* and *D. s. sumatrensis*, were present in the sample. For *D. bicornis*, there were 13 specimens from Kenya, seven from Tanzania, and eight from unknown localities. Based on subspecific distributions from Hillman-Smith and Groves (1994), the Kenyan specimens were either *D. b. ladoensis* or *D. b. michaeli*, and the Tanzanian specimens were *D. b. minor*. At least two subspecies were therefore present in the sample.

Subspecific differences in morphology exist in the extant rhinos. Groves (1975) found that *C. s. simum* has slightly larger cranial dimensions than *C. s. cottoni*. The *D. sumatrensis* subspecies are primarily distinguished by skull length, occiput size, and zygomatic breadth (Groves 1965, 1967). Variations in skull size exist among the *D. bicornis* subspecies as well (Hillman-Smith and Groves 1994).

As the samples contain several subspecies, potential subspecific differences in the sample must be addressed. Upon visual inspection of the samples, no subspecific differences in morphological development were apparent. Each species' specimens formed uniform developmental series, and all individuals were included in ontogenetic descriptions.

3.2 AGE CLASSIFICATION

To make meaningful comparisons, an age classification method with applicable ageing criteria for all species must be used. Two dental ageing methods are commonly used on extant

rhino specimens. Cementum line counting is a method that estimates chronological age with annual growth increments in teeth. Teeth are sectioned to visually count the internal cementum lines (Hitchins 1978). Cementum line counting can provide precise age estimations, but the method can be time-consuming, expensive, and destructive, especially on fragile fossil specimens. Dental eruption and wear classification groups individuals into classes based on dental developmental stages. The stages are demarcated using sequential tooth eruptions and wear patterns as criteria, and relative ages are assigned to groups. Although not as precise as cementum line counting, dental classification can be quick, inexpensive, safe, and informative.

Previous studies have supplemented relative dental ages with chronological ages for *D. bicornis* (Goddard 1970, Hitchins 1978) and *C. simum* (Hillman-Smith et al. 1986). Goddard (1970) distinguished 20 mandibular age classes and provided chronological estimates for each class using known-age individuals. Hitchins (1978) distinguished 18 mandibular and maxillary age classes, and provided chronological estimates using cementum line counts; age estimations were refined and supported using known-age individuals. Hillman-Smith et al. (1986) distinguished 17 maxillary and mandibular age classes and provided age estimates with cementum line counts and known-age individuals. No comprehensive dental development studies have been completed for *R. unicornis* or *D. sumatrensis*.

Among these three studies, Goddard (1970) and Hitchins (1978) provided the most detail for eruption timings and morphological wear patterns of each stage, especially for mandibular dentition. Mandibular dentition in the *T. major* sample was better preserved than maxillary dentition. Ventral crania were often fragile and fractured, thus limiting maxillary age classification feasibility. Between these two studies, only Hitchins (1978) used both cementum

line counts and known-age individuals for estimating chronological ages, so I assessed this age classification method for consistency in the extant rhinos and *T. major*.

To use a single age classification method, eruption and wear patterns must be consistent across all species. The *D. bicornis* eruption sequence for deciduous (d) and adult teeth as described and depicted by Hitchins (1978) is dp2, dp3, p1, dp4, m1, p2, p3, m2, p4, m3. This sequence is the order of teeth becoming fully erupted and beginning to wear. Two sets of teeth have near synchronous eruptions: p1 and dp4, and p2, p3, and m2. Similar eruption sequences, including the synchronous eruption of p2, p3, and m2, have been recognized in other extant rhinos as well as in *Teleoceras*. Groves (1967) and Hillman-Smith et al. (1986) both reported comparable sequences for *D. sumatrensis* and *C. simum*, respectively. Mihlbachler (2001) also found the same eruption sequence in *T. proterum*. Upon inspection of the samples, the extant rhinos and *T. major* all share the same eruption sequence.

Similar wear patterns among species must also be confirmed. The following are the *D. bicornis* mandibular molariform wear patterns as described and depicted by Hitchins (1978), and summarized by Mihlbachler (2001). Wear stage criteria for age classification are depicted and described in Figure 3-1. Tooth-by-tooth wear stages are provided in Table 3-2.

The mandibular molariform teeth (dp3, dp4, p3, p4, m1, m2, and m3) are considered erupting when they are just above the bone surface. The anterior lophid erupts slightly ahead of the posterior lophid. Molariform teeth are fully erupted when both lophids are equal in height and begin to show wear on the enamel polish. The anterior lophid begins to wear first, and it remains ahead of the posterior lophid throughout the wear process.

As wear continues, dentine becomes exposed as a thin, lingually curved crescent on each lophid; anterior and posterior exposed dentine is not initially joined. Dentine is exposed as a

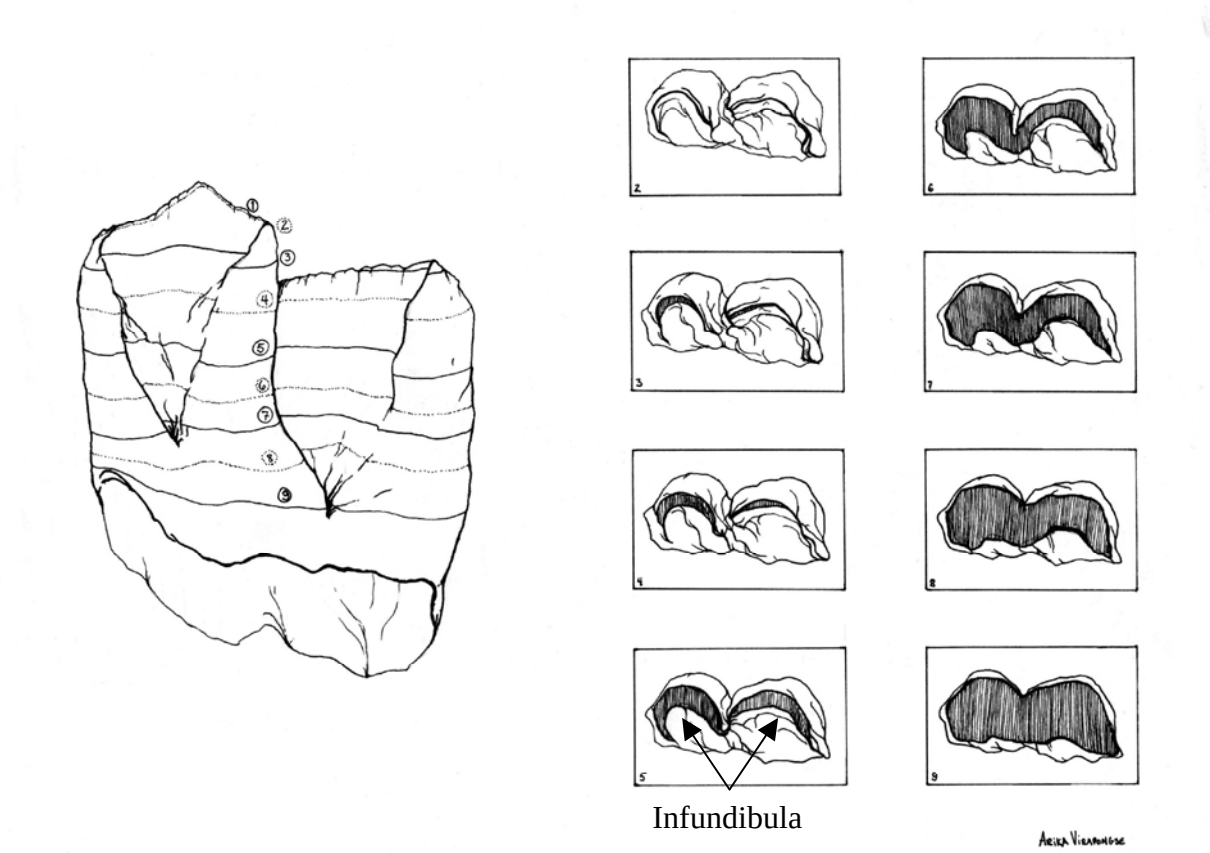

1. Tooth is erupting above the bone surface.
2. Anterior lophid has slight wear on the enamel polish.
3. Anterior lophid dentine is exposed and posterior lophid has slight wear on enamel polish.
4. Anterior and posterior lophid dentine is exposed but not joined.
5. Anterior and posterior lophid dentine is joined.
6. Anterior and posterior lophid dentine is wider with a constriction between the lophids.
7. Constriction between lophids is reduced and anterior infundibulum reduced to enamel notch.
8. Anterior infundibulum is worn away and posterior infundibulum is reduced to enamel notch.
9. Anterior and posterior lophid enamel is worn away, forming a rectangular dentine surface.

Figure 3-1. Molariform wear sequence for age class demarcation. Lingual and occlusal views of the wear stages are provided for mandibular molariform dentition in rhinos, from Mihlbachler (2001).

Table 3-2. Wear stage criteria for age classification. Wear stages of the mandibular molariform teeth are provided for each Age Class, as described by Hitchins (1978).

Age Class / Tooth	dp3	dp4	m1	p3	m2	p4	m3
0							
1	1						
2	1						
3	2, 3	2, 3					
4	3, 4	3, 4	1				
5	5, 6, 7	5, 6	2, 3				
6	7, 8	6, 7	3, 4				
7		7	4	1	1		
8			4	2, 3	2, 3	1	
9			4, 5	3, 4	3, 4	3, 4	1
10			5, 6, 7	4, 5	4, 5	4, 5	1, 2
11			6, 7	5	4, 5	4, 5	2
12			7	6	6	5, 6	3, 4
13			8	6, 7	7	6, 7	4, 5
14			8, 9	7, 8	7	7	5, 6, 7
15			8, 9	8, 9	8	8	6, 7, 8
16			9	9	8	8, 9	7, 8
17			9	9	8, 9	9	7, 8

crescent because each lophid is lingually curved and hollow, an infundibulum. The infundibulum narrows towards the root like a funnel. As wear increases, anterior and posterior dentine crescents widen and eventually join. A buccal constriction develops between lophids, forming an m-shaped dentine surface. Anterior and posterior dentine widens as infundibula shrink with increased wear. Gradually, the buccal constriction widens and infundibula become small enamel notches. The anterior infundibulum disappears, and the lophid becomes a flat and straight dentine surface. When the posterior infundibulum disappears, all occlusal enamel on the molariform tooth is worn away.

3.3 DESCRIPTIVE MORPHOLOGY

Following age classification, crania and mandibles were articulated, and each species sample was demarcated into groups based on shared morphological similarities among age classes. The 12 character differences among grazers and browsers, as summarized by Janis (1995) and Mendoza et al. (2002), were assessed and described in each species. The skull morphologies of each species' ontogenetic sequence were then described using right lateral and dorsal viewpoints. Morphological changes of the dorsal cranium and lateral skull were described in detail, with special attention given to the temporalis and masseter muscle attachment sites, tusks, and horns. Captive specimens were assessed for dental and skull development inconsistencies among non-captive specimens of similar ages.

3.4 TRADITIONAL MORPHOMETRICS

3.4.1 Measurements

Nineteen cranial, mandibular, and dental measurements were selected to statistically investigate functional and ontogenetic differences in the species' skulls. The measurements are described in Table 3-3 and depicted in Figure 3-2.

Measurement 1 was selected as an overall size dimension. Total cranial length (TCL) has been used to estimate body size in extant and extinct ungulates, and it has been used as the standard in comparing mammalian skull shape changes (Radinsky 1981, McKinney and Schoch 1985, Wayne 1986). The measurement's landmarks vary among studies; the anterior margin (basion) and posterior margin (opisthion) of the foramen magnum are common posterior landmarks, and the anterior-most premolar, premaxilla-maxilla junction, and premaxilla tip are common anterior landmarks. Among the specimens in this study, the premaxilla and basion

were often disarticulated or fractured, so the anterior-most premolar and the opisthion were chosen as landmarks.

Measurements 2-5 were cranial dimensions selected to address ontogenetic changes, as preliminary observations suggested these dimensions disproportionately change with growth. Anterior cranial length (ACL) addresses the facial region. Medial cranial length (MCL) addresses the orbit and zygomatic arch. Posterior cranial length (PCL) addresses the braincase length, which is also a character of functional significance. Supraorbital width (SW) addresses medial cranial width, possibly related to the frontal horn.

Previous ungulate studies have correlated these measurements with muscle size and function. Occipital height (OH) has been related to temporalis size and exertion force (Pérez-Barbería and Gordon 1999). Zygomatic width (ZW) has been correlated with temporalis size (Joeckel 1990). Mandibular length (ML) has been used to approximate the mandibular lever arm during mastication (Homberger and Walker 2004). Ramus length (RL) was measured to approximate masseter insertion size, and condyle width (CW) has been associated with masseter function while grinding (Joeckel 1990).

Measurements 11-19 were orthal and dental dimensions selected for functional investigations, as correlations among these measurements have been used to predict ungulate feeding preferences. Diastema width (DW) and maxillary posterior premolar width (MXPPW) are similar to muzzle dimensions used in distinguishing grazers from mixed feeders and browsers (Janis and Ehrhardt 1988). Anterior premolar width of the maxilla (MXAPW) was also used to functionally assess the shape of the muzzle. The ratio of premolar row length to molar row length has been used to distinguish grazers from browsers, so both maxillary (MXPL, MXML) and mandibular (MNPL, MNML) dimensions were taken (Janis 1995). The total dental

length of both the maxilla and mandible (MXDL, MNDL) were measured to address ontogenetic changes of the total tooth row.

The above non-dental measurements were applicable for all ages and species. All anatomical left and right measurements were taken for all length dimensions. Disarticulated and fractured specimens prevented some cranial and mandibular dimensions from being measured. The number of specimens with all cranial and mandibular dimensions measured is provided in Table 3-5. All dental measurements were taken on the bone surface from the furthest buccal corner of fully erupted teeth. Alveoli of shed teeth were not used as measurement landmarks.

An 80 cm aluminum caliper was used for measurements greater than 15 cm. A digital caliper was used for measurements less than 15 cm. To address total potential error of an individual measurement from the measurer and tools, a series of five repeated measurements were taken on a *D. bicornis* specimen (AMNH 85175).

Table 3-3. Nineteen measurements taken on each specimen from all species. * indicates length measurements with both right and left dimensions measured when possible.

Number	Name	Abbreviation	Type	Description
1	Total Cranial Length*	TCL	Cranial	opisthion to anterior-most premolar
2	Posterior Cranial Length*	PCL	Cranial	opisthion to lateral-most point of zygomatic arch condyle
3	Medial Cranial Length*	MCL	Cranial	lateral-most point of zygomatic arch condyle to anterior-most point of orbit
4	Anterior Cranial Length*	ACL	Cranial	anterior-most point of orbit to posterior-most point of nasal incision
5	Supraorbital Width	SW	Cranial	lateral-most point of left supraorbital process to corresponding right process

Table continued

6	Occipital Height	OH	Cranial	opisthion to posterior-most midline point of occipital crest
7	Zygomatic Width	ZW	Cranial	lateral-most point of left zygomatic arch condyle to corresponding right condyle
8	Mandibular Length*	ML	Mandibular	lateral-most point of mandibular condyle to anterior-most point of mandibular symphysis
9	Ramus Length*	RL	Mandibular	posterior-most m to posterior-most point of posterior ramus bulge
10	Condyle Width	CW	Mandibular	lateral-most point of left mandibular condyle to corresponding right condyle
11	Diastema Width	DW	Cranial	left ventral-lateral premaxilla-maxilla junction to corresponding right junction
12	Maxillary Anterior Premolar Width	MXAPW	Dental	left anterior-most PM to corresponding right PM
13	Maxillary Posterior Premolar Width	MXPPW	Dental	left posterior-most PM to corresponding right PM
14	Maxillary Premolar Length*	MXPL	Dental	anterior-most PM to posterior-most PM
15	Maxillary Molar Length*	MXML	Dental	anterior-most M to posterior-most M
16	Maxillary Dentition Length*	MXDL	Dental	anterior-most PM to posterior-most PM
17	Mandibular Premolar Length*	MNPL	Dental	anterior-most pm to posterior-most pm
18	Mandibular Molar Length*	MNML	Dental	anterior-most m to posterior-most m
19	Mandibular Dentition Length*	MNDL	Dental	anterior-most pm to posterior-most m

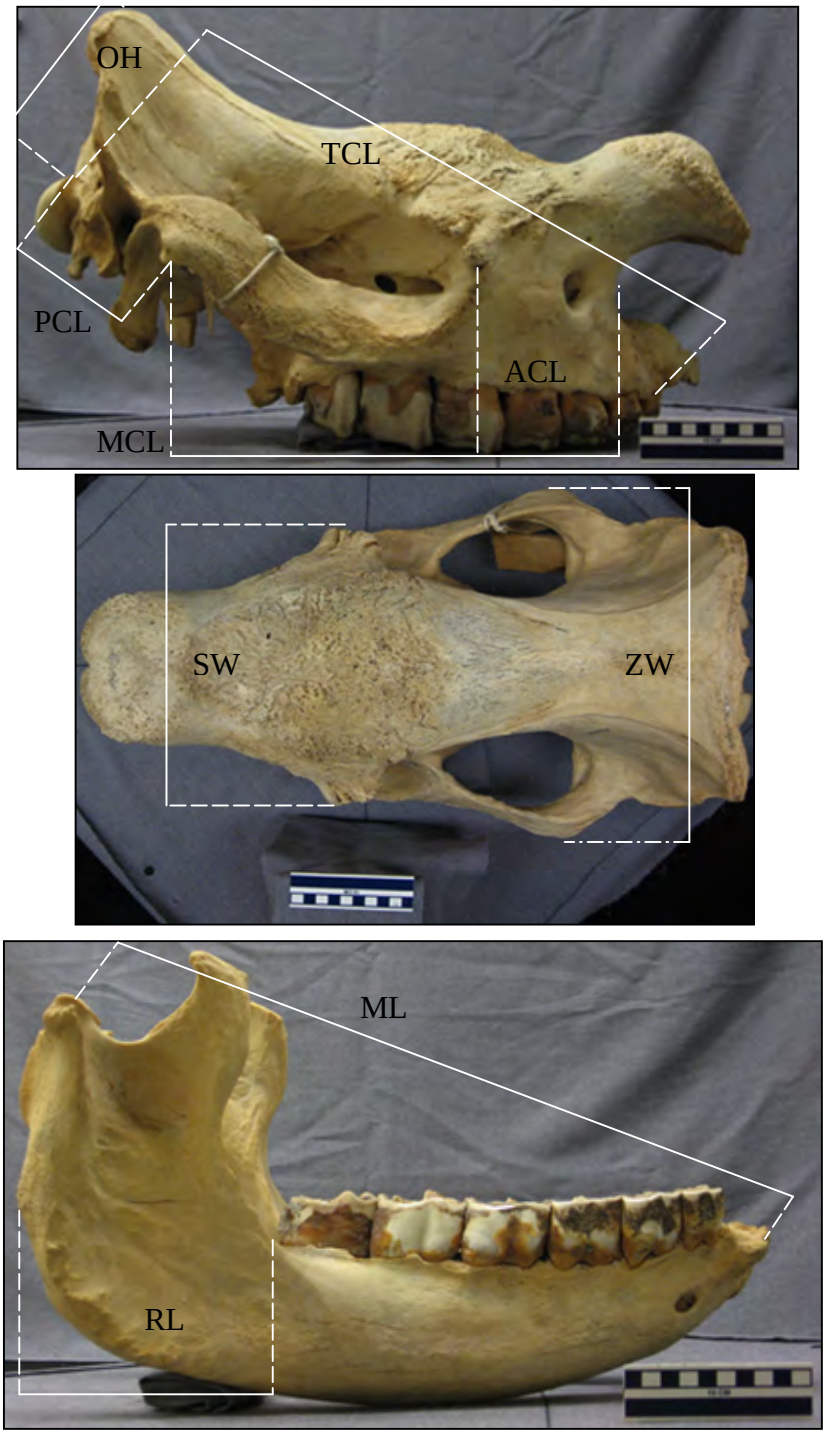

Figure 3-2a. Cranial and mandibular measurements taken for morphological analyses (*D. bicornis* specimen, FMNH 22366). See Table 3-3 for measurement abbreviation explanations.

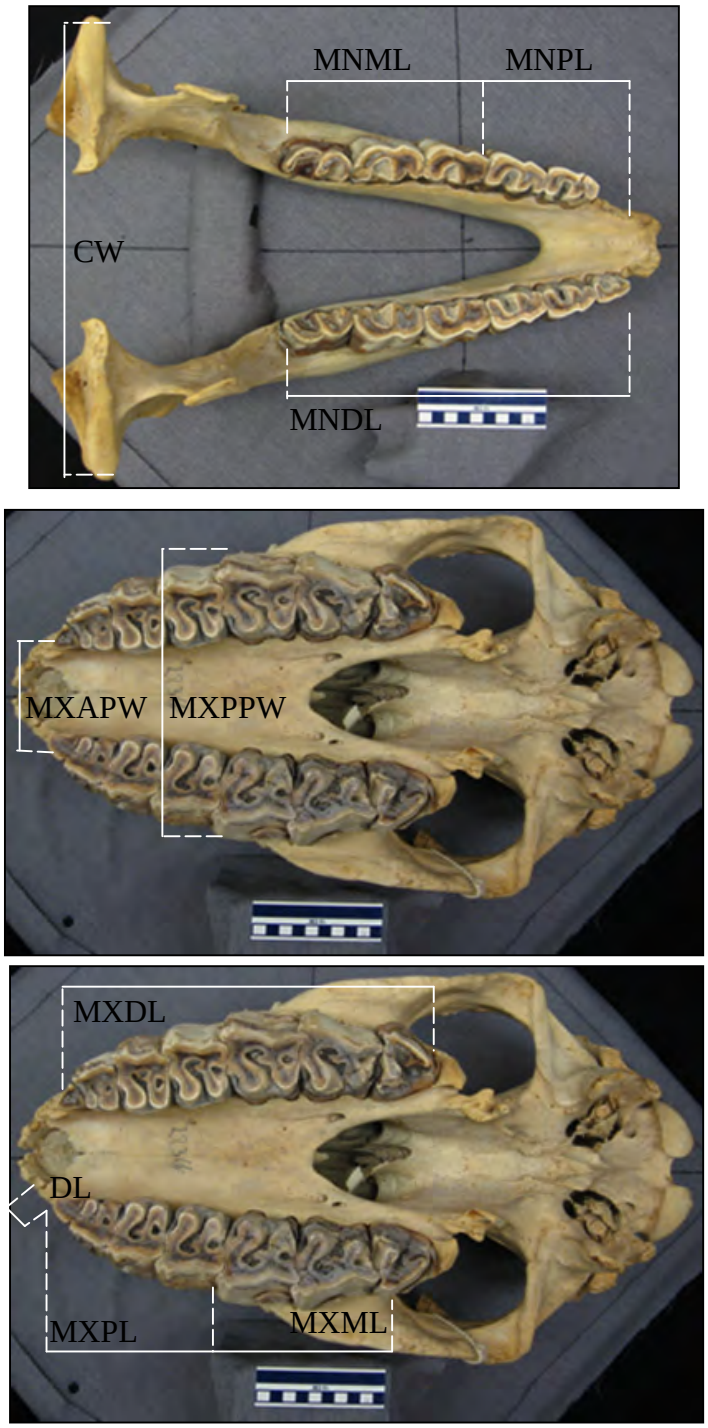

Figure 3-2b. Mandibular and dental measurements taken for morphological analyses (*D. bicornis* specimen, FMNH 22366). See Table 3-3 for measurement abbreviation explanations.

3.4.2 Measurement Error

Basic statistics were determined with PAST (Hammer et al. 2009) for each set of five repeated measurements from an adult *D. bicornis* specimen to assess measurement error. The coefficient of variation (CV) of a sample measures variability relative to the sample mean. CV is an appropriate measure for sample comparisons of a wide range of magnitudes (Goto and Mascie-Taylor 2007). With repeated measurements varying between 48.84mm (DW) and 523mm (TCL), CV was the measure of variability used for assessing measurement error.

The following statistics were reported for the repeatedly measured *D. bicornis* specimen in Appendix 1: minimum, maximum, mean, standard deviation (SD), and CV. The CVs for all measurements ranged between 0.146% (MXML) and 2.870% (DW), with a mean of 0.557%. With the DW value removed, the mean was 0.480%.

A small CV difference exists between the two measurement tools (Table 3-6). For the ten manual caliper measurements (>15 cm), the CV mean was 0.423%. For the nine digital caliper measurements (<15 cm), the CV mean was 0.720%. However, when the diastema measurements were removed from the digital caliper sample, the CV mean was only 0.555%, closer to the manual caliper's CV mean.

Table 3-4. Coefficient of variation (CV) results for the manual and digital calipers.

Measure	**%**
CV Mean	0.55743
CV Non-Diastema Mean	0.48033
CV Manual Mean	0.42316
CV Digital Mean	0.72046
CV Non-Diastema Digital Mean	0.55508

3.4.3 Asymmetry

Asymmetry between right and left sides is common in an organism, and the degree of asymmetry in a population is a result of both genetic and environmental influences (Hammer 2002). Asymmetry in fossil specimens also could be a result of postmortem warping. As asymmetry could arise from several influences, assessing the degree of asymmetry could elucidate developmental differences among species.

Assessing the degree of asymmetry is also important to maximize specimen coverage in statistical analyses. Acknowledging and understanding the degree of difference between right and left sides across ages and species is necessary for specimens with only one measurable side dimension. More specimens could be included in the analyses if specimens with missing side dimensions were comparable to specimens with both side dimensions measured.

To assess asymmetry, an Asymmetry Index was calculated for each of a specimen's 12 left-right measurements. The index is a size-independent percentage of asymmetry comparable for all ages with the right measurement chosen as the standard (Rossi et al. 2003).

$$AsymmetryIndex = \left(\frac{Right - Left}{Right} \right) \times 100$$

Using PAST (Hammer et al. 2009), the Kruskal-Wallis test for equality of medians was used to assess asymmetry in the 12 dimensions among groups. The Kruskal-Wallis test has no sample size or normality assumptions, a non-parametric equivalent to ANOVA (Hammer 2002). For all Kruskal-Wallis tests with multiple pairwise comparisons, a significance level of 0.05 was used for the overall test significance H-statistic. Following test significance, PAST reported Bonferroni-corrected p-values for all pairwise comparisons. A value of 0.05 was used to test for significance for these p-values.

The specimens were divided into four age groups based on subsequent molar eruption: Age Classes 1-4 (m1 not yet fully erupted), Age Classes 5-7 (m1 fully erupted), Age Classes 8-9 (m2 fully erupted), and Age Classes 10-17 (m3 fully erupted). *Teleoceras major*, *C. simum*, and *D. bicornis* were each tested for equality in asymmetry among age groups for the cranial and mandibular dimensions using the Kruskal-Wallis test. Due to small sample sizes, the age groups of *R. unicornis* and *D. sumatrensis* were not tested using the Kruskal-Wallis test. Instead, the total samples of *R. unicornis* and *D. sumatrensis* were tested for normality using the Shapiro-Wilk test with a significance level of 0.05. Specimen counts are provided in Appendix 2.

3.4.4 Sex and Subspecies Differences

Two methods were used to assess sexual and subspecific differences in ten cranial and mandibular variables in *R. unicornis*, *C. simum*, and *D. bicornis*. *Teleoceras major* was excluded from this assessment because the Ashfall Fossil Beds sample reflects a population, and Mead (2000) previously identified dimorphism in the same *T. major* sample. *Dicerorhinus sumatrensis* also was excluded because of small sample size; only 4 specimens were from adults and only 4 specimens' sex was identified. For the first method, each set of variables for adults of each species was tested for a unimodal distribution using the Shapiro-Wilk test for normality with a significance level of 0.05. Deviations from a unimodal distribution could be indicative of morphological differences between sexes or subspecies. Second, permutation t-tests were used to test characters for differences between male and female adult specimens of each species. Permutation t-tests test the standard t-statistic with 10,000 random pairs of replicate comparisons from the data set. The results are more accurate than standard t-tests for small sample sizes (Hammer 2009). A significance level of 0.05 was used for each test. Both Shapiro-Wilk and

permutation t-tests were completed using PAST (Hammer et al. 2009). Specimen counts for tests are provided in Appendix 2.

3.4.5 Function

The following measurements and ratios were investigated for skull dimension differences among species associated with feeding ecology: PCL, OH, RL, MXPL to MXML, MNPL to MNML, DW to MXPPW, and MXAPW TO MXPPW (Table 3-3 for abbreviations). Adult specimens (Age Classes 10-17) from each species were tested for differences in these functional characters. The mean of left and right side measurements were used for dimension lengths. Specimen counts are provided in Appendix 2.

Seven measurements and ratios were each tested for equality among species using the Kruskal-Wallis test in PAST (Hammer et al. 2009). For all Kruskal-Wallis tests with multiple pairwise comparisons, a significance level of 0.05 was used for the overall test significance H-statistic. Following test significance, PAST reported Bonferroni-corrected p-values for all pairwise comparisons. A value of 0.05 was used to test for significance for these p-values.

3.4.6 Allometry

Linear curve fitting techniques are the most common method for investigating allometric changes, in which a dimension of interest (dependent variable) is fitted against a size estimator (independent variable) (Hammer 2002). The slope of the fitted line between the dependent and independent variables is used as the growth ratio (Klingenberg 1998).

The primary equation for assessing allometry is Huxley's (1932) bivariate equation, $Y = b X^{a}$, where Y is the shape variable of interest, X is a measure of size, and a and b are the coefficients that describe the fit (German and Meyers 1989). To transform the line of fit into a straight line for ease in comparisons, morphometric data are often log-transformed, resulting in

the equation Y = log b + a log X. When Y is regressed on X, the growth ratio, a, is a change in Y for every unit X. Positive allometry of a shape variable has slope >1, negative allometry has slope <1, and isometry (no change in shape with size) has a slope =1 (Gould 1966).

If multiple variables are involved, Jolicoeur's (1963) multivariate generalization of allometry is often used instead of numerous bivariate regressions. A principal component analysis (PCA) produces linear combinations of the variables (components) to explain the most variation in the sample (Hammer 2002). A PCA of log-transformed morphometric data produces allometric growth estimations (Shea 1985). Jolicoeur (1963) found that the variable loading ratios (eigenvectors) are proportional to Huxley's bivariate slope estimations. Size is considered to inherently affect all variables in a PCA, and it can be assessed and scaled equally using the eigenvector of the first principal component (Giannini 2004).

With a large number of variables and species in this study, a PCA was the preferred method to describe ontogeny and compare shape change of skull dimensions in the extant rhinos and *T. major*. Cranial variables were tested separately from mandibular and dental variables because some juvenile specimens were missing several mandibular and dental measurements. The first variable set included 7 cranial variables with 91 specimens, and the second variable set included 7 mandibular and dental variables with 86 specimens. The following specimens were excluded from the second set of variables due to numerous missing measurements: UNSM 51101 (*T. major*, Age Class 4), AMNH 274636 and USNM 574963 (*R. unicornis* Age Class 1), AMNH 54764 (*D. sumatrensis*, Age Class 2), and USNM 182019 (*D. bicornis* Age Class 0). In the two variable sets, *T. major*, *C. simum*, and *D. bicornis* specimens represent a full range of ages, but *R. unicornis* and *D. sumatrensis* specimens have less age coverage.

Using PAST (Hammer et al. 2009), a PCA was completed for both data sets of each species to estimate allometric coefficients for each variable. All data sets included a few missing data points, which were accounted for by column average substitution PAST. Specimen and missing data counts are provided in Appendix 2.

3.5 GEOMETRIC MORPHOMETRICS

To further assess and compare skull ontogenetic shape changes between *T. major* and the extant rhinos, geometric morphometrics were used. Geometric morphometrics shape analysis techniques can be used to assess, describe, and depict morphological shape. Landmark-based methods use the coordinates of selected landmarks on specimen images as quantitative variables for analyses (Zelditch et al. 2004).

Digital images were captured for all specimens using orthographic projection techniques developed by the lab of Dominique Homberger and student Michelle L. Osborn. A rotating surface with perpendicular axes was created for consistent skull placement for all species. Crania and mandibles were articulated, and the occlusal planes were kept parallel with the rotating surface (Figure 3-3). On the x-axis, skulls were aligned with the anteroposterior axis. On the y-axis, skulls were aligned with the anterior orbit of the right and left sides. The camera was placed at an equal height to the right zygomatic arch and aligned perpendicular to the y-axis; the right lateral view of each specimen was captured.

For biologically meaningful shape comparisons among specimens and across groups, landmarks must be anatomically homologous, and of an intersection, point, or tip of a structure (Zelditch et al. 2004). Fifteen homologous landmarks were digitized using tpsDIG2 (Rohlf 2008) on all specimen images possessing the complete set of landmarks (52 total specimens). Landmarks were chosen to fully cover the skull and to track ontogenetic shape changes. (Teeth

were not used as landmarks to maximize inclusion of specimens from all ages.) Landmarks are depicted in Figure 3-4 and described in Table 3-5, and specimen counts for each species are provided in Appendix 2.

Landmark coordinates were entered into MorphoJ (Klingenberg 2008) for data manipulation. Six data sets were created, one for each of five species and one with all five species together. Landmarks were normalized across specimens using Procrustes superimposition, which scales, rotates, and aligns the specimens by least squares distances among corresponding landmarks (Hammer 2002). Procrustes superimposition does not change the shape of the structure, and the shape becomes independent of size.

Specimen outliers were then assessed in MorphoJ using the squared Mahalanobis distance, which estimates how unusual a specimen is from the sample; no significant outliers were apparent. A wireframe outline joining the landmarks was created in PAST and MorphoJ for each of six data sets to aid in depicting shape change among related landmarks (Figure 3-5).

Normalized shape variables in MorphoJ were used for two statistical analyses, PCA and CVA (canonical variate analysis) to compare shape variation within and among groups. A PCA is an ordination technique that produces new variables (components) with linear combinations of original variables (Zelditch et al. 2004). The new variables can simplify the patterns of variation among individuals in a sample. Multiplying shape variables by the PC coefficients results in vector displacements of the landmarks that correspond to each component and depict shape variation. A PCA of shape variables was completed in MorphoJ for each of the five species to compare ontogenetic shape changes. The significant components in each analysis were used to assess the landmarks that contribute most to the variation and shape change within a species. A minimum of 10% of the variance explained was the basis of cutoff for significant components.

Figure 3-3. Orthographic alignment of specimens (*D. bicornis* specimen, FMNH 127849).

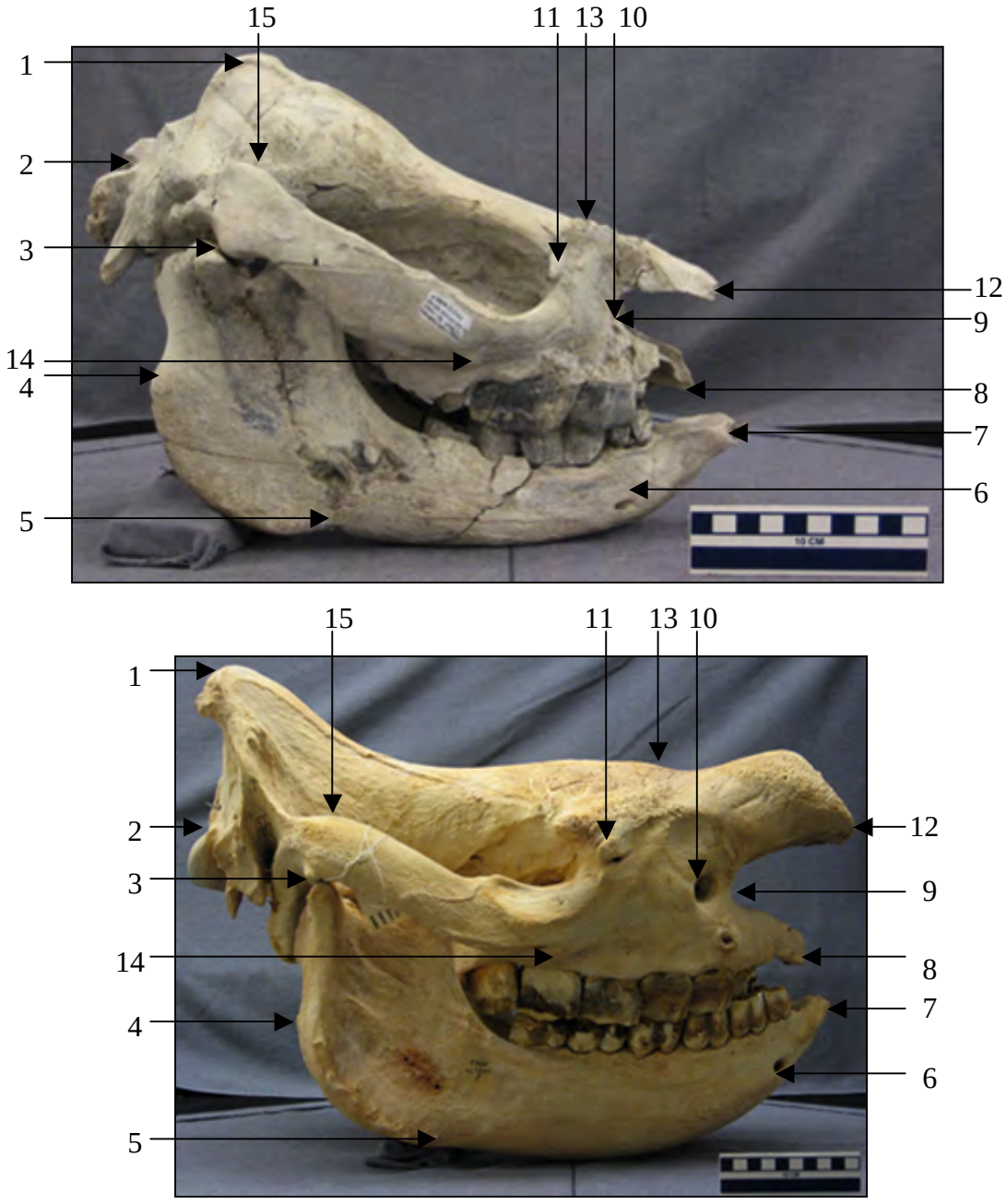

Figure 3-4. Landmark depictions for geometric morphometric analyses. The 15 landmarks are depicted on a *T. major* juvenile specimen, UNSM 52245 (above) and a *D. bicornis* adult specimen, FMNH 127849 (below). See Table 3-10 for the list of landmarks.

Table 3-5. Morphological descriptions of the landmarks, as shown in Figure 3-4.

Landmark	Description
1	The dorsal-most point of the occipital crest
2	The dorsal junction of the occipital condyle with the occipital plate
3	The dorsal-most point of the mandibular condyle
4	The posterior-most projection of the mandibular muscle attachment band
5	The anterior-most extension of the mandibular muscle attachment band
6	The center of the mental foramen
7	The anterior-most point of the mandible
8	The ventral-most junction of the maxilla and premaxilla
9	The posterior-most point of the nasal incision
10	The center of the infraorbital foramen
11	The center of the anterior orbital prominence
12	The anterior-most point of the nasals
13	The dorsal-most junction of the nasals and frontals
14	The anterior-most point of the jugal facial crest
15	The dorsal-most point of the zygoma

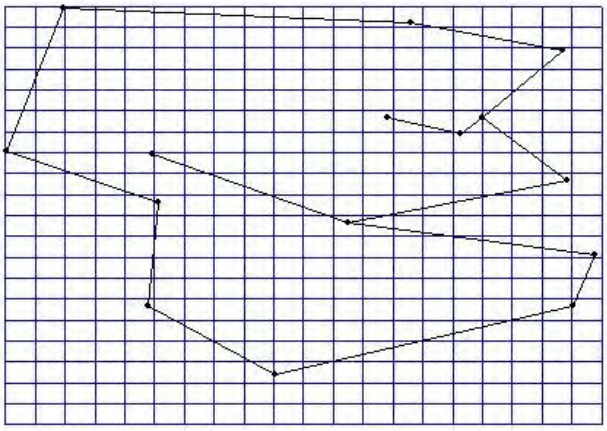

Figure 3-5. Wireframe outline of connected landmarks used to depict skull shape changes.

Different from PCA, CVA is a discrimination technique used to describe group differences (Zelditch et al. 2004). A CVA linear uses linear combinations of original variables like PCA, but group differences are used to maximize the separation of groups and to scale new coordinate axes. Multiplying the shape variables by the CV coefficients produces vector

displacements that help in visualizing the variables that best discriminate groups. A CVA of the five species grouped Procrustes coordinates was completed in MorphoJ to distinguish shape differences among the species' ontogenies. CV specimen plots and landmark displacements were assessed for the discriminating shape differences among species. A minimum of 10% of the variance explained was the basis of cutoff for significant components.

Another method for visually assessing shape change uses the change in coordinates of a specimen compared to a source configuration (Hammer 2002). Visual representations of this deformation, termed thin-plate splines, can yield insight into shape changes within a species. Deformation is broken down into uniform and non-uniform components. The uniform component represents linear deformation such as scaling and stretching. The non-uniform component is described by the partial warps, which are ordered from global changes to local changes (Hammer 2002).

The landmark coordinates were entered into PAST for assessing each species thin-plate splines. Five data sets were created, one for each species, and Procrustes superimposition was performed on each data set. The partial warps were calculated, and the total ontogenetic deformation (uniform and non-uniform together) for each species was visualized using thin-plate splines. To assess allometric growth factors, local expansion and contraction of the grids, which indicate changes in the primary growth centers through ontogeny, were assessed. The youngest specimen was used as the reference configuration to display ontogenetic deformation.

CHAPTER 4. RESULTS

4.1 AGE CLASSIFICATION

Upon inspection of extant rhino and *T. major* dentition, *D. bicornis* mandibular wear patterns were consistent in all pre-adult specimens. In heavily worn teeth of old adults, two inconsistencies were common. First, species occasionally displayed inconsistent wear stages of the full tooth row compared to age class descriptions of Hitchins (1978). Mihlbachler (2003) cited similar inconsistencies between *T. proterum* and *D. bicornis*. Mihlbachler (2003) used development of the most recently erupted teeth for classification because they would have been least affected by wear rate differences among individuals. The same age classification rationale and methodology was used in this study.

A second inconsistency was development of isolated, ovular infundibula in the premolars of old adult *C. simum* specimens. *Ceratotherium simum* molariform teeth have narrower lingual dentine at comparable stages of wear in other rhinos. As premolars wear, dentine lingually joins, forming an isolated infundibulum in Wear Stage 6. With heavy wear, infundibula gradually shrink and disappear. Despite this difference in premolar development, all other aspects of *C. simum* molariform wear were consistent with Hitchins (1978).

Overall, mandibular eruption and wear patterns described by Hitchins (1978) were accurate and applicable in extant rhinos and *T. major*. Hitchins's (1978) criteria were therefore used confidently for age classification in this study. Using these criteria, each specimen was placed into the most appropriate age class. Counts of species' specimen numbers for each age class are provided in Table 4-1.

Table 4-1. Age Class specimen counts for each species

Age Class / Species	*T. major*	*R. unicornis*	*D. sumatrensis*	*C. simum*	*D. bicornis*
0					2
1		2		1	1
2	3		1	2	
3	1	1		3	3
4	2			1	1
5	5	1		1	1
6		1		1	1
7			1	1	1
8	2	1	1	1	2
9	1			2	1
10	2	1	2	1	1
11	5	3	1	2	2
12	3	3		3	4
13		2	1		2
14	2			1	2
15	1				1
16					
17					1

4.2 DESCRIBED FUNCTIONAL CHARACTERS

Adult skull images of the five rhino species are provided in Figure 4-1 for depiction of the functional characters described below. Refer to Table 2-3 and Figure 2-4 for explanations of the functional characters.

Teleoceras major

The anterior maxilla above the premolars is short and shallow, and the nasal incision and orbit are contracted (Appendix 3). In Age Classes 10-15, the ventral maxilla is rugose and deeper, but still small in area. The posterior maxilla is thin and narrow below the jugal. However, the jugal is dorsal-ventrally broad, and it expands significantly throughout ontogeny, forming a very broad surface with the posterior maxilla.

The anterior jugal angles anteriorly-dorsally and extends past the anterior orbit border. In Age Class 4, the jugal develops a rugose ventral edge that gradually becomes sharper. The orbit location is anterior. In Age Class 2, the anterior orbit is above the anterior of P3. In Age Class 15, the anterior orbit is above the middle of M1. The anterior skull appears contracted.

The mandibular condyle is even with the anterior orbital tubercle, forming a parallel plane with the occlusal surface. The mandibular body is thin and anteriorly tapered in Age Classes 2-3, and it deepens slightly in Age Classes 4-9. In Age Class 10, the mandibular body is deep with less curvature. The mandibular angle is large and strongly curved with a pronounced muscle attachment band. A substantial increase in curvature and size occurs in Age Class 10.

Rhinoceros unicornis

The anterior maxilla above the premolars is deep and narrow. The nasal incision and orbit are close in Age Classes 1-8, and they separate from each other in Age Classes 11-13 (Appendix 3). In Age Classes 11-13, the maxilla increases in height, depth, and rugosity. The posterior maxilla and posterior jugal deepen through ontogeny, forming an overall broad and deep surface.

The anterior jugal ends behind the anterior orbit border. The jugal is parallel with the occlusal surface, having a ventral edge that sharpens gradually. The orbit location is anterior. The anterior orbit is above the anterior of P3 in Age Class 1 and above the posterior of P4 in Age Classes 11-13.

The mandibular condyle is above the anterior orbital tubercle. The mandibular body is thin and curved in Age Class 1. In Age Classes 3-13, the mandibular body is deeper and anteriorly tapered, but overall is thin. The mandibular angle changes significantly. In Age Class

1, the mandibular angle is small and gently curved. In Age Classes 11-13, the mandibular angle is large and strongly curved with a pronounced muscle attachment band.

Dicerorhinus sumatrensis

The anterior maxilla above the premolars is high and wide. The nasal incision and anterior orbit continually expand (Appendix 3), and the anterior maxilla heightens in Age Classes 7-13. In Age Classes 10-13, the ventral maxilla is rugose. The posterior maxilla is thin and the posterior jugal is narrow in Age Classes 2-8. In Age Classes 10-13 the maxilla and jugal deepen slightly.

The anterior jugal ends behind the anterior orbit border. The jugal is parallel with the occlusal surface, and the ventral edge sharpens in Age Classes 7-13. The orbit location is medial. In Age Class 2, the anterior orbit is above the anterior of P3. In Age Class 13, the anterior orbit is above the posterior of M1.

The mandibular condyle is slightly below the anterior orbital tubercle. The mandibular body is very thin in Age Class 2 and only slightly deeper in Age Classes 7-13. In Age Class 2, the mandibular angle is small and gently curved. In Age Classes 7-13, the mandibular angle increases in curvature and size, but it remains small and not strongly curved.

Ceratotherium simum

The anterior maxilla is long, high, and smooth. In Age Classes 1-3, the nasal incision and anterior orbit are close, but in Age Classes 4-14 they expand (Appendix 3). The anterior maxilla increases in height and remains smooth. The posterior maxilla and posterior jugal are thin early in ontogeny. In Age Classes 7-14, both the maxilla and jugal expand in depth, but they remain moderately deep.

The anterior jugal angles anteriorly-ventrally and extends past the anterior orbit border. The rugose ventral edge of the jugal in Age Class 3 sharpens in Age Classes 7-14; the ventral edge is long through ontogeny. The orbit location is posterior. In Age Class 1, the anterior orbit is above the posterior of P3. In Age Class 14, the anterior orbit is above the middle of M2.

The mandibular condyle is even with the anterior orbital tubercle, forming a plane parallel with the occlusal plane. The mandibular body is very deep and slightly curved. The body deepens throughout ontogeny. The mandibular angle is gently curved. Mandibular angle curvature and muscle attachment band robustness slightly increase in Age Classes 5-14.

Diceros bicornis

The anterior maxilla is large and rugose. In Age Classes 1-6, the nasal incision and anterior orbit are close, but in Age Class 7-17, the two diverge (Appendix 3). Anterior maxilla height and rugosity increase in Age Classes 7-17. The posterior maxilla and the posterior jugal are thin. The jugal gradually expands ventrally and the maxilla below remains thin.

The anterior jugal ends behind the anterior orbit border. The jugal is parallel with the occlusal surface, and in Age Class 5 a rugose ventral edge develops that sharpens through ontogeny. The orbit location is medial. The anterior orbit is above the middle of P3 in Age Class 1 and above the middle of M1 in Age Classes 14-17.

The mandibular condyle is below the anterior orbital tubercle. The mandibular body is medial in depth. In Age Classes 0-3, the mandibular body is thin and gently curved, and in Age Classes 4-17, the body deepens and straightens. The mandibular angle changes significantly. In Age Classes 0-3, the mandibular angle is weakly curved. In Age Classes 10-17, the mandibular angle is large and strongly curved, with a pronounced muscle attachment band.

Figure 4-1. Adult skull images for depiction of described functional characters. Refer to Table 2-3 and Figure 2-4 for explanations of the functional characters. Top left: *T. major* (UNSM 52288); top right: *R. unicornis* (AMNH 54454); center: *D. sumatrensis* (AMNH 81892); bottom left: *C. simum* (AMNH 51856); bottom right: *D. bicornis* (FMNH 127849).

4.3 DESCRIBED SKULL ONTOGENY

Teleoceras major

Ontogenetic Sequence

The *Teleoceras major* specimens were morphologically and developmentally divided into 4 groups: Age Classes 2-3, 4-5, 8-9, 10-15. The ontogenetic sequence based on dental development is provided in Appendix 4. Lateral skull images of specimen representatives for each age group are provided in Figure 4-2.

Dorsal Cranium

Dorsal crania in Age Classes 2-3 are short, wide, and globular. Rounded, slightly rectangular frontals join wider, rounder parietals posteriorly. The occipital crest is faint and concave. The zygomatic arches have a slight U-shaped outline, flaring laterally at the jugal-squamosal articulation. Temporal lines are not visible. The nasals are short and narrow to a point. In Age Class 3, the posterior frontals are more stretched and narrowed, forming a smoothly rounded hourglass shape with the parietals.

Dorsal cranium elongation distinguishes Age Classes 4-5 from other groups. The frontals are further elongated, forming a rounded and stretched diamond. The parietals are laterally rounded with a narrow, flat, midline surface bounded by the temporal lines, first appearing in Age Class 4. The occipital crest is more prominent and slightly less concave. The nasals are elongated and the zygomatic arches are longer with an increase in flare and robustness.

Frontal and parietal widening with the development of strong crests characterizes Age Classes 8-9. The frontal diamond is wider and flatter, distinct from adjacent nasals and parietals. The posterior frontals are narrowed, and the frontal-parietal suture is not visible beginning in

Age Class 8. Near the frontal-parietal junction, the temporal lines have converged to a single crest that connects with the occipital crest.

In Age Classes 10-15, the frontals and parietals are wider, but the posterior frontals and anterior parietals narrow to a short cylinder between the zygomatic arches. Overall zygomatic arch robustness has increased, and the dorsal-lateral edges are more medially rounded. The nasals are also wider, and the nasal-frontal suture remains apparent in all Age Classes 10-15 specimens. The occipital crest is strongly concave.

Lateral Skull

Early-developed muscle attachment sites on a short and rounded skull distinguish Age Classes 2-3. The mandibular angle is robust and strongly curved with ventral and posterior bulges. The facial crest is long and sharp, and the lateral zygomatic arch is broad and robust. The occiput, although small in size, has a sharp occipital crest. The parietal slope is inclined and rounded, and the frontals and nasals are flat. The premaxillae parallel the nasals, and the zygomatic arch parallels the dorsal parietal slope. The mandibular body is thin, curved, and anteriorly tapered.

Mandibular and facial enlargements characterize Age Classes 4-5. The mandibular body is deeper and longer, more proportional with the wide ramus. The mandibular angle is stronger and more robust. The ventral-posterior maxilla is deeper, and the anterior facial crest is curved dorsally. The premaxilla and nasals have lengthened. The occipital crest is sharper and oriented dorsal-anteriorly, but the braincase is still round. The lateral zygomatic arch is broader and more robust. All temporalis and masseter attachment sites increase in size in Age Classes 4-5.

Expansion of muscle attachment sites and overall lengthening of the skull characterize Age Classes 8-9. The zygomatic arch is anteriorly-posteriorly expanded and the facial crest is

broader. The mandibular ramus is wider with a stronger curve. The parietals are expanded posteriorly and the parietal slope is flatter; the occipital slope is vertical. The frontals, nasals, and mandibular body lengthen considerably.

Overall skull dimensions in Age Classes 10-15 are similar to Age Classes 8-9, but muscle attachment sites are exaggerated. The zygomatic arch, facial crest, and mandibular ramus are expanded. The occiput is more robust and its parietal slope is higher; the occipital slope is still vertical. The mandibular body deepens considerably. All facial sutures are visible in Age Class 10 specimens. Sutures usually close in Age Classes 11-12, but all sutures are noticeable in UNSM 5273 (Age Class 14). The jugal-zygoma suture is present in all individuals.

Figure 4-2. Lateral skull images representing the ontogenetic sequence for *T. major*. Top left: Age Class 2 (UNSM 52245); top right: Age Class 5 (UNSM 52234); bottom left: Age Class 8 (UNSM 52232); bottom right: Age Class 14 (UNSM 52288).

Horns

A slight nasal bump appears on the nasal tip in Age Class 5, and a small rugose area appears in Age Class 10. The nasals are consistently parallel to the premaxillae in all age classes, and little structural support is apparent. The most significant increases in nasal length and robustness occur within Age Classes 5 and 8.

Tusks

The exact timing of lower second incisor (i2) tusk eruption cannot be determined from the specimens available. In Age Classes 2-5, di2 are small, rounded, and peg-like. In an Age Class 8 specimen (UNSM 52232), the i2 have erupted, having a lozenge or teardrop shape. The tusks are short, suggesting they were recently erupted. The other Age Class 8 representative (UNSM 52230) still has di2. There were no Age Class 6-7 specimens available for data collection. These data suggest that di2 are shed between Age Classes 6-8, possibly during Age Class 8.

During tusk growth, a change in tusk orientation occurs. Prior to tusk eruption the di2 are anteriorly oriented, parallel to each other along the midline. In Age Classes 8-10 the tusks are slightly splayed laterally, no longer parallel to the midline. Beginning in Age Class 11, as the tusks further erupt and the mandibular symphysis widens, the tusks splay further laterally. All specimens from Age Classes 11-15 have significantly splayed tusks.

Sexual dimorphism is apparent. Two of the 16 adult specimens have significantly longer and wider tusks (UNSM 52272, UNSM 52288). These specimens are of Age Classes 11 and 14, respectively. The other 14 specimens have negligible tusk differences other than wear. Specimens UNSM 52272 and UNSM 52288 were interpreted as adult males.

Non-Molariform Dentition

No specimens possess a mandibular p1. The mandibular permanent p2 is commonly shed in adults, earliest evidence being in Age Class 10 (UNSM 52238), coinciding with m3 eruption. Adults with m3 in wear occasionally retain p2. In the sample, 5 of 13 (38%) specimens Age Class 10 and older retain at least one p2. The maxillary P1 is occasionally shed in adults; the earliest evidence is Age Class 10 (UNSM 52238), coinciding with M3 eruption. Adults with M3 in wear often retain P1. Overall, 8 of 13 (62%) specimens Age Class 10 and older retain at least one P1.

The specimens retain rudimentary first lower incisors (i1) or open i1 alveoli, in all age classes. The incisors are short, thin, and rounded; they are located at bone level, or slightly above. In the sample, 11 of 27 specimens (41%) have lower incisors, while 17 of 27 specimens (63%) have i1 or empty i1 alveoli. All specimens without evidence of lower incisors have fractured mandibular symphyses.

Rhinoceros unicornis

Ontogenetic Sequence

The *Rhinoceros unicornis* specimens were morphologically and developmentally divided into 4 groups: Age Classes 1, 3-5, 6-8, 11-13. The ontogenetic sequence based on dental development is provided in Appendix 4. Lateral skull images of specimen representatives for each age group are provided in Figure 4-3.

Dorsal Cranium

Rounded frontals and parietals with slender zygomatic arches characterize the dorsal crania in Age Class 1. The frontals and parietals are globular and similar in size, with the frontals narrower than the parietals. The frontal-parietal juncture is slightly V-shaped, forming a

bilobed dorsal surface. The occipitals are thin, having a straight and unpronounced occipital crest. The nasals are short, rounded, and triangular. The zygomatic arch outline is straight, and the arches are slender, especially anteriorly. Temporal lines are not visible.

The development and subsequent stretching of a diamond-shaped dorsal surface characterize Age Classes 3-5. This surface forms as frontals have posteriorly lengthened and narrowed, and the postorbital processes are protruding. The nasals are longer, more robust, and anteriorly rounded. The nasals and frontals together form a flat, stretched diamond across much of the dorsal surface. The temporal lines, which appear in Age Class 3, form prominent posterior edges of the diamond-shaped surface. The temporal lines converge then diverge on the parietals, posteriorly joining with the occipital crest. The occipital crest is pronounced with a slightly concave posterior edge. The zygomatic arches are longer and larger.

Further transformations to the diamond-shaped dorsal surface distinguish Age Classes 6-8. The diamond-shape is further stretched and narrowed posteriorly, culminating as a thin and sharp surface bounded by the temporal lines. The temporal lines and occipital crest are sharper, and the occipital crest is more concave. Lateral of the temporal lines, the parietals are concavely sloped, no longer convexly rounded. The parietal-occipital suture is not visible in Age Class 6, while the frontal-parietal suture is no longer visible in Age Class 8.

Exaggerations of the nasals, frontals, and parietals characterize Age Classes 11-13. The temporal crests are more prominent, and laterally, the parietal slope is steeper. The zygomatic arches are more robust and the dorsal-lateral edges are medially rounded. The nasals are wider and bulbous, and the posterior frontals are narrower. The nasal-frontal suture has disappeared in Age Class 12.

Lateral Skull

An undeveloped braincase, mandible, and muscle attachment sites typify Age Class 1. The parietals are round with an inclined dorsal slope. The occipital slope is anteriorly inclined. Thin zygomatic arches parallel the parietal slope. The facial crest is not pronounced. The dorsal nasal surface is posteriorly flat, and it curves and thins to a point anteriorly-ventrally. The mandibular body is thin, curved, and tapered anteriorly. The mandibular angle is gently curved with a slight posterior bulge.

Transformations to the occiput, facial crest, and mandible distinguish Age Classes 3-5. The parietals are higher and angular, shaped as a rounded triangle. The parietal slope is further inclined, beginning above the anterior orbit; the occipital slope is nearly vertical. Anterior of the nasal swelling, the nasals curve sharply ventrally. The zygomatic arch is more robust with a sharp and short facial crest. The zygomatic arch is higher, paralleling the dorsal parietal slope. The mandibular ramus is deeper and more strongly curved with the development of a peripheral muscle attachment band. The peripheral band has anterior and posterior bulges. The mandibular body is deeper and still curved and tapered anteriorly.

Continued transformations to the muscle attachment sites typify Age Classes 6-8. The occiput is higher and more triangular. The parietal slope begins further posteriorly, above the posterior orbit. The anterior zygomatic arch is broader, and the facial crest is longer and sharper. The nasal swelling is higher. The mandible is overall more robust with the mandibular angle more strongly curved dorsally. Both mandibular angle bulges are prominent, and the peripheral muscle attachment band is posterior-ventrally extended and exaggerated in size. The mandibular body is deeper.

Age Classes 11-13 are characterized by exaggerations to the muscle attachment sites. The parietal slope is more inclined and the occipital slope is nearly vertical, resulting in a high, angular occiput. Zygomatic arch height, broadness, and robustness have increased, especially anteriorly. The facial crest is sharper, and the maxilla anterior of the facial crest is broader. Nasal curvature has increased anteriorly. The mandibular angle is strongly exaggerated, anteriorly curving dorsal of the posterior bulge. The peripheral attachment band is expanded and robust, having extremely prominent bulges. The mandibular body is deeper with a greater anterior taper. All Age Class 11 specimens have visible sutures but no facial sutures are visible in Age Class 12.

Figure 4-3. Lateral skull images representing the ontogenetic sequence for *R. unicornis*. Top left: Age Class 1 (USNM 574963); top right: Age Class 5 (AMNH 119475); bottom left: Age Class 8 (AMNH 54456); bottom right: Age Class 12 (AMNH 54454).

Captive Specimens

One *R. unicornis* captive specimen, UNSM ZM13844, had a suspect age classification because its visible jugal-zygoma suture implied an older age than the dentition. The jugal-zygoma suture is no longer visible; all Age Class 11 specimens have noticeable jugal-zygoma sutures. UNSM ZM13844 is the only classified Age Class 10 individual in the sample. The specimen also had distinct skull morphology not present in the rest of the sample. It had a steep parietal slope and zygomatic arch, steeper than all other specimens. The facial crest and jugal are both unusually short. The characteristic smooth-sloped transition from the anterior parietal slope to the nasal bulge is not present. Instead, the steep parietal slope transitions to a short orbital bulge followed by a steep nasal inclination. A higher occiput and an anteriorly-posteriorly compressed orbital region compared to other adult specimens result in an uncharacteristic morphology, so UNSM ZM13844 was removed from the ontogenetic sequence.

Another captive *R. unicornis* specimen, FMNH 140833, was incomplete and damaged, preventing a full assessment of its morphology; it was removed from ontogenetic descriptions. The third captive *R. unicornis* specimen, FMNH 57639, displayed no age inconsistencies or morphological distinctions, so it was included in the ontogenetic sequence.

Horns

Horn development is not constant through ontogeny. In Age Class 1, the nasals are sloped anteriorly and ventrally. There is no dorsal swelling or rugosity present. In Age Classes 3-8, the dorsal swelling is present and it gradually increases. Anterior of the swelling, the nasals curve sharply ventrally. The nasal horn rugosity first appears in Age Class 8, and it becomes more robust throughout Age Classes 11-13.

Tusks

A relatively complete ontogenetic sequence allows an estimate of di2 shedding and tusk eruption. In Age Classes 1-6, di2 are small, rounded, and peg-like, and little size increase occurs. By Age Class 8, the tusks are erupted, having a teardrop shape. Representatives of Age Class 7 were unavailable for collection. The i2 eruption is estimated to occur in Age Classes 7-8.

A change in tusk orientation occurs during development. Prior to tusk eruption, di_2 are anteriorly oriented and parallel to each other along the midline. In Age Class 8, the tusks are slightly splayed laterally, not parallel to the midline. In Age Classes 11-13, as the tusks erupt further and the mandibular symphysis widens, the tusks are splayed further. There are no noticeable tusk size or shape differences between sexes, likely due to the small sample size.

Non-Molariform Dentition

The mandibular p1 is lost in all nine specimens Age Class 11 and older. No Age Class 9 or 10 specimens were in the sample, but an Age Class 8 specimen still retains p1. Therefore, the p1 is likely shed with m3 eruption. The maxillary P1 is occasionally lost in adults, the earliest evidence being in Age Class 11, coinciding with M3 eruption. Adults with m3 in wear often retain P1. Overall, 5 of 9 (56%) specimens Age Class 11 and older retain at least one P1.

The rudimentary i1 is occasionally present in the sample. The incisors are short, thin, and rounded. All 15 specimens have i1 alveoli, and 4 of 15 (27%) specimens have i1 present. Some i1 are retained in adults; for example, two Age Class 13 specimens (FMNH 25707, 57639) have i1. Rudimentary second upper incisors (I2) are also present early in ontogeny. The I2 are short, rounded nubs at the bone surface in Age Class 1 (AMNH 274636, USNM 574963). The premaxillae of Age Class 3 and Age Class 5 specimens are not preserved, and Age Class 6 and older specimens show no sign of I2.

Dicerorhinus sumatrensis

Ontogenetic Sequence

The *Dicerorhinus sumatrensis* specimens were morphologically and developmentally demarcated into 3 groups: Age Classes 2, 7-8, 10-13. The ontogenetic sequence based on dental development is provided in Appendix 4. Lateral skull images of specimen representatives for each age group are provided in Figure 4-4.

Dorsal Cranium

Rounded frontals and parietals with thin zygomatic arches characterize the dorsal cranium in Age Class 2. The frontals are fairly rectangular while the parietals are slightly larger, more rounded, and narrowed posteriorly. The occipitals are thin and the occipital crest is a short, straight, unpronounced line. The nasals are short, rounded, and triangular. The zygomatic arches are straight and thin with no lateral flare. Temporal lines are not visible.

Elongated frontals, nasals and zygomatic arches typify Age Classes 7-8. The frontals and parietals are rounded and narrowed posteriorly. The occipital crest is slightly concave. The nasals are longer and terminally rounded, with a rugosity appearing in Age Class 8. The zygomatic arches are long, straight, and robust posteriorly near the occipital articulation. Temporal lines are visible but unpronounced in Age Class 8. The parietal-occipital and frontal-parietal sutures are not visible in Age Classes 7 and 8, respectively.

Age Classes 10-13 are characterized by frontal-parietal continuity and nasal exaggerations. The frontals and parietals are dorsally flattened and smoothly connected by the temporal lines. In Age Class 13, the frontals are wider and rounder as the frontal rugosity develops. Throughout Age Classes 10-13, the anterior nasals become rounder and wider, and the nasal rugosity gradually expands. The nasal-frontal suture is not visible in Age Class 10. The

temporal lines are pronounced and parallel to the midline. The parietals are rectangular, and the occipital crest remains slightly concave. The zygomatic arches are robust in Age Classes 10-11, and in Age Class 13 they are laterally extended.

Lateral Skull

A globular occiput, undeveloped muscle attachment sites, and thin mandible characterize Age Class 2. A rounded parietal slope and an inclined occipital slope form a globular occiput. The zygomatic arch is thin and parallel to the parietal slope, and the facial crest is indistinct. The nasals thin to a point, curving ventrally. The thin mandibular body slightly tapers anterior of the premolars. The mandibular angle is slightly curved with a weak posterior bulge.

An angular occiput and weak muscle attachment crests typify Age Classes 7-8. The occiput is sharply triangular, having a further inclined parietal slope and a vertical occipital slope. The occipital crest and temporal lines are visible but not prominent. The squamosal is thin, the jugal is short and broad, and the facial crest is apparent but not prominent. The nasals have a slight dorsal swelling, and in Age Class 8 the nasal rugosity develops. The mandibular ramus is narrow with a rounded mandibular angle and noticeable anterior and posterior bulges. The slender mandibular body tapers from the premolars to the incisors.

Increases in nasal and frontal swelling and slight muscle attachment site enlargements characterize Age Classes 10-13. The parietal slope is increased, and the temporal lines and occipital crest are sharper. A frontal swelling appears in Age Class 10; it enlarges through Age Classes 11-13. The nasal swelling rises and the nasal tip curves more ventrally in Age Classes 10-13. The jugal is considerably broader. The facial crest is longer and sharper, and anteriorly the maxilla is broader and extended. The mandibular angle is stronger and deeper with a peripheral band. The anterior and posterior bulges are more prominent, especially in Age Class

13. The facial sutures close in Age Class 10 except for the jugal-zygoma suture (Age Class 11) and maxilla-jugal suture (after Age Class 11).

Figure 4-4. Lateral skull images representing the ontogenetic sequence for *D. sumatrensis*. Top: Age Class 2 (AMNH 54764); bottom left: Age Class 8 (FMNH 63878); bottom right: Age Class 13 (AMNH 81892).

Horns

Nasal development mostly occurs in Age Classes 10-13. The nasals have a slight dorsal swelling in Age Classes 2-8. In Age Classes 10-13, the nasal swelling becomes higher and the nasal tip curves steeper ventrally. The nasal rugosity appears in Age Class 8, increasing through Age Class 11, and the frontal rugosity appears in Age Class 11.

Tusks

The sample is small and incomplete, so the timing of di2 shedding and tusk eruption was estimated based on two specimens. In Age Class 7, the alveoli are empty and the tusks are

erupting, still below bone level. In Age Class 8, the tusks are erupted, and they have a lozenge shape. These two specimens suggest that di_2 are shed in Age Class 7. During tusk growth and development, a change in tusk orientation occurs. In Age Classes 8-11, the tusks are anteriorly oriented, parallel to each other along the midline. In Age Class 13, the tusks are longer and splayed laterally. The mandibular symphysis does not appear to have widened among these stages. Due to the small sample size, size or shape differences between sexes are not discernible.

Non-Molariform Dentition

The mandibular p1 is present in all specimens Age Classes 1-8 and lost in all specimens Age Class 10 and older. Mandibular p1 loss may be associated with m3 eruption because m3 eruption occurs in Age Classes 9-10. The maxillary P1 is also shed, possibly earlier than the mandibular p1. An Age Class 7 specimen (AMNH 173576) has heavily worn P1, while an Age Class 8 specimen (FMNH 63878) has empty P1 alveoli. In specimens Age Class 10 and older, P1 are lost with no alveoli remaining. Maxillary P1 loss may be associated with the synchronous eruption of P2, P3, and M2, which were erupted with no wear in FMNH 63878. There is no evidence of rudimentary lower or upper incisors in the sample.

Ceratotherium simum

Ontogenetic Sequence

The *Ceratotherium simum* specimens were morphologically and developmentally demarcated into 5 groups: Age Classes 1-2, 3-4, 5-7, 8-9, 10-14. The ontogenetic sequence based on dental development is provided in Appendix 4. Lateral skull images of specimen representatives for each age group are provided in Figure 4-5.

Dorsal Cranium

Rounded parietals and rectangular frontals characterize Age Classes 1-2. The parietals are round, and the occipitals are narrow with a concave occipital crest. Postorbital processes protrude from rectangular, posteriorly narrowed frontals. The nasals are rounded, slightly narrowing anteriorly. The zygomatic arches are straight and robust.

Lengthened frontals and parietals, and bulbous nasals distinguish Age Classes 3-4. Posteriorly the frontals are lengthened and concavely narrowed, forming a cylindrical junction with the lengthened parietals. The parietal-occipital junction is triangular, deeper than the occipital crest. The nasals are wider and more bulbous.

Overall lengthening with frontal and occiput flattening and widening characterizes Age Classes 5-9. The frontals are anteriorly wider with a more exaggerated posterior narrowing. The parietals are medially cylindrical and laterally wide. The squamosals are narrow, flat shelves near the parietal articulation. The occipital crest is medially deeper with posterior-lateral flares. The nasals are particularly more bulbous with a slight midline indentation in Age Class 9. The zygomatic arches are extended with medially rounded dorsal-lateral edges. In Age Class 6, the frontal-parietal suture is not visible while the temporal lines are apparent. The temporal lines are narrow and parallel near the suture, and they diverge posteriorly. In Age Class 9, the temporal lines are fully prominent. The parietal-occipital suture disappears between Age Classes 6-8.

Nasal, frontal, and occipital exaggerations distinguish Age Classes 10-14. The frontals and nasals are further rounded and widened. In Age Class 10, nasal and frontal rugosities develop; both the nasal and nasal-frontal sutures are not visible in Age Class 11. The nasals and frontals are completely covered by rugosity in Age Class 12. The temporal lines are posteriorly

sharper, diverging along wider and deeper occipital flares. The occipitals are broader than the frontals, and the squamosal shelves are wider. The zygomatic arches are overall more robust.

Lateral Skull

A posteriorly oriented, angular occiput and deep mandibular body characterize Age Classes 1-2. The occiput has a gentle parietal slope and a vertical occipital slope. A slender zygomatic arch parallels the parietal slope. The facial crest is short and slightly prominent. The nasals are bulbous with a slight dorsal swelling and steep terminal slope. All facial sutures are visible. The mandibular body is deep and gently curved, tapering to a point anterior of the premolars. The mandibular ramus is also deep, having a posterior bulge and weak mandibular angle. Dorsal of the bulge the ramus is almost vertical.

Parietal and facial elongations characterize Age Classes 3-4. The parietals are oriented further posteriorly but the parietal slope has not changed; the occipital slope is vertical. The maxilla is longer and the premaxilla is projecting further past the premolars. The zygomatic arch is more robust and the facial crest is sharper and longer. The nasals are larger with a higher swelling. The mandible undergoes slight developments in Age Classes 3-4. The mandibular body maintains its shape and depth. The ramus is wider and the mandibular angle is stronger. The posterior bulge is more prominent and a thin peripheral muscle attachment band is present.

A posteriorly stretched occiput and transformed zygomatic arch characterize Age Classes 5-9. The cranium has significantly increased in length and height. The parietals are stretched posteriorly and more shallowly sloped, making the occiput long and triangular. The nasals are longer and the nasal swelling is higher. Significant increases in the nasal swelling occur through Age Classes 5-9. The zygomatic arch becomes more robust with a change in orientation, but still paralleling the lowered parietal slope. The jugal becomes broader and flatter while the

squamosal becomes inclined, staying parallel to the parietal slope. The facial crest becomes a long, sharp attachment area. The mandible gradually becomes deeper and wider. The body deepens and its ventral profile flattens. The ramus widens and the mandibular angle becomes stronger and longer. In Age Classes 7-9, the posterior bulge is no longer apparent, as the peripheral muscle attachment band becomes longer and more robust.

Age Classes 10-14 are characterized by horn swellings, facial suture closings, and increases in robustness. A slight frontal swelling develops, and the nasal swelling increases through Age Classes 10-14. The mandibular body is deeper, and the zygomatic arch, facial crest, and peripheral band are more robust. All facial sutures are closed in Age Class 10. The jugal-zygoma suture disappears in Age Class 12.

Figure 4-5. Lateral skull images representing the ontogenetic sequence for *C. simum*. Top left: Age Class 1 (AMNH 51918); top right: Age Class 5 (AMNH 51870); bottom left: Age Class 8 (AMNH 51931); bottom right: Age Class 12 (AMNH 51856).

Horns

Nasal development is gradual with shape and size transformations occurring in Age Classes 5-9. The nasal and frontal rugosities develop in Age Classes 8 and 10, respectively. The rugosities and swellings steadily increase in Age Classes 11-14.

Non-Molariform Dentition

The mandibular p1 is lost in specimens Age Class 8 and older. An Age Class 8 specimen (AMNH 51931) has open p1 alveoli, and two Age Class 9 specimens (AMNH 54125, 51865) show no evidence of p1. Mandibular p1 loss may be associated with synchronous eruption of p2, p3, and m2, which are recently erupted in AMNH 51931. The maxillary P1 is lost in all specimens Age Class 8 and older. An Age Class 8 specimen (AMNH 51931) has open P1 alveoli, and two Age Class 9 specimens (AMNH 54125, 51865) have near closed P1 alveoli. Maxillary P1 loss may be associated with synchronous eruption of P2, P3, and M2, which are not fully erupted in AMNH 51931.

No rudimentary incisors are present in the sample. However, shallow upper and lower incisor alveoli with no teeth are present in Age Classes 2 (AMNH 51882), 8 (AMNH 51931), and 9 (AMNH 51865). No specimens Age Class 10 and up have incisor alveoli. Only 1 of 10 premaxillae are articulated in Age Classes 1-7, so incisor alveoli may be common in pre-adults.

Diceros bicornis

Ontogenetic Sequence

The *Diceros bicornis* specimens were morphologically and developmentally demarcated into 6 groups: Age Classes 0, 1-3, 4-5, 6-7, 8-10, 11-17. The ontogenetic sequence is based on dental development provided in Appendix 4. Lateral skull images of specimen representatives are provided in Figure 4-6.

Dorsal Cranium

A rounded cranium with thin, straight zygomatic arches distinguishes Age Class 0. The frontals are long and rectangular while the parietals are shorter but equal in width. The occipitals widen posteriorly and the occipital crest is convexly curved. The nasals are triangular and distally rounded.

Significant nasal, frontal, and parietal lengthening occurs in Age Classes 1 and 3. The nasals become longer and more rounded terminally. The frontals and parietals lengthen considerably; both are rectangular. The zygomatic arches lengthen and slightly extend laterally. The occipital crest is straight.

Posteriorly narrowed frontals and laterally extended zygomatic arches typify Age Classes 4-5. The frontals narrow posteriorly and the parietals narrow anteriorly, forming a concave juncture. The occipitals are longer with a concave occipital crest. The zygomatic arches are more robust and laterally extended. A narrow squamosal shelf is present near the articulation with the parietals.

Anteriorly rounded frontals and posteriorly widened parietals form a dorsal hourglass shape in Age Classes 6-7. The parietals widen laterally, the occipital crest is straight, and the squamosals form wide, flat shelves. The zygomatic arches are wider and more robust. Appearing in Age Class 6, the temporal lines are faint, unpronounced, and concave along the dorsal hourglass shape.

Rugosity development and muscle attachment site pronouncements distinguish Age Classes 8-10. The frontals and nasals become rounder and wider in Age Classes 8-10, with rugosities appearing in Age Class 8. Wider frontals and parietals between pronounced temporal

lines form a more distinct dorsal hourglass. The zygomatic arches are more pronounced and robust. In Age Class 8, the frontal-parietal and parietal-occipital sutures are not visible.

Pronounced nasals, frontals, temporal lines, zygomatic arches, and occipital crest characterize Age Classes 11-17. The nasals and frontals become exceptionally round and rugose. Anteriorly the temporal lines become narrower, and posteriorly they become wider, joining the occipital crest. The temporal lines and occipital crest are sharper, and the zygomatic arches are more robust. The nasal-frontal suture is not visible in Age Class 11.

Lateral Skull

An undeveloped occiput and mandible with a broad jugal distinguish Age Class 0. The frontals and parietals are flat and inclined. The occipital slope is anteriorly inclined. The nasals are short and pointed with a small dorsal swelling. The jugal is broader and more robust than the squamosal. An undeveloped mandible has a thin, curved body; a short, narrow, ramus; and a sharp mandibular angle.

Occiput, zygomatic arch, and mandible muscle attachment site developments characterize Age Classes 1-3. The parietal slope is steeper and the occipital slope is almost vertical, together forming an angular occiput. The jugal and squamosal are equally broad, and the zygomatic arch is inclined, paralleling the parietal slope. The facial crest is long and fairly sharp. The nasals are steeply sloped on both sides of the pronounced dorsal swelling. All facial sutures are visible. The mandibular ramus is wide and vertical, and the mandibular body tapers anteriorly. The mandibular angle has a thin peripheral band and posterior bulge.

Increases in parietal, zygomatic arch, and mandibular angle robustness distinguish Age Classes 4-5. The parietals are enlarged and extended vertically, forming a more angular occiput. The occipital slope is vertical. The jugal is broader than the squamosal, the zygomatic arch is

more inclined, and the facial crest is longer and sharper. The nasals have a slightly higher vertical swelling. The mandibular body is deeper. The ramus is more robust with a pronounced posterior bulge and peripheral band.

Muscle attachment site transformations distinguish Age Classes 6-7. The parietals are higher and more sharply sloped. The zygomatic arch and facial crest are longer. The nasals are rounder and more robust, with a higher dorsal swelling. The mandibular ramus is deeper and the mandibular body is flatter and deeper.

Frontal swelling and rugosity development typify Age Classes 8-10. Dorsal of the anterior orbit, a slight frontal swelling with rugosity appears in Age Class 8. The nasal rugosity also appears in Age Class 8. The occipital crest is directly dorsal of the foramen magnum. The zygomatic arch is broader, the facial crest is sharper, and the facial region is deeper. The facial sutures are faint but still apparent. In Age Classes 8-10, the mandibular angle is nearly vertical, and it curves anteriorly dorsal of the posterior bulge. The mandibular body and ramus are deeper, and the peripheral band is more pronounced.

Age Classes 11-17 are characterized by a gradual increase in frontal and nasal rugosity, and muscle attachment site increases. The frontal and nasal swellings increase throughout Age Classes 11-17, and the rugose areas gradually spread. The occiput, zygomatic arch, and mandibular angle become more robust, and the facial crest becomes longer and more pronounced. The jugal-zygoma and facial sutures disappear in Age Class 12.

Captive Specimens

One captive specimen, FMNH 60784, was advanced morphologically for its age classification. Although it was the only Age Class 9 specimen, it was larger and more robust than Age Class 10-11 specimens. Increased robustness of the zygomatic arch and occiput, and

Figure 4-6. Lateral skull images representing the ontogenetic sequence for *D. bicornis*. Top: Age Class 1 (USNM 182030); center left: Age Class 3 (USNM A34718); center right: Age Class 5 (USNM 240884); bottom left: Age Class 8 (USNM 161925); bottom right: Age Class 12 (FMNH 127849).

highly developed nasal and frontal rugosities are comparable in development to Age Class 12. The jugal-zygoma and facial sutures are still visible, which disappear approximately in Age Class 12. Overall development of FMNH 60784 was characteristic of Age Class 12. Due to age class inconsistencies, FMNH 60784 was removed from the ontogenetic sequences

Another captive specimen, FMNH 166520, was incomplete and damaged, preventing a full assessment of its morphology; it was removed from the ontogenetic sequence. The other two captive specimens, FMNH 121646 and FMNH 57809, displayed no age inconsistencies or morphological distinctions; they were included in the ontogenetic sequence.

Horns

Nasal horn development is gradual in Age Classes 0-17. The nasal swelling is present in all specimens. The swelling gradually increases, and in Age Class 8 the nasals become more robust and the rugosity develops. The nasal rugosity gradually increases from Age Classes 10-17. Frontal horn development begins in Age Class 8 with the appearance of a frontal swelling. The frontal rugosity also appears in Age Class 8, steadily increasing in Age Classes 10-17.

Non-Molariform Dentition

The mandibular p1 is lost in all specimens by Age Class 12. Mandibular p1 loss may be associated with m3 eruption, as all 11 specimens with m3 fully erupted have lost p1. The maxillary P1 is rarely missing in adults, as only 3 of 12 specimens (25%) have lost P1. Specimens in Age Classes 12 (FMNH 127849), 15 (FMNH 57809), and 17 (USNM 182195) are the only specimens missing P1.

Rudimentary lower incisors are present in all ages, from Age Class 1 (USNM 182030) to Age Class 15 (FMNH 57809). Overall, 9 of 26 specimens (35%) have rounded incisor nubs at bone level, and 14 of 26 specimens (54%) have incisors or open alveoli. Rudimentary upper incisors are retained in all age ranges, from Age Class 1 (USNM 182030) to Age Class 12 (FMNH 22366). The incisors are small, round protuberances at bone level. Among the 13 of 26 specimens (50%) with premaxillae articulated, 5 of 13 (38%) have upper incisors.

4.4 TRADITIONAL MORPHOMETRICS

4.4.1 Measurements

The 19 dimensions were measured on each specimen for all ages and species. Due to disarticulated bones for extant species specimens and fractured skulls for *T. major* specimens, not all measurements were available on each specimen. The percentage of specimens with all dimensions measured is provided in Table 4-2

Table 4-2. Specimen numbers and percentages with all dimensions measured for each species.

	T. major	***R. unicornis***	***D. sumatrensis***	***C. simum***	***D. bicornis***
Specimens with all measurements	17	11	5	15	19
Total specimens	27	15	7	20	26
% of specimens	63%	73%	71%	75%	73%

4.4.2 Asymmetry

Testing the Asymmetry Index among age groups for *T. major*, *C. simum*, and *D. bicornis* revealed no significant differences from equality for any cranial or mandibular dimensions with the Kruskal-Wallis test (Table 4-3). The Shapiro-Wilk tests of normality for *R. unicornis* and *D. sumatrensis* resulted in only one dimension, ACL of *R. unicornis*, with a significant p-value ($p = 0.000009154$) (Table 4-4). This sample contained one specimen, UNSM ZM13844, with an Asymmetry Index of -31%. This specimen is a captive individual that was removed from ontogenetic assessments because of inconsistencies with the *R. unicornis* sample. When UNSM ZM13844 was removed from the ACL asymmetry analysis, the sample was not significantly different from normality ($p = 0.1824$). No dimensions for any species were found to have

significant differences in asymmetry among age groups, and specimen UNSM ZM13844 was removed from all subsequent analyses of asymmetry and function.

Table 4-3. Kruskal-Wallis test results for asymmetry among age groups. H-statistics and p-values are provided for tests for asymmetry among age groups for *T. major*, *C. simum*, and *D. bicornis*.

	T. major	***C. simum***	***D. bicornis***
TCL	H: 1.74 p: 0.6281	H: 1.937 p: 0.5856	H: 5.79 p: 0.1223
PCL	H: 0.7465 p: 0.8622	H: 2.054 p: 0.5613	H: 6.18 p: 0.1032
MCL	H: 1.443 p: 0.6955	H: 6.478 p: 0.09055	H: 1.416 p: 0.7019
ACL	H: 4.786 p: 0.1882	H: 3.299 p: 0.3477	H: 0.1896 p: 0.9792
ML	H: 1.261 p: 0.7384	H: 5.487 p: 0.1394	H: 3.605 p: 0.3075
RL	H: 1.336 p: 0.7207	H: 0.4641 p: 0.9267	H: 4.113 p: 0.2495

Table 4-4. Shapiro-Wilk test for normality results for asymmetry among age groups. W-statistics and p-values are provided among age groups for *R. unicornis* and *D. sumatrensis*. ACL* is with captive specimen UNSM ZM13844 removed.

	R. unicornis	***D. sumatrensis***
TCL	W: 0.9182 p: 0.2375	W: 0.9531 p: 0.7578
PCL	W: 0.9574 p: 0.6809	W: 0.9282 p: 0.5665
MCL	W: 0.9535 p: 0.5815	W: 0.8931 p: 0.3345
ACL	W: 0.5499 p: 0.000009154	W: 0.9936 p: 0.9980
ML	W: 0.9668 p: 0.8305	W: 0.8934 p: 0.2926
RL	W: 0.9623 p: 0.8161	W: 0.8501 p: 0.1578
ACL*	W: 0.9144 p: 0.1824	

Following age group comparisons within species, adult groups among species were tested for equality in asymmetry for all 12 dimensions using the Kruskal-Wallis test. Only one cranial dimension (MCL, p = 0.000298) and one mandibular dimension (ML, p = 0.001012) had significant p-values (Table 4-5). No dental dimensions deviated from equality.

For MCL, *R. unicornis* was found to differ significantly from two species, *T. major* (p = 0.001613) and *C. simum* (p = 0.02143). Within these samples, there were no significant outlier

Table 4-5. Kruskal-Wallis test results for asymmetry among adults. H-statistics and p-values are provided among adult samples of the species.

TCL	H: 6.329 p: 0.175
PCL	H: 4.021 p: 0.403
MCL	H: 21.14 p: 0.0002975
ACL	H: 9.229 p: 0.055
ML	H: 18.44 p: 0.001012
RL	H: 9.345 p: 0.053

MXPL	H: 2.99 p: 0.559
MXML	H: 1.687 p: 0.793
MXDL	H: 1.138 p: 0.888
MNPL	H: 4.053 p: 0.398
MNML	H: 6.301 p: 0.177
MNDL	H: 2.735 p: 0.603

MCL	***T. major***	***R. unicornis***	***D. sumatrensis***	***C. simum***
T. major				
R. unicornis	0.001613			
D. sumatrensis	0.1058	1		
C. simum	1	0.02143	0.6825	
D. bicornis	0.171	0.4884	1	1

ML	***T. major***	***R. unicornis***	***D. sumatrensis***	***C. simum***
T. major				
R. unicornis	0.04228			
D. sumatrensis	0.362	1		
C. simum	0.3937	0.06536	1	
D. bicornis	0.04295	0.2789	1	1

specimens. The *R. unicornis* sample had a strong left asymmetry, with a sample minimum of –3.15%, a maximum of 0%, and a median of -2.45%, while the *T. major* (0%, 5.08%, 2.00%) and *C. simum* (-1.39%, 5.15%, 1.33%) samples had strong right asymmetries (Appendix 5).

For ML, *T. major* was found to differ significantly from two species, *R. unicornis* ($p = 0.04228$) and *D. bicornis* ($p = 0.04295$). The *T. major* sample had a wide range of positive and negative values, with a minimum of -5.62%, a maximum of 6.81%, and variance of 9.39. The other species had minima and maxima between -1.72% and 1.88%, and variances under 1.00.

The analyses indicate no asymmetry differences in age groups within species and minimal adult differences in asymmetry in extant rhinos. The stronger asymmetric values of *T. major* are not unexpected, as several mandibular condyles were significantly warped postmortem. Comparing specimen counts of asymmetry and symmetry for each dimension using 0.5% difference as a threshold (Table 4-6), the difference between *T. major* and extant rhinos is more apparent, as several cranial and mandibular lengths (MCL, ACL, ML, RL) are right side dominated in *T. major*. To address asymmetries, a right and left measurement mean was used for each length in statistical analyses using measurement data. Specimens with one side dimension measured were included in analyses as only a few characters had large asymmetric values.

4.4.3 Sex and Subspecies Differences

Testing the adult samples for sexual dimorphism and subspecies differences resulted in only one significant difference. The Shapiro-Wilk tests for normality for sex and subspecies differences yielded no p-values below the threshold of 0.05, giving no signs of deviation from unimodal distributions among the adult samples (Table 4-7). Permutation t-tests for sex differences yielded one significant p-value among the 30 tests for *R. unicornis, C. simum,* and *D.*

Table 4-6. Asymmetry Index counts for right-left dimensions in the species. Specimens are categorized as right asymmetric, left asymmetric, and symmetric, with 0.5% difference as the threshold. See Table 3-3 for measurement abbreviations.

	T. major			***R. unicornis***			***D. sumatrensis***			***C. simum***			***D. bicornis***		
Asymmetry	**Right**	**Left**	**Even**	**Right**	**Left**	**Even**	**Right**	**Left**	**Even**	**Right**	**Left**	**Even**	**Right**	**Left**	**Even**
TCL%	4	15	6	3	4	7	2	2	3	6	0	12	5	4	16
PCL%	11	14	1	8	4	2	0	5	1	4	10	5	13	8	3
MCL%	20	4	3	1	11	3	2	4	0	8	7	5	10	14	2
ACL%	16	3	4	9	4	2	3	3	1	7	12	1	10	10	6
ML%	20	5	0	2	7	5	1	3	3	9	4	7	5	11	7
RL%	18	7	1	5	6	1	3	2	1	9	6	4	10	7	6
MXPL%	13	10	3	5	7	1	5	1	0	7	7	5	8	12	5
MXML%	8	10	2	5	2	4	3	2	1	5	6	2	5	9	4
MXDL%	16	6	4	5	4	4	2	2	2	6	6	7	11	5	9
MNPL%	13	9	4	3	5	5	0	3	3	9	5	6	9	10	6
MNML%	4	14	3	5	5	1	3	0	3	3	6	4	9	6	4
MNDL%	9	11	5	4	6	4	2	3	1	5	5	10	7	5	13

Table 4-7. Shapiro-Wilk test for normality results for sex and subspecies. W-statistics and p-values are provided for sex and subspecies differences among adults in *R. unicornis*, *C. simum*, and *D. bicornis*. The significance threshold was $p < 0.05$. See Table 3-3 for abbreviations.

	R. unicornis	***C. simum***	***D. bicornis***
TCL	W: 0.9689	W: 0.8438	W: 0.9266
	p: 0.8905	p: 0.1401	p: 0.3072
PCL	W: 0.911	W: 0.9873	W: 0.9643
	p: 0.4029	p: 0.9817	p: 0.8185
MCL	W: 0.9311	W: 0.8291	W: 0.9353
	p: 0.5261	p: 0.0785	p: 0.3994
ACL	W: 0.9309	W: 0.8638	W: 0.9706
	p: 0.5244	p: 0.1637	p: 0.9011
SW	W: 0.9438	W: 0.8958	W: 0.8925
	p: 0.6484	p: 0.3061	p: 0.1056
OH	W: 0.893	W: 0.9833	W: 0.9534
	p: 0.2906	p: 0.9667	p: 0.6507
ZW	W: 0.9155	W: 0.9346	W: 0.957
	p: 0.3946	p: 0.591	p: 0.7077
ML	W: 0.9624	W: 0.8447	W: 0.9381
	p: 0.833	p: 0.1099	p: 0.4327
RL	W: 0.9505	W: 0.925	W: 0.9126
	p: 0.7165	p: 0.509	p: 0.1993
CW	W: 0.8936	W: 0.9061	W: 0.8774
	p: 0.294	p: 0.3692	p: 0.08107

Table 4-8. Permutation t-test results for sex and subspecies differences. P-values are provided for sex and subspecies differences among adults in *R. unicornis*, *C. simum*, and *D. bicornis*. The green shaded value indicates a significant p-value of < 0.05. See Table 3-4 for abbreviations.

	R. unicornis	***C. simum***	***D. bicornis***
TCL	p: 0.0286	p: 1	p: 0.6812
PCL	p: 0.108	p: 0.1027	p: 0.9696
MCL	p: 0.7605	p: 0.2033	p: 0.6855
ACL	p: 0.7605	p: 0.9336	p: 0.8822
SW	p: 0.658	p: 0.1026	p: 0.9389
OH	p: 0.6503	p: 0.1968	p: 0.3782
ZW	p: 0.3144	p: 0.1015	p: 0.9193
ML	p: 0.5532	p: 0.3064	p: 1
RL	p: 1	p: 0.7111	p: 0.4187
CW	p: 0.8975	p: 0.0972	p: 0.4282

bicornis (Table 4-8). The *R. unicornis* female sample had a significantly larger TCL than the male sample (p=0.0286). As no subspecies differences and one sex difference resulted from all tests, the inclusion of all ages and subspecies in the allometry sample was done with confidence.

4.4.4 Functional Characters

The Kruskal-Wallis tests for equality of medians in seven functional characters resulted in significant H-statistics for each test (Table 4-9). All species comparisons for functional characters had several significant Bonferroni-corrected p-values < 0.05. Each character's test results are discussed in detail below (Table 4-10 and the sample statistics are provided in Appendix 6. Rankings and groupings of the species for each character are based on test results and sample statistics.

Posterior Cranial Length

The PCL analysis resulted in several significant p-values among species, placing the species into two groups: *R. unicornis*, *D. sumatrensis*, and *D. bicornis* in Group 1, and *T. major* and *C. simum* in Group 2. Most pairwise comparisons of a Group 1 species with a Group 2 species were significant (<0.05). Within group comparisons yielded no p-values close to the significance level. *Dicerorhinus sumatrensis* was not significantly different from any species, but based on nearly significant p-values and sample statistics, it was placed in Group 2.

Occipital Height

The OH analysis resulted in several significant differences among species, with *R. unicornis* differentiating from all species with significant p–values except for *D. sumatrensis*. Another significant p-value (0.04619) resulted between *C. simum* and *D. bicornis*. Similar to PCL, *D. sumatrensis* was not significantly different from any species in OH. Based on sample

statistics, the species ranked into three groups: Group 1 with *T. major* and *C. simum*; Group 2 with *D. bicornis* and *D. sumatrensis*; and Group 3 with *R. unicornis*.

Ramus Length

The RL analysis resulted in two *D. bicornis* comparisons with significant p-values: *T. major* (0.00085) and *R. unicornis* (0.00932). Based on test results and sample statistics, the species ranked into three groups: Group 1 with *T. major* and *R. unicornis*; Group 2 with *C. simum* and *D. sumatrensis*; and Group 3 with *D. bicornis.*

Premolar Row Length to Molar Row Length

The MXPL to MXML and MNPL to MNML analyses indicated that *T. major* was significantly different from all the extant rhinos. Of the eight comparisons between *T. major* and the extant rhinos, seven p-values were significant. Further, of the 12 comparisons among the extant rhinos, only one p-value was significant, which was between *R. unicornis* and *C. simum* for the mandible (p=0.03569). Based on the test results and sample statistics, the species were placed into two groups: Group 1 with *T. major*; and Group 2 with *D. sumatrensis*, *D. bicornis, C. simum,* and *R. unicornis*.

Premaxilla Width to Palate Width

The DW to MXPPW analysis resulted in four of ten comparisons with significant p-values. Three of the significant p-values were from comparisons between *T. major* and *R. unicornis*, *D. sumatrensis,* and *C. simum*. The only other comparison with a significant p-value was between *C. simum* and *D. bicornis.* The rankings and groupings of this character are: Group 1 with *C. simum, D. sumatrensis,* and *R. unicornis*, Group 2 with *T. major* and *D. bicornis*.

Anterior Premolar Width to Palate Width

The MXAPW to MXPPW analysis resulted in two *T. major* comparisons with significant p-values: *D. sumatrensis* (0.03495) and *C. simum* (0.02988). Based on test results and sample statistics, the rankings and groupings of this character are: Group 1 with *C. simum* and *D. sumatrensis*, and Group 2 with *R. unicornis*, *T. major*, and *D. bicornis*.

Table 4-9. Kruskal-Wallis test results for functional character differences among species. H-statistics and p-values are provided for differences among functional characters. With a threshold of < 0.05, all seven tests indicated significant differences.

PCL	H: 25.86 p: 0.0000337
OH	H: 25.4 p: 0.00004185
RL	H: 18.1 p: 0.00118
MXPL/ MXML	H: 23.48 p: 0.0001014
MNPL/ MNML	H: 31.42 p: 0.000002513
DW/ MXPPW	H: 24.62 p: 0.00005987
MXAPW/ MXPPW	H: 16.25 p: 0.002701

4.4.5 Cranial Allometry

In the cranial variable set, each species' PCA had over 91% of the variation explained by the first principal component, while the second component varied between 0.7-6.2% (Appendix 7). Although the second component explained some of the variance, the Joliffe cut-off value indicated that only the first principal component was significant in each species' PCA.

The five species all had positive variable loadings on the first component, but the loadings were not equal, having both high and low positive scores (Appendix 8). The specimen

Table 4-10. Kruskal-Wallis test results for pairwise comparisons of functional characters. Bonferroni-corrected p-values are provided, with shaded values indicating significance (< 0.05).

PCL	*T. major*	*R. unicornis*	*D. sumatrensis*	*C. simum*
T. major				
R. unicornis	0.02988			
D. sumatrensis	0.06768	0.21860		
C. simum	1	0.00939	0.08475	
D. bicornis	0.01406	1	0.16870	0.04619

OH	*T. major*	*R. unicornis*	*D. sumatrensis*	*C. simum*
T. major				
R. unicornis	0.00152			
D. sumatrensis	1	0.1379		
C. simum	1	0.00939	0.74530	
D. bicornis	1	0.00152	1	0.04619

RL	*T. major*	*R. unicornis*	*D. sumatrensis*	*C. simum*
T. major				
R. unicornis	1			
D. sumatrensis	1	1		
C. simum	1	1	1	
D. bicornis	0.00085	0.00932	1	0.44070

MXPL/MXML	*T. major*	*R. unicornis*	*D. sumatrensis*	*C. simum*
T. major				
R. unicornis	0.00372			
D. sumatrensis	0.29470	1		
C. simum	0.00597	1	1	
D. bicornis	0.00440	0.47220	1	1

MNPL/MNML	*T. major*	*R. unicornis*	*D. sumatrensis*	*C. simum*
T. major				
R. unicornis	0.00372			
D. sumatrensis	0.04889	1		
C. simum	0.00082	0.03569	1	
D. bicornis	0.00039	1	1	0.21490

DW/MXPPW	*T. major*	*R. unicornis*	*D. sumatrensis*	*C. simum*
T. major				
R. unicornis	0.00248			
D. sumatrensis	0.04375	1		
C. simum	0.06019	1	1	
D. bicornis	0.25110	0.09218	0.10730	0.04938

Table continued

MXAPW/MXPPW	*T. major*	*R. unicornis*	*D. sumatrensis*	*C. simum*
T. major				
R. unicornis	0.63120			
D. sumatrensis	0.03495	0.37240		
C. simum	0.02988	0.60601	1	
D. bicornis	1	0.63121	0.79732	0.26540

plots on the first component also indicate that the specimens were distributed according to overall size (Figure 4-7). As explained by Shea (1985), positive but unequal first component variable loadings and specimen distribution according to size together indicate that the first component reflects growth allometry, not just size. Further, calculated allometric coefficients from the variable loading ratios yielded positive allometric, negative allometric, and isometric variables for each species, another sign that the cranial PCA summarized each species' growth allometry (Table 4-11).

The cranial PCA resulted in allometric coefficient groupings among the species. For example, *C. simum* and *T. major* had nearly isometric growth for TCL and MCL, while *R. unicornis, D. bicornis,* and *D. sumatrensis* had negative allometric coefficients. Conversely, *D. bicornis, R. unicornis,* and *D. sumatrensis* all had strong positive allometric scores for OH, while *C. simum* and *T. major* had strong negative allometric scores.

Two variables, PCL and ZW, had noticeable groupings of coefficients. For PCL, *T. major*, *D. bicornis,* and *R. unicornis* had strong negative allometric scores, while *C. simum* and *D. sumatrensis* had slight negative allometric scores. For ZW, *D. sumatrensis* and *T. major* had isometric scores, *R. unicornis* had a slight negative allometric score, and *C. simum* and *D. bicornis* had strong negative allometric scores.

The variables ACL and SW had a three species grouping and two species with isolated scores. For ACL, *T. major* had a strong positive allometric score, *C. simum, D. sumatrensis,* and

R. unicornis had slight positive allometric scores, and *D. bicornis* had a slight negative allometric score. For SW, *C. simum* had a positive allometric score, *D. bicornis*, *T. major*, and *R. unicornis* had near isometric scores, and *D. sumatrensis* had a negative allometric score.

4.4.6 Mandibular and Dental Allometry

In the mandibular and dental variable set, each species' PCA had over 88% of the variation explained by the first principal component, while the second component varied between 2.8-7.4% (Appendix 9). Like the cranial variable set, the Joliffe cut-off value indicated that only the first principal component was significant.

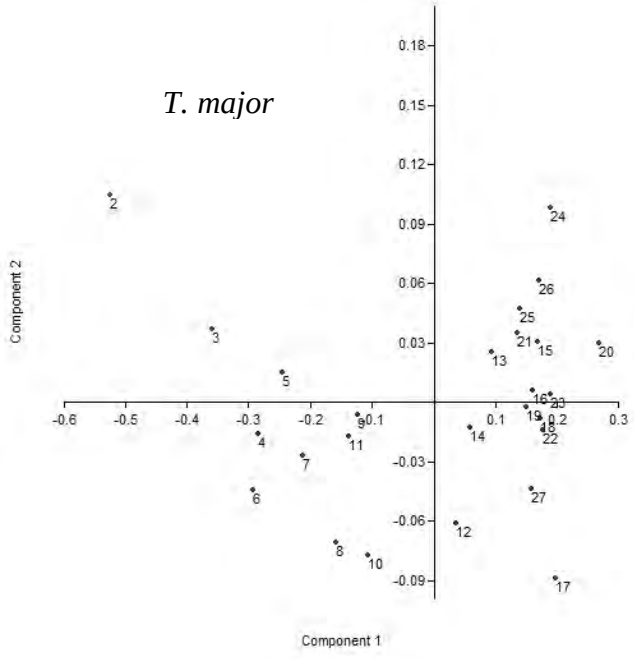

Figure 4-7a. Cranial PCA specimen plots of PC1-PC2 for *T. major*. Specimen numbers increase with Age Class along PC1, a sign that PC1 distributes specimens according to overall size and that growth allometry is reflected. Clustered specimens on PC1 are specimens of similar size.

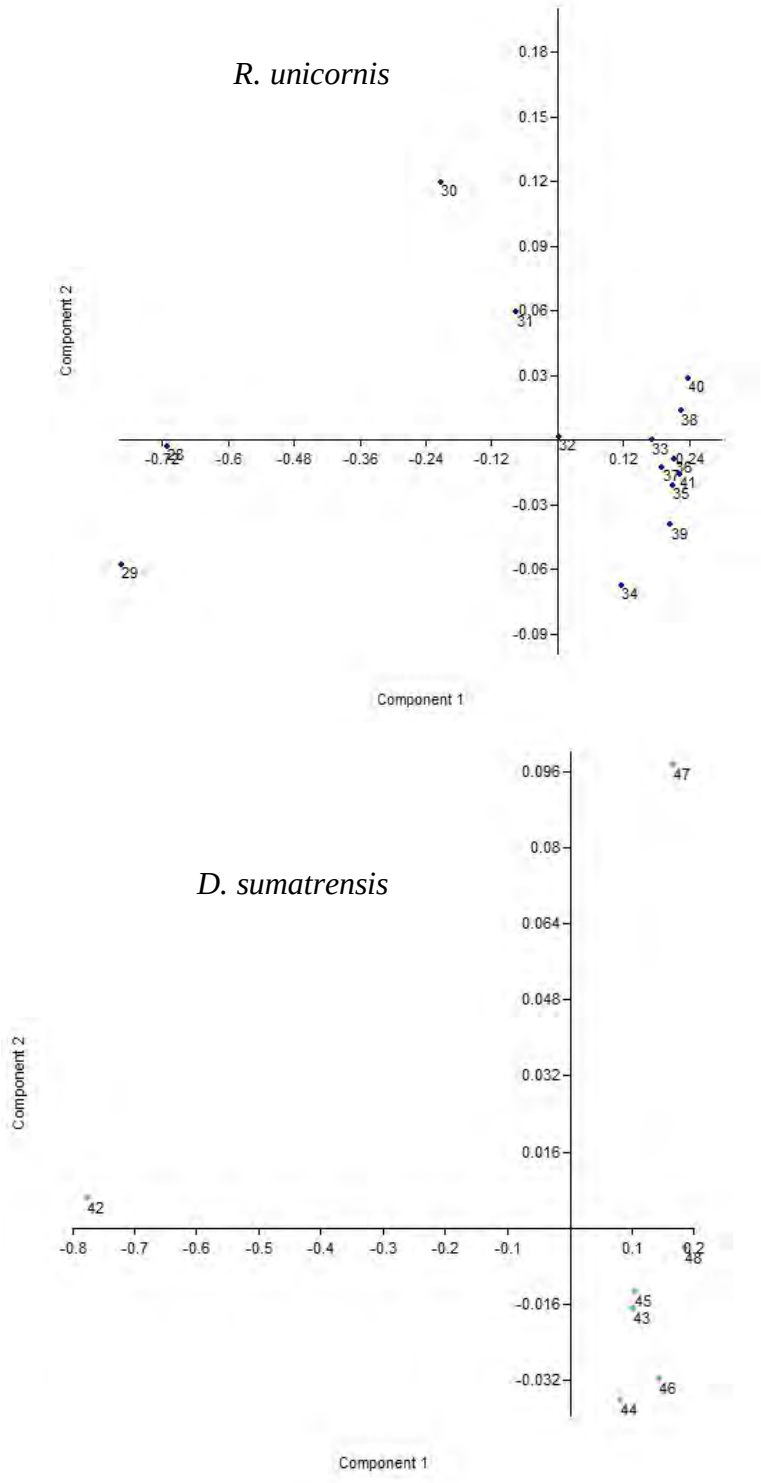

Figure 4-7b. Cranial PCA specimen plots of PC1-PC2 for *R. unicornis* and *D. sumatrensis*. Specimen numbers increase with Age Class along PC1, a sign that PC1 distributes specimens according to overall size and that growth allometry is reflected. Clustered specimens on PC1 are adult specimens of similar size.

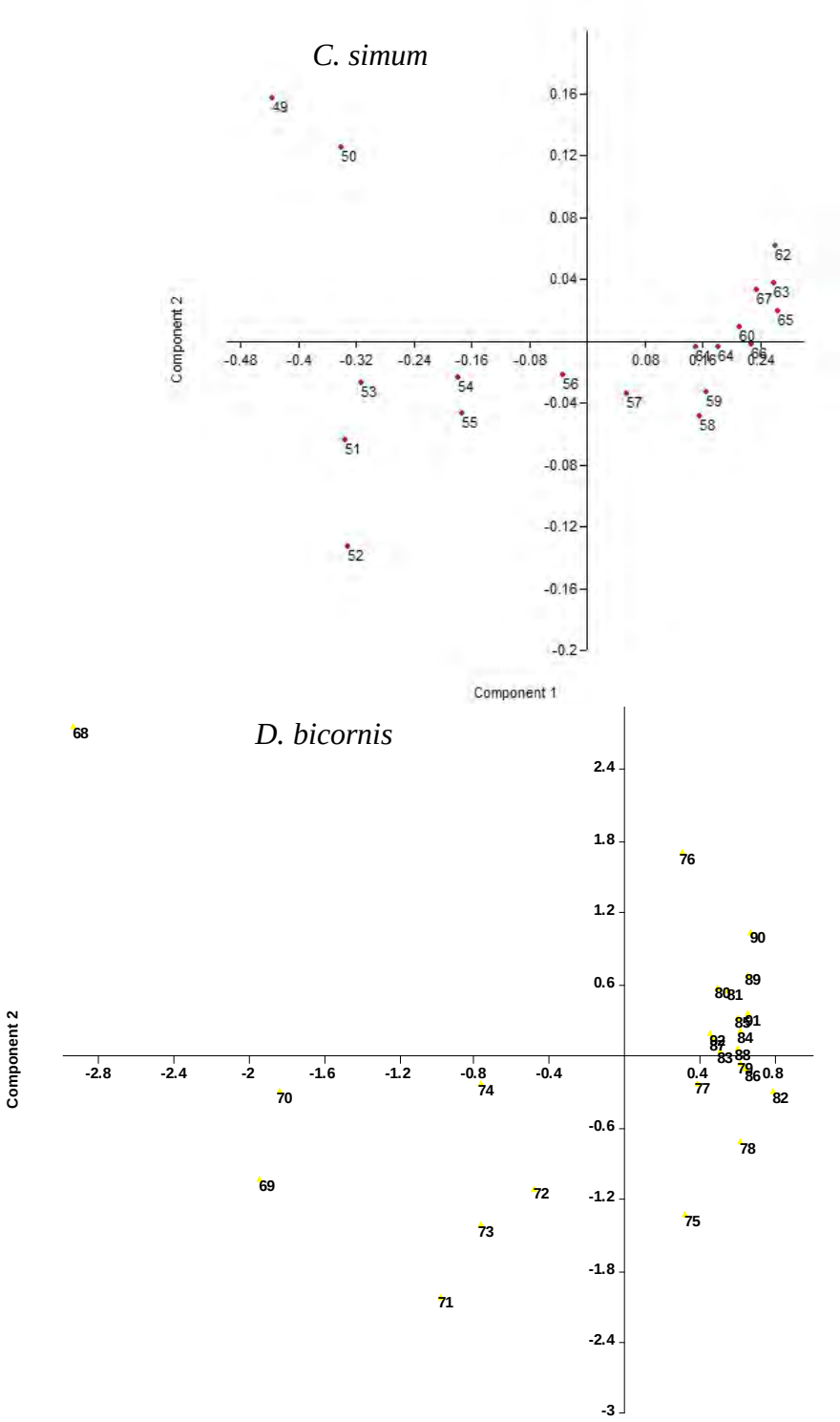

Figure 4-7c. Cranial PCA specimen plots of PC1-PC2 for *C. simum* and *D. bicornis*. Specimen numbers increase with Age Class along PC1, a sign that PC1 distributes specimens according to overall size and that growth allometry is reflected. Clustered specimens on PC1 are adult specimens of similar size.

Table 4-11. Allometric coefficients PCA cranial dimensions.

	T. major	*R. unicornis*	*D. sumatrensis*	*C. simum*	*D. bicornis*
TCL	0.9988	0.9281	0.8694	1.0410	0.8916
PCL	0.7821	0.8212	0.9155	0.9117	0.8118
MCL	1.0190	0.9378	0.9175	1.0260	0.9291
ACL	1.3980	1.0940	1.1520	1.1740	0.9486
SW	0.9775	0.9695	0.9293	1.1120	0.9825
OH	0.8175	1.3160	1.1830	0.8608	1.5650
ZW	1.0070	0.9335	1.0340	0.8740	0.8710

Four of the species, *D. sumatrensis* excluded, had positive variable loadings on the first component, and the loadings were unequal, having both high and low positive scores (Appendix 8). Positive and negative variable loadings for *D. sumatrensis* indicate that the first component did not reflect growth allometry like in the other four species, and consequently, mandibular and dental allometry were not discussed for *D. sumatrensis*. Specimen plots on the first component also indicate that the specimens were distributed according to overall size (Figure 4-8).

Most of the allometric coefficients were similar across all species with only slight differences (Table 4-12). For ML, all the species' allometric coefficients were isometric, and all the MXDL coefficients were positive. MNDL had strong positive allometric coefficients for all species except *D. bicornis*, which had isometric coefficients.

Three variables, MNPPW, RL, and CW, had negative allometric coefficients for all species. For MNPPW, *R. unicornis* had a significantly lower coefficient than other species. For RL, *D. bicornis* had a significantly higher score than *T. major* and *C. simum*. The very low coefficient of *R. unicornis* for RL was probably strongly affected by a lack of young specimens, so it is not regarded as accurate. For CW, *C. simum* had the highest score while *D. bicornis* had the lowest score; *T. major* and *R. unicornis* had intermediate scores.

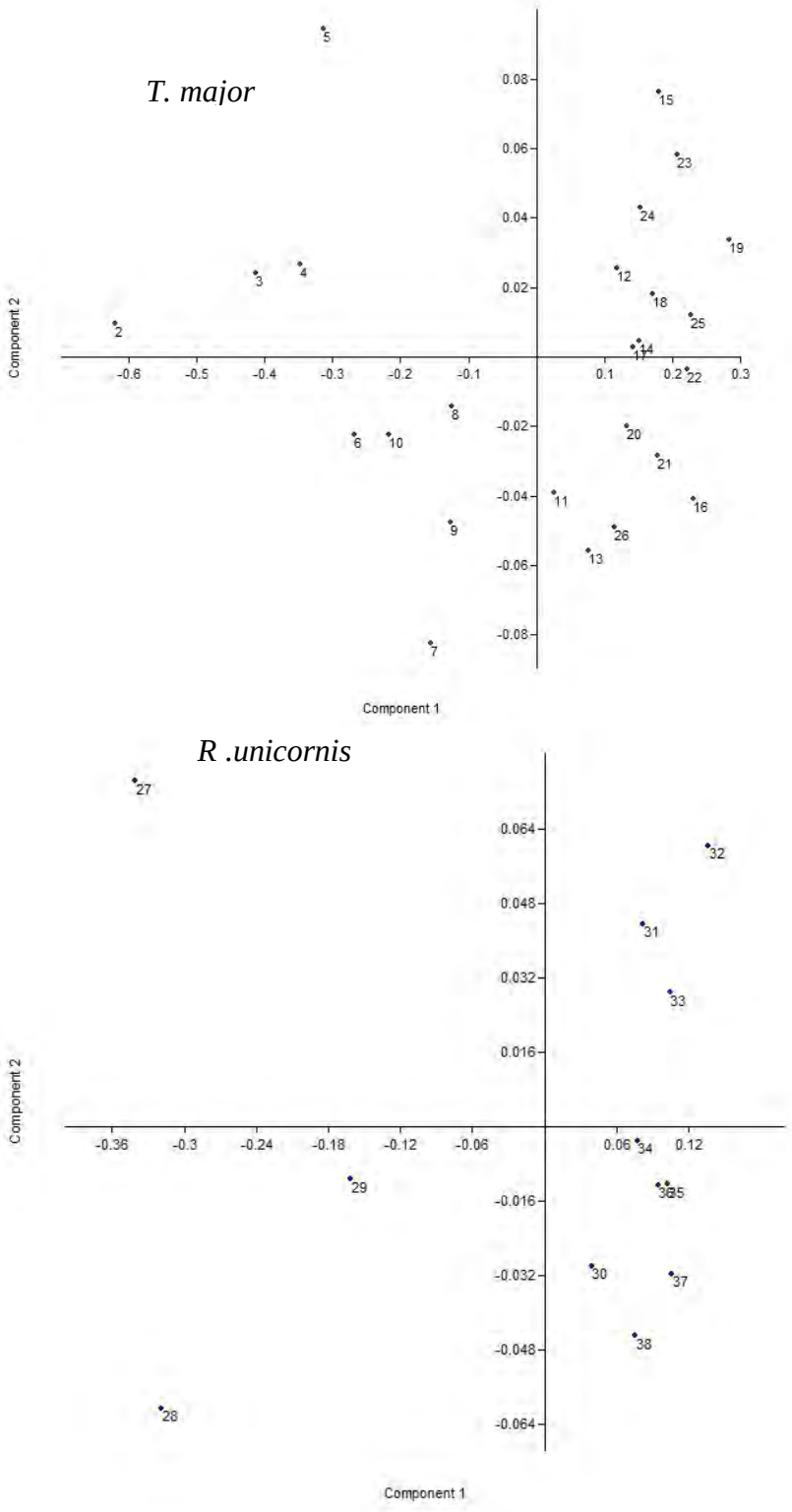

Figure 4-8a. Mandibular and dental PCA plots of PC1-PC2 for *T. major* and *R. unicornis*. Specimen numbers increase with Age Class along PC1, a sign that PC1 distributes specimens according to overall size and that growth allometry is reflected. Clustered specimens on PC1 are adult specimens of similar size.

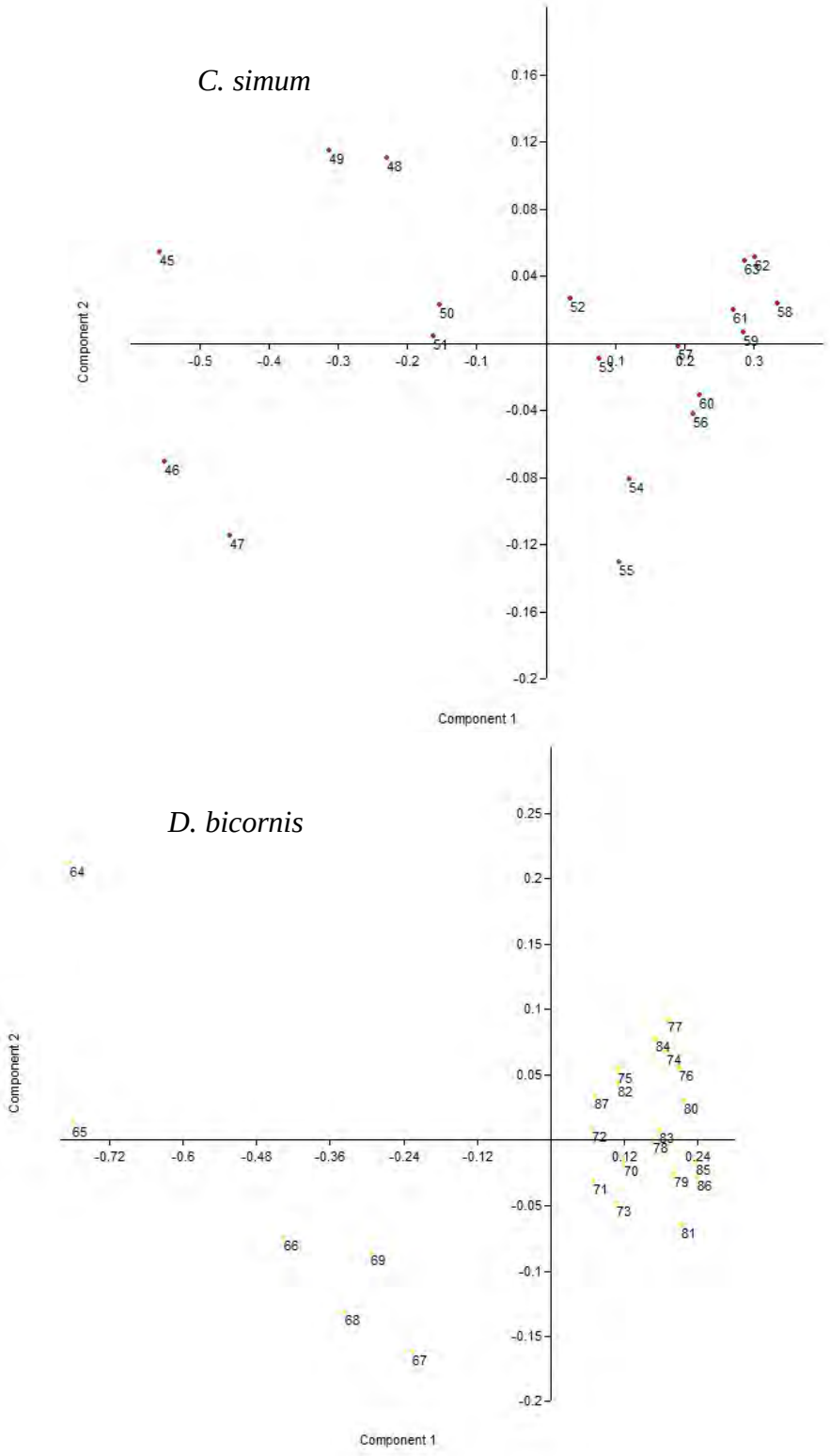

Figure 4-8b. Mandibular and dental PCA plots of PC1-PC2 for *C. simum* and *D. bicornis*. Specimen numbers increase with Age Class along PC1, a sign that PC1 distributes specimens according to overall size and that growth allometry is reflected.

One variable, MNAPW, had the most variation in allometric coefficients across species. *Diceros bicornis* had a strong positive coefficient, *R. unicornis* and *T. major* had isometric coefficients, and *C. simum* had a strong negative coefficient.

Table 4-12. Allometric coefficients for PCA mandibular and dental dimensions. Green shaded values indicate allometries removed from analysis. See Table 3-3 for abbreviations.

	T. major	***R. unicornis***	***D. sumatrensis***	***C. simum***	***D. bicornis***
ML	0.9910	1.0020	-0.2310	0.9790	1.0140
RL	0.4986	0.1105	-7.3620	0.4218	0.8705
CW	0.8018	0.8415	0.6516	0.9234	0.7259
MXDL	1.4650	1.7050	5.5090	1.6860	1.3580
MNDL	1.4920	1.8480	5.7910	1.7220	1.0680
MNAPW	1.0230	1.0330	1.4700	0.5113	1.3110
MNPPW	0.7289	0.4593	1.1710	0.7565	0.6528

4.5 GEOMETRIC MORPHOMETRICS

4.5.1 Principal Component Analysis

Teleoceras major

The PCA for *T. major* resulted in 11 components that explained the total variance within the sample. The first three components each explained over 10% of the variance, and together they accounted for 68.6% (Appendix 10). PC1, which explained 42.0% of the variance, summarized the most fundamental shape differences within the ontogenetic sample. The wireframe outline for *T. major* indicates that four characters had the most ontogenetic variation: occipital slope angle, zygomatic arch length and height, nasal length and height, and mandibular angle curvature (Figure 4-9a).

PC2, which explained 14.5% of the variance, displayed large-scale vertical variance in both the cranium and mandible. In the cranium, the occipital, parietal, and facial regions all varied in vertical depth. In the mandible, the body and ramus varied in vertical depth, and

mandibular angle curvature also showed variation. PC3, which explained 11.9% of the variance, had only two characters with slight local variances: zygomatic arch anterior-posterior extension and infraorbital foramen ventral displacement.

Rhinoceros unicornis

The PCA for *R. unicornis* resulted in two out of 10 significant components, with PC1 and PC2 explaining 50.4% and 21.8% of the variance, respectively. PC1 displayed significant variances in four characters: occipital slope angle, zygomatic arch height, mandibular angle curvature, and nasal height and length. PC2 summarized variation in two areas: occipital extension posteriorly and mandibular angle and body extension anteriorly.

Dicerorhinus sumatrensis

The PCA for *D. sumatrensis* resulted in five total components, with the first four components each explaining over 10% of the variance and accounting for 94.7% in total. PC1, which explained 53.3% of the variance, displayed shape variation in three characters: occipital angle slope, mandibular angle curvature, and nasal length. PC2, which explained 20.6%, primarily summarized global cranial variation. The occiput, zygomatic arch, and maxilla all demonstrated anterior-posterior extension; occipital dorsal-ventral extension was also present.

PC3 and PC4, which explained 10.6% and 10.1% of the variance, respectively, displayed relatively little shape variation. PC3 summarized some variation in mandibular body depth. PC 4 displayed global anterior-posterior variation in the zygomatic arch and facial region, similar to PC2 shape variation.

Ceratotherium simum

The PCA for *C. simum* resulted in 10 total components, with the first three components each explaining over 10% of the variance and accounting for 75.8% in total. PC1, which

explained 48.5% of the variance, depicted shape variation in two characters: nasal extension, and anterior-posterior and dorsal-ventral occipital extension. PC2, explaining 17.2%, summarized variance in zygomatic arch height and length, and mandibular angle curvature. PC3, which explained 10.0%, described further variation in zygomatic arch height and nasal length and height, as well as mandibular body depth.

Diceros bicornis

The PCA for *D. bicornis* resulted in 11 total components, with the first four components each explaining over 10% of the variance and accounting for 81.7% in total. PC1 explained 34.0% of the variance, and displayed shape variation in four characters: occipital angle slope, zygomatic arch length and height, mandibular angle curvature, and nasal length. PC2, which explained 24.2%, summarized vertical variations in mandibular body depth and nasal height.

PC3, explaining 13.2% of the variance, demonstrated shape variation in frontal depth, occipital extension posteriorly and dorsally, and mandibular extension posteriorly. In PC4, which explained 10.2%, frontal depth was the only character with noticeable variance.

4.5.2 Canonical Variate Analysis

The CVA produced four canonical variates that explained 100% of the total variation among the five species (Table 4-13). The first three variates explained at least 10% of the variance each, and the fourth variate explained almost 5%. CV specimen score plots of the six variate-combinations indicate that CV1 and CV2 were significant species discriminators, while CV3 and CV4 weakly discriminated the species (Figure 4-10). Although some species were grouped together, no specimens were misclassified into different species for all CVs.

Canonical variate 1 (CV1), which explained 62.8% of the variance, separated all species except for *D. sumatrensis* and *D. bicornis*, which were grouped together. The wireframe outline

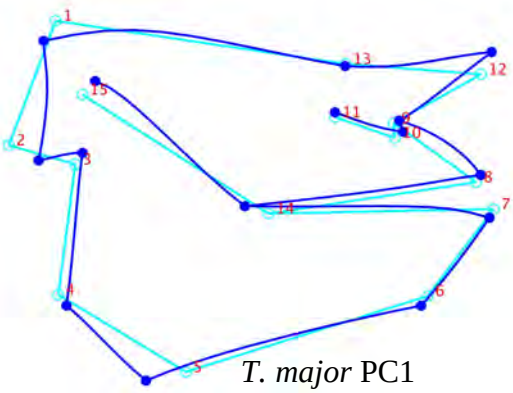

T. major PC1

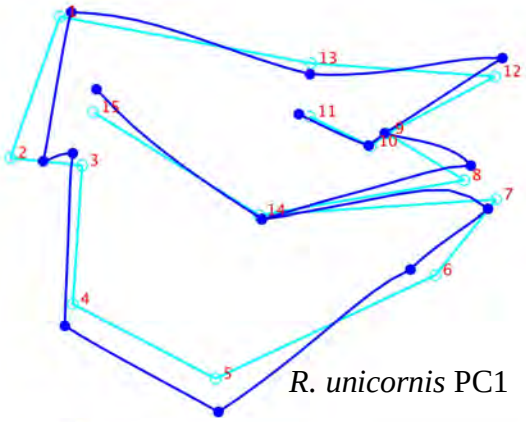

R. unicornis PC1

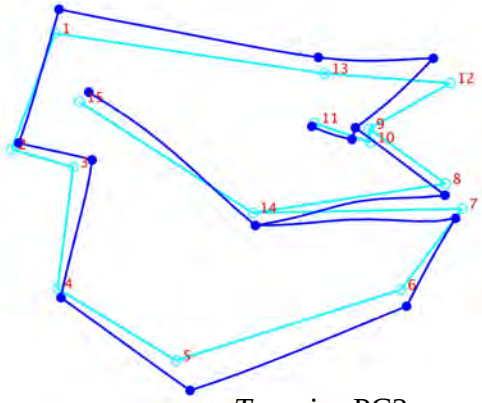

T. major PC2

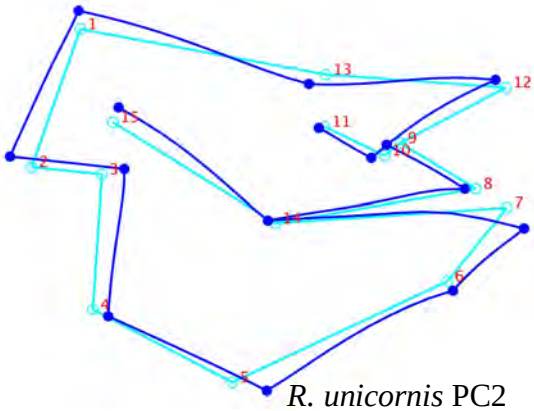

R. unicornis PC2

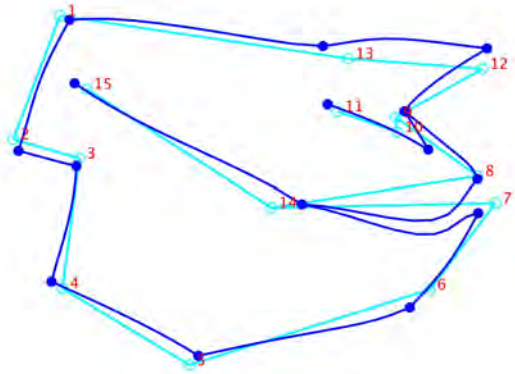

T. major PC3

Figure 4-9a. PCA shape transformations for *T. major* and *R. unicornis*. Shape transformations are summarized by significant PCs in each species. Numbers refer landmarks. The light blue outline signifies the mean shape for the sample. The dark blue line signifies the shape summarized by the PC.

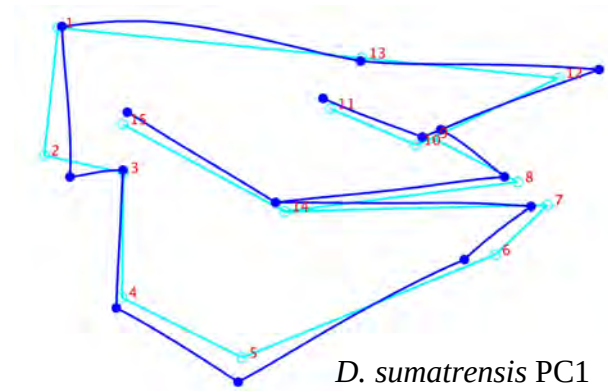

D. sumatrensis PC1

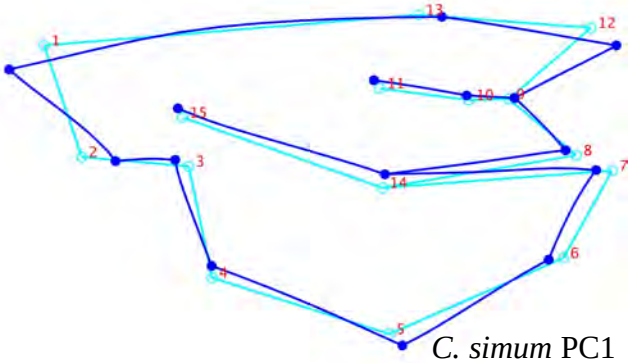

C. simum PC1

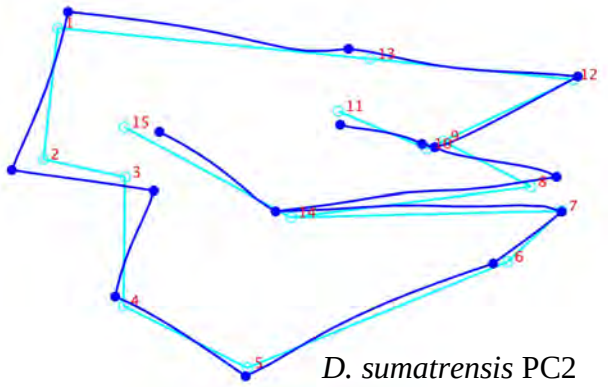

D. sumatrensis PC2

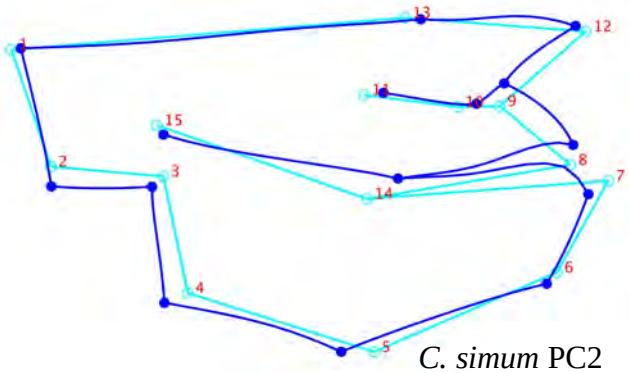

C. simum PC2

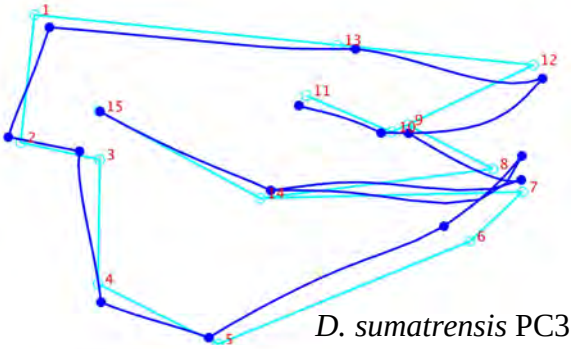

D. sumatrensis PC3

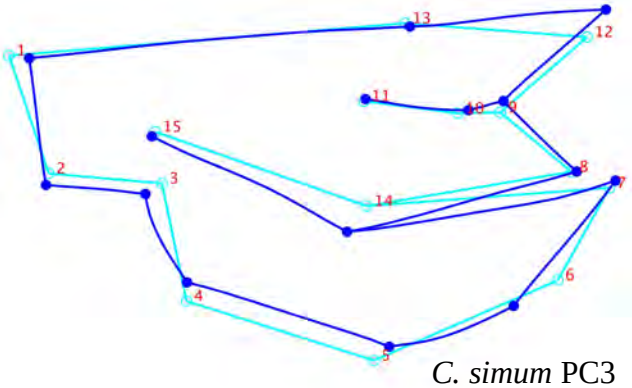

C. simum PC3

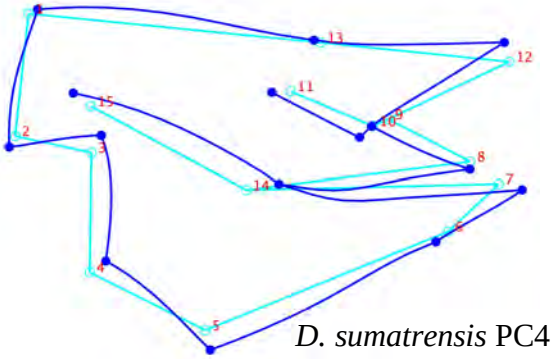

D. sumatrensis PC4

Figure 4-9b. PCA shape transformations for *D. sumatrensis* and *C. simum*. Numbers refer landmarks. The light blue outline signifies the mean shape for the sample. The dark blue line signifies the shape summarized by the PC.

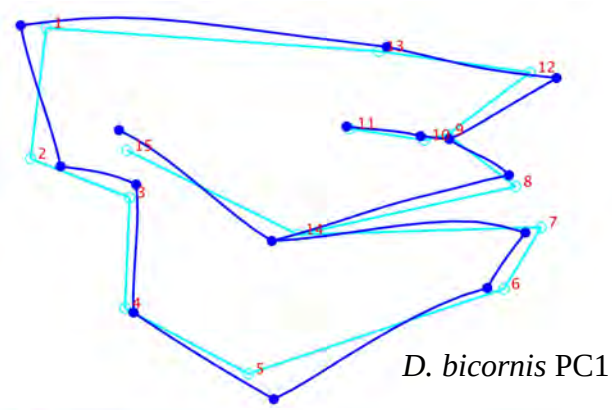

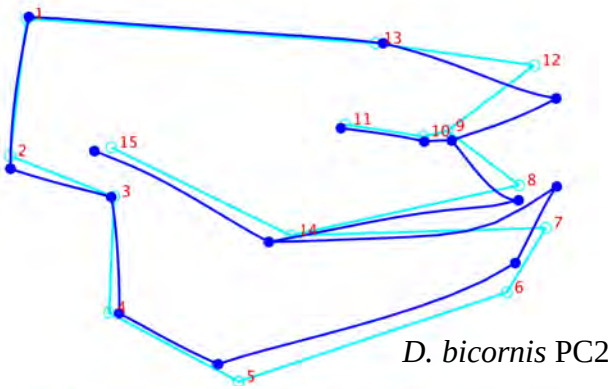

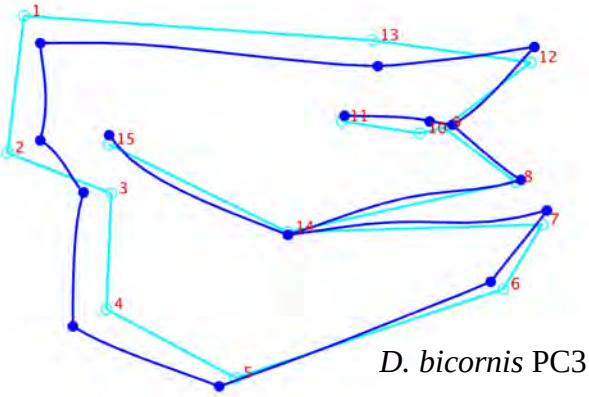

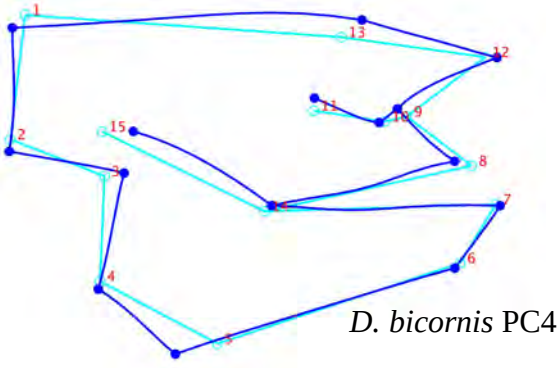

Figure 4-9c. PCA shape transformations for *D. bicornis*. Numbers refer landmarks. The light blue outline signifies the mean shape for the sample. The dark blue line signifies the shape summarized by the PC.

of the Procrustes coordinates for CV1 depicted four distinct shape differences for strong positive scores on CV1: occiput orientation, mandibular angle size, facial length and nasal depth (Figure 4-11). Based on the specimen scores, these characters were shown to be present in the ontogenetic samples of *T. major* and *R. unicornis*, while the opposite characters were present in *C. simum, D. bicornis*, and *D. sumatrensis*.

Canonical variate 2 (CV2), which explained 21.4% of the variance, separated the species into three groups. Three shape differences described strong positive scores for CV2 based on the wireframe graph: mandibular body depth, occiput height, and anterior jugal length. These characters were shown to be present in *D. sumatrensis*, *R. unicornis*, and *D. bicornis*, while the opposite characters were present in *C. simum* and *T. major*.

Canonical variate 3 (CV3) explained 10.7% of the variance and separated the species into three groups that formed a continuum of CV scores. Three shape differences distinguished the three groups of species: zygomatic arch length, anterior extension of the masseteric attachment band, and mandibular condyle height. These characters were shown to be present in *R. unicornis* and *C. simum*, while the opposite characters were present in *D. bicornis* and *D. sumatrensis*.

Canonical variate 4 (CV4), which explained 4.9% of the variance, only slightly separated *D. sumatrensis* from the other species. Both *D. bicornis* and *R. unicornis* grouped together with strong positive scores, *C. simum* and *T. major* grouped together with neutral scores, and *D. sumatrensis* had strong negative scores. The only shape difference described by CV4 was medial and posterior cranial depth, which was shown to be present in *D. bicornis* and *R. unicornis*, and the opposite condition was present in *D. sumatrensis*.

4.5.3 Thin-Plate Splines

Teleoceras major

Local expansion (green) and contraction (purple) factors for the *T. major* sample indicate changes in primary growth centers in ontogeny (Figure 4-12). With an Age Class 2 specimen as the reference, large expansion factors in Age Classes 4-5 were located in the anterior facial and nasal regions, specifically around the orbit and nasal incision. The mandibular ramus and zygomatic arch had strong expansion factors in Age Classes 4-5. Large contraction areas in Age Classes 4-5 were located along the anterior mandible and posterior occiput.

Table 4-13. Eigenvalues and % variance of each CV for the grouped species CVA.

CV	Eigenvalue	% Variance	Cumulative %
1	79.12922686	62.825	62.825
2	26.99395954	21.432	84.258
3	13.56330317	10.769	95.026
4	6.26442722	4.974	100

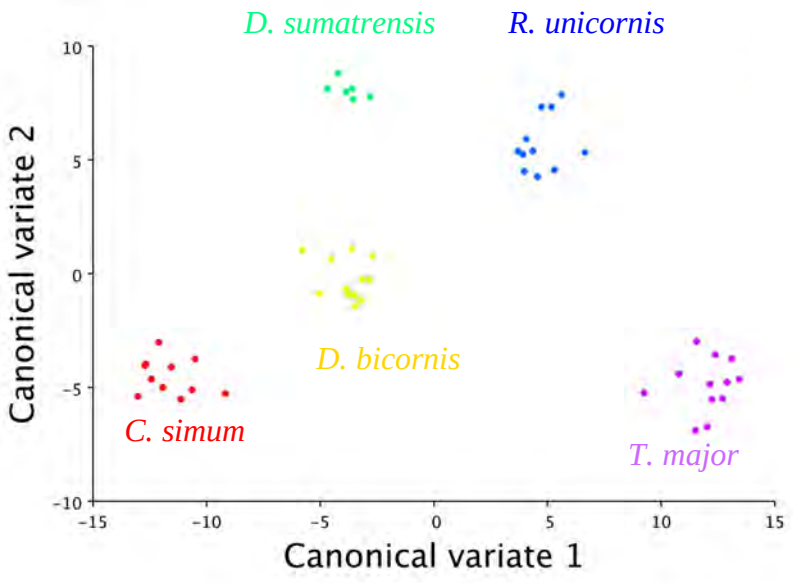

Figure 4-10a. Specimen plots for comparisons with CV1-2. CV1-2 accurately discriminate the species, as the species are separated. Species with similar scores for a CV have similar ontogenetic morphological changes for the traits characterized by that CV (Figure 4-11).

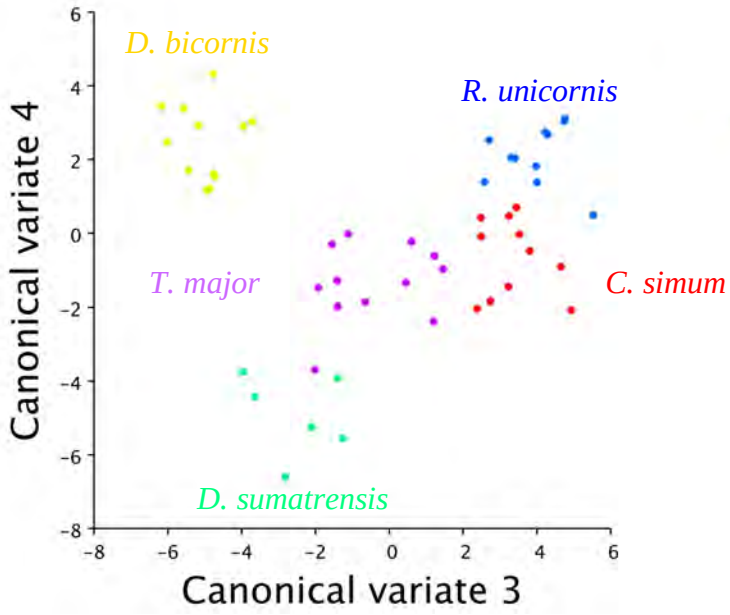

Figure 4-10b. Specimen plots for comparisons with CV3-4. CV3-4 do not accurately discriminate species, as the species are overlapping. Species with similar scores for a CV have similar ontogenetic morphological changes for the traits characterized by that CV (Figure 4-11).

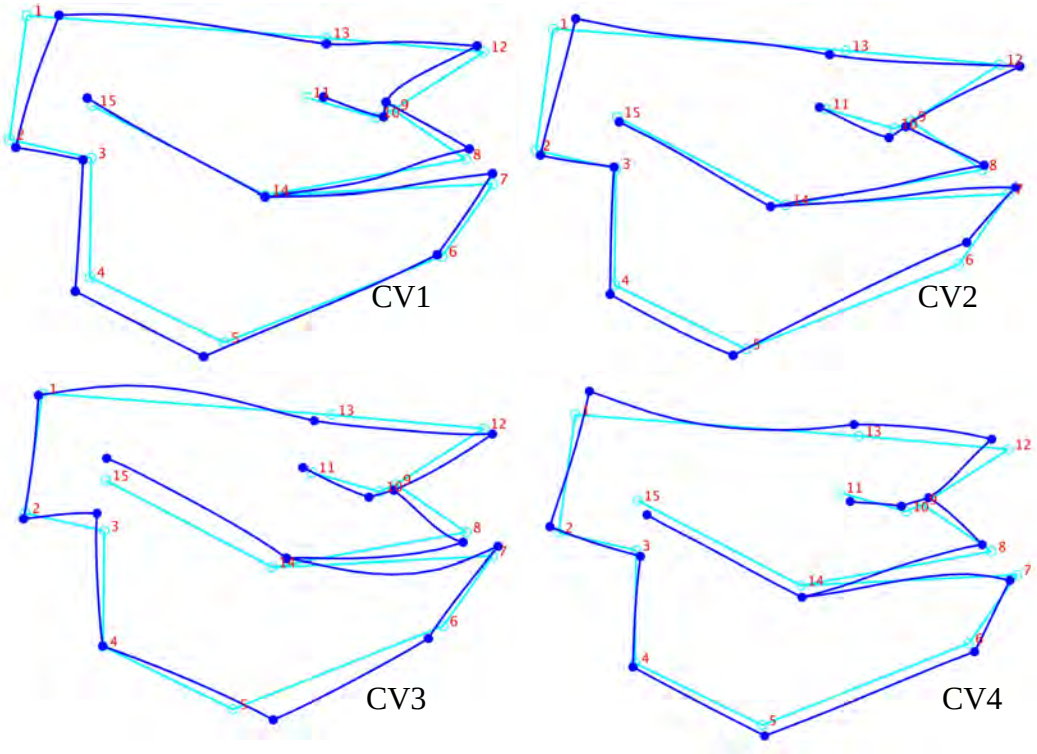

Figure 4-11. Shape transformations summarized by CVs in the grouped species CVA. Numbers refer landmarks. The light blue outline signifies the mean shape for the sample. The dark blue line signifies the shape summarized by the CV. Species with similar scores on a CV (Figure 4-10) have similar ontogenetic morphological changes depicted here.

Similar expansion and contraction factors were present in Age Class 8, but beginning in Age Class 9, the mandibular body and ventral maxilla both had strong expansion factors. Age Classes 10-12 showed strong expansions of the mandibular body and nasal-frontal regions, with strong contractions in the occiput and posterior mandible. The anterior facial region retained strong expansion factors through Age Classes 4-12.

Rhinoceros unicornis

The *R. unicornis* sample displayed relatively consistent expansion (green) and contraction (purple) factors through ontogeny (Figure 4-13). Using an Age Class 1 specimen as the reference, expansion factors in Age Classes 3-5 were located along the mandibular angle and the anterior mandible and nasals. Strong contraction areas in Age Classes 3-5 were located at the nasal incision and across the braincase between the orbit and posterior zygomatic arch. In Age Class 6, the mandibular ramus had a stronger expansion factor, while the anterior mandible and nasals retained similar expansion factors. The contraction factor of the occiput was stronger in Age Class 6, but also more localized posteriorly.

The expansion factors of Age Classes 3-6 remained similar through Age Classes 8-13, with the mandibular ramus continuing to expand strongly. In Age Class 8, a stronger contraction factor was present in the frontal region between the orbit and nasal-frontal suture. Both the posterior occiput and frontal region retained strong contraction factors from Age Classes 8-13.

Dicerorhinus sumatrensis

The incomplete *D. sumatrensis* sample displayed consistent expansion (green) and contraction (purple) factors in ontogeny (Figure 4-14). With an Age Class 2 specimen as the reference, strong expansion factors were present in three regions in Age Classes 7-8: the mandibular ramus, the anterior mandible, and the anterior facial region between the orbit and

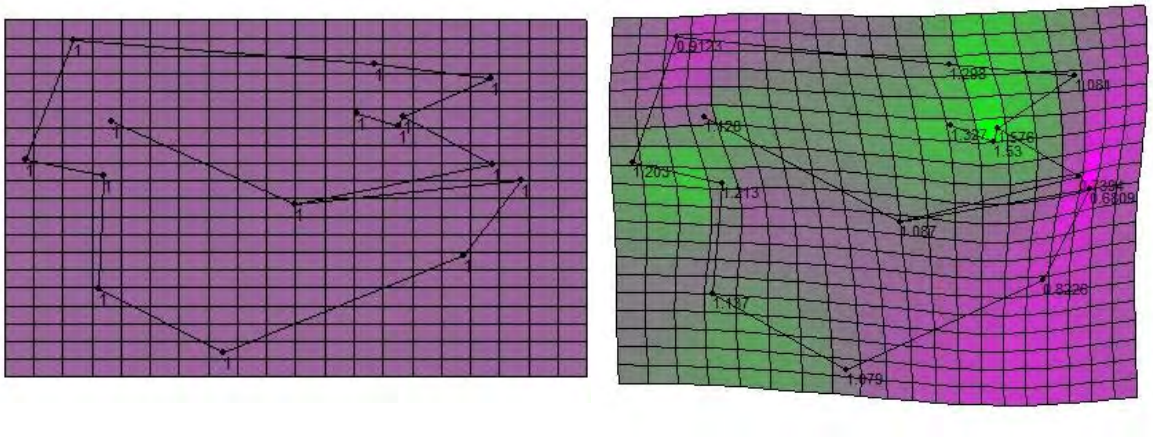

Age Class 2 (source configuration) Age Class 4

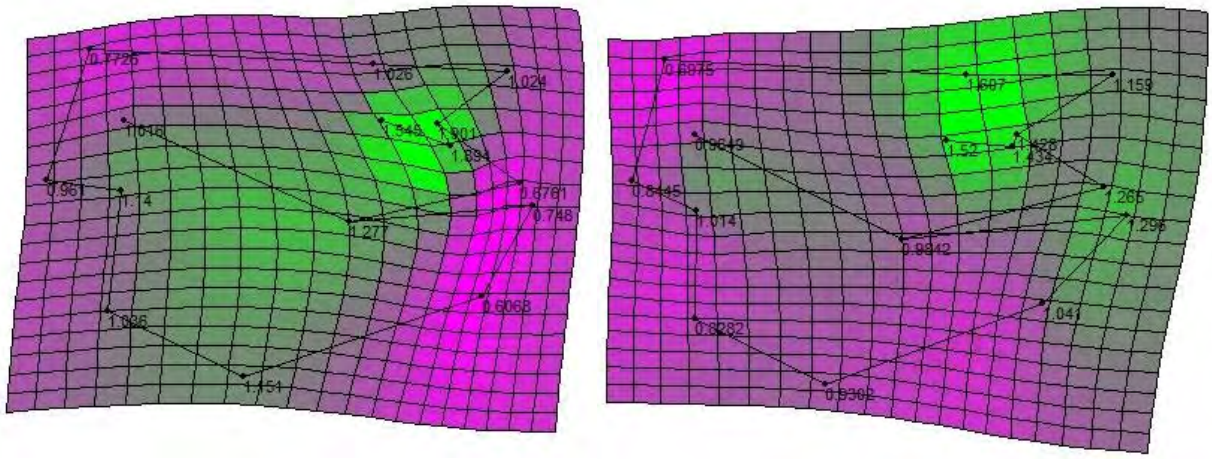

Age Class 5 Age Class 8

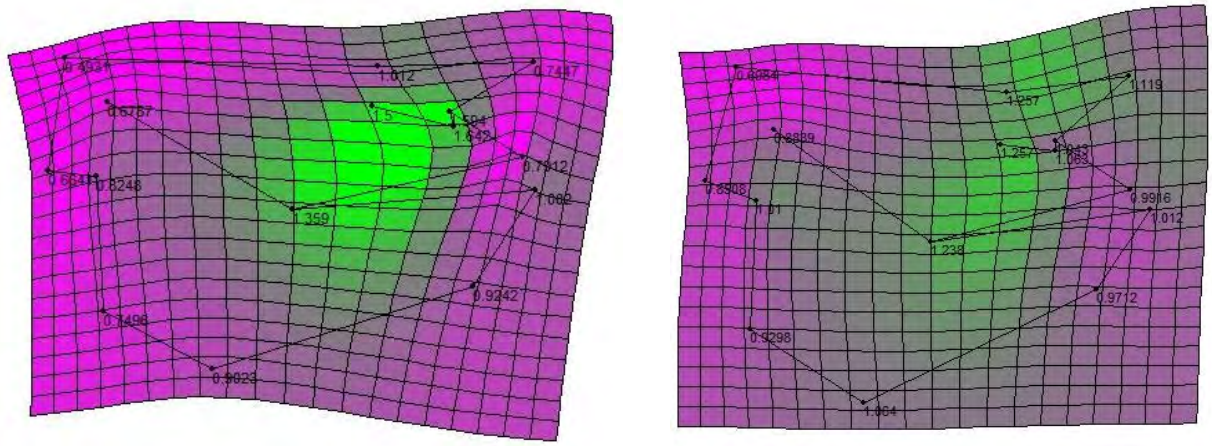

Age Class 10 Age Class 12

Figure 4-12. Thin-plate splines depicting shape transformations in *T. major*. Green areas indicate centers of expansion and purple areas indicate centers of contraction. Bright areas represent stronger expansion/contraction than dark areas.

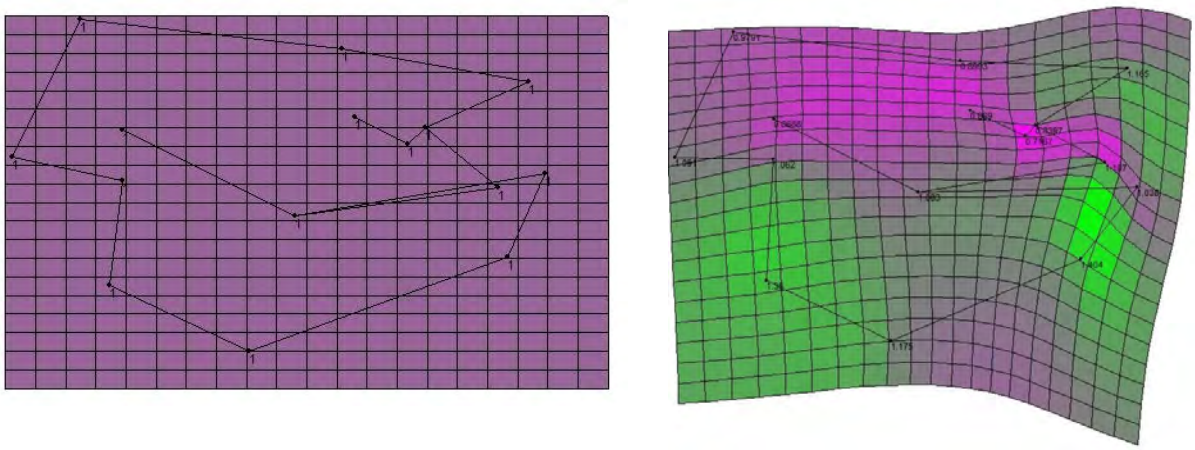

Age Class 1 (source configuration) Age Class 3

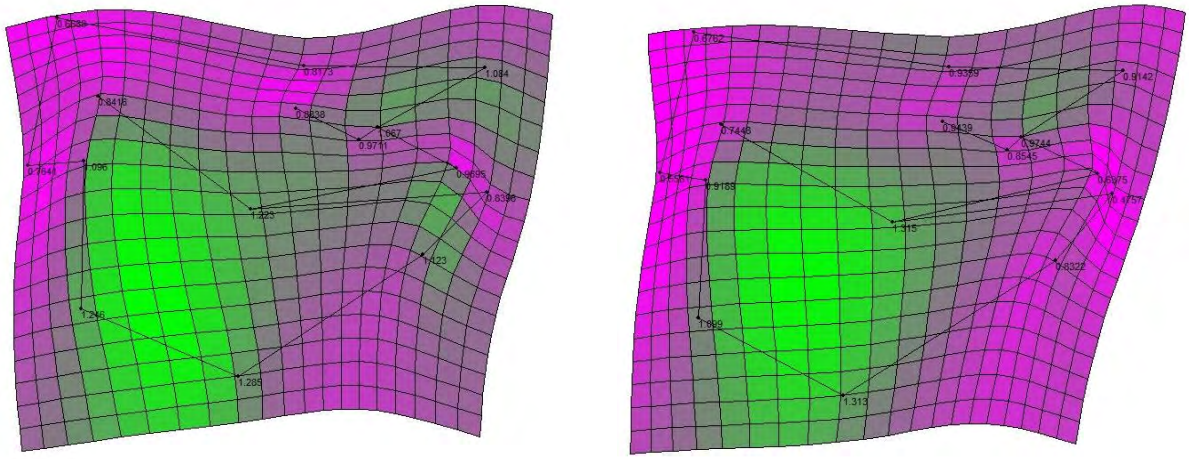

Age Class 5 Age Class 8

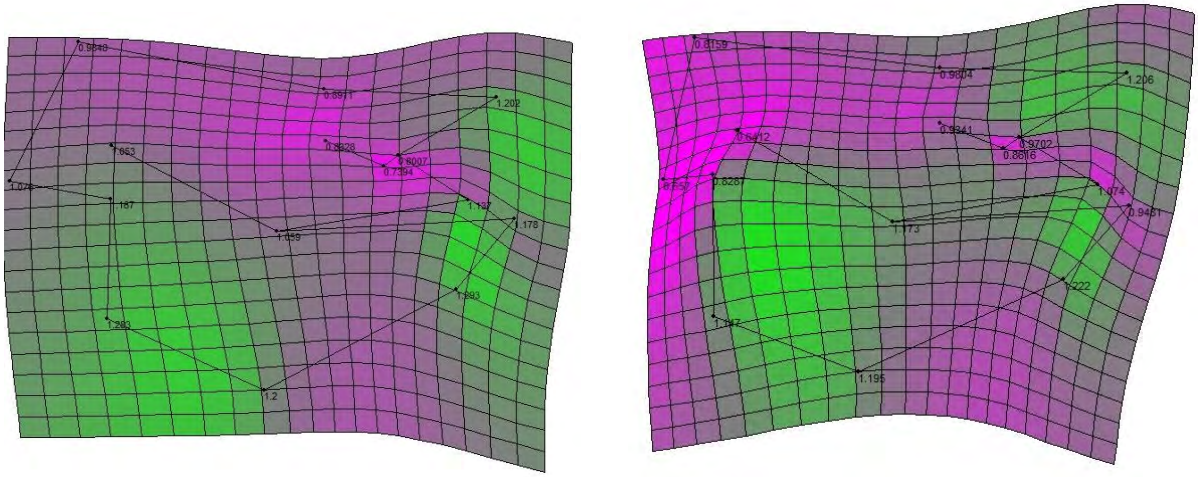

Age Class 11 Age Class 13

Figure 4-13. Thin-plate splines depicting shape transformations in *R. unicornis*. Green areas indicate centers of expansion and purple areas indicate centers of contraction. Bright areas represent stronger expansion/contraction than dark areas.

posterior-ventral maxilla. Strong contraction factors in Age Classes 7-8 were located at the posterior occiput and the nasal incision.

These expansion and contraction factors remained mostly consistent in Age Classes 10-11, only slightly changing in location and strength. The most noticeable changes were the stronger expansion of the nasals and the stronger contraction of the braincase anterior of the occiput.

Ceratotherium simum

Local expansion (green) and contraction (purple) factors for the *C. simum* sample indicate relatively weak growth changes through most of ontogeny (Figure 4-15). With an Age Class 2 specimen as the reference, no strong expansion or contraction factors were present in Age Classes 3-4. Slight expansion factors were found at the anterior facial region, nasals, and anterior ramus, and a slight contraction factor was present at the posterior occiput.

In Age Classes 5-7, the mandibular body, anterior facial region, anterior ramus, and nasals had slightly stronger expansion factors, while the posterior occiput and anterior mandible had slightly stronger contraction factors. These expansion and contraction areas remained unchanged in Age Classes 8-9.

Age Class 11 had the strongest expansion and contraction factors in the ontogenetic sample. The anterior ramus and posterior body of the mandible had strong expansion factors, while the anterior facial region and posterior occiput had strong contraction factors.

Diceros bicornis

Local expansion (green) and contraction (purple) factors for the *D. bicornis* sample displayed gradual growth center transitions in ontogeny (Figure 4-16). With an Age Class 3 specimen as the reference, three primary areas had strong expansion factors in Age Classes 5-6:

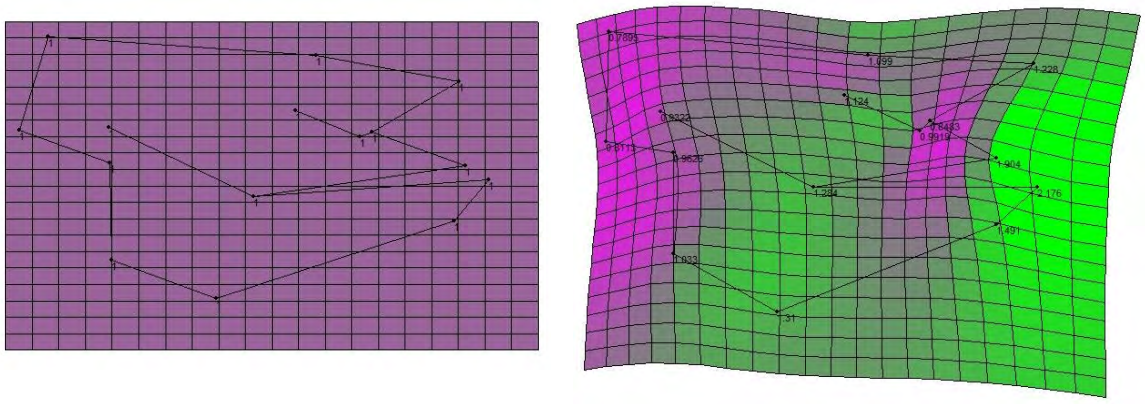

Age Class 2 (source configuration) Age Class 7

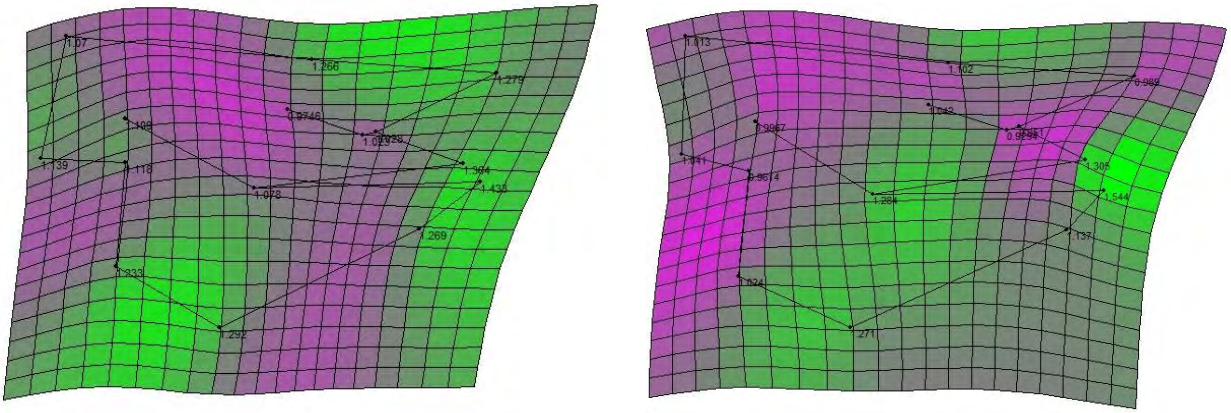

Age Class 8 Age Class 10

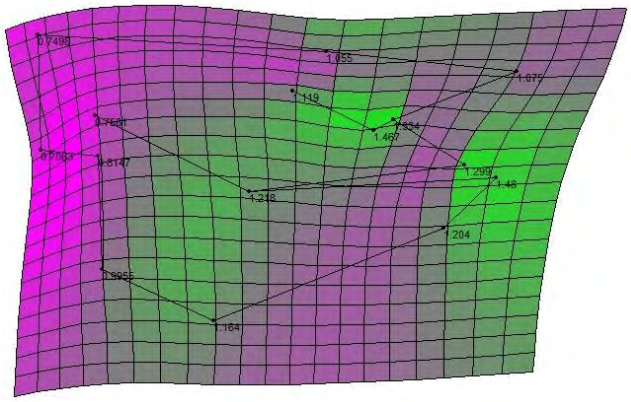

Age Class 11

Figure 4-14. Thin-plate splines depicting shape transformations in *D. sumatrensis*. Green areas indicate centers of expansion and purple areas indicate centers of contraction. Bright areas represent stronger expansion/contraction than dark areas.

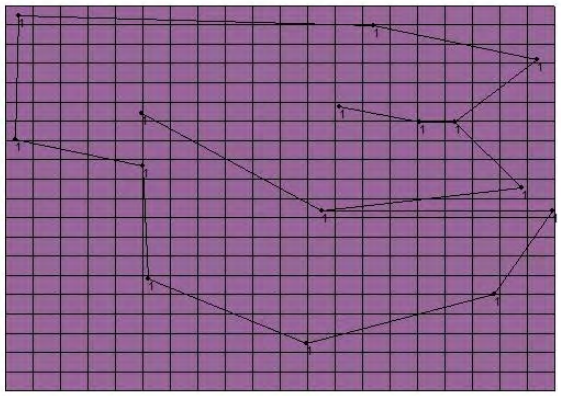

Age Class 2 (source configuration)

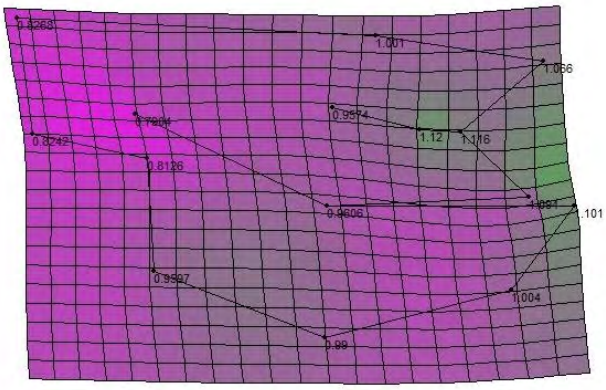

Age Class 4

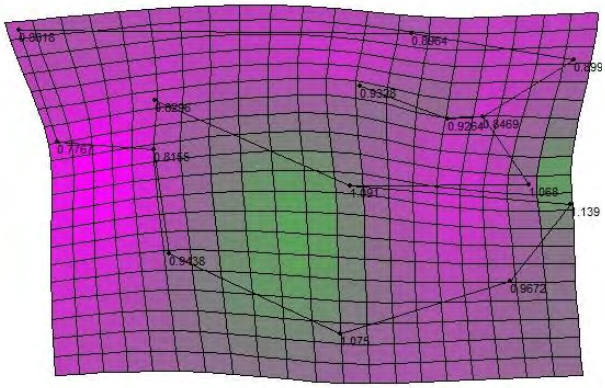

Age Class 6

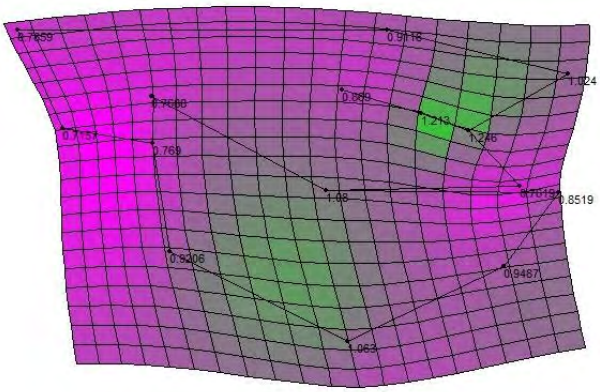

Age Class 8

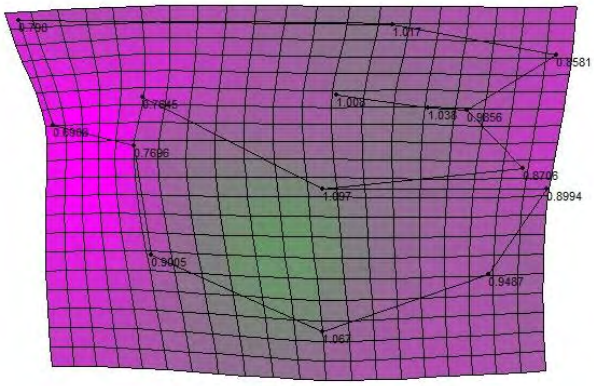

Age Class 9

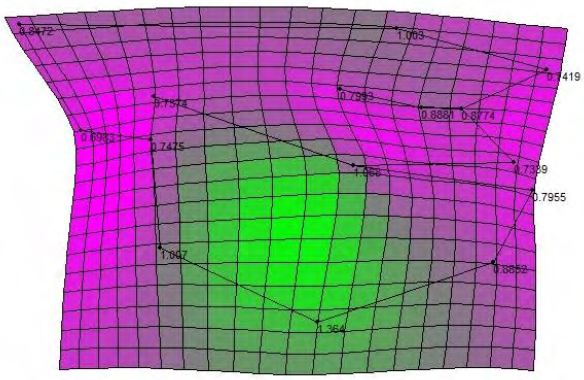

Age Class 11

Figure 4-15. Thin-plate splines depicting shape transformations in *C .simum*. Green areas indicate centers of expansion and purple areas indicate centers of contraction. Bright areas represent stronger expansion/contraction than dark areas.

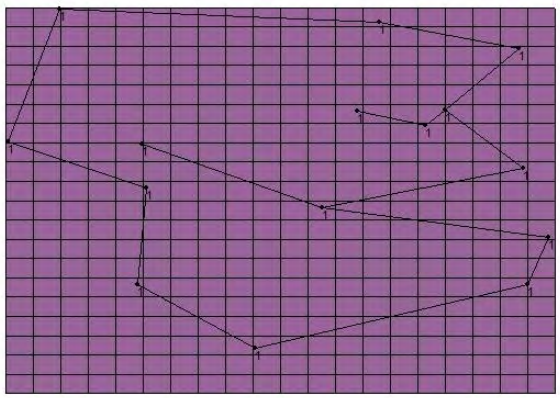

Age Class 3 (source configuration)

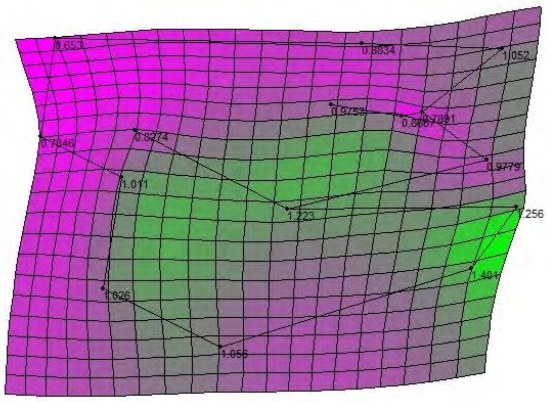

Age Class 5

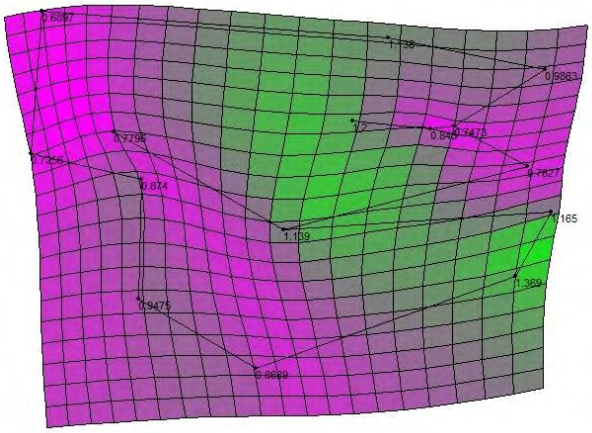

Age Class 7

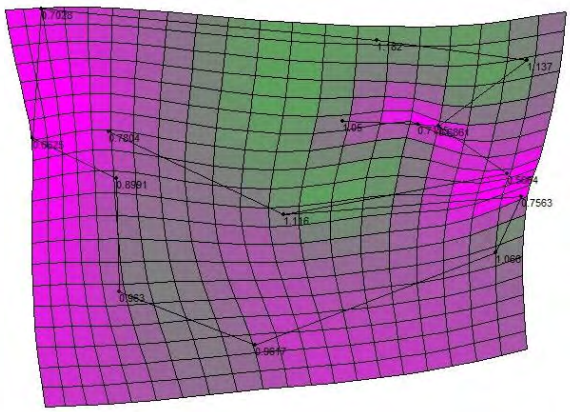

Age Class 8

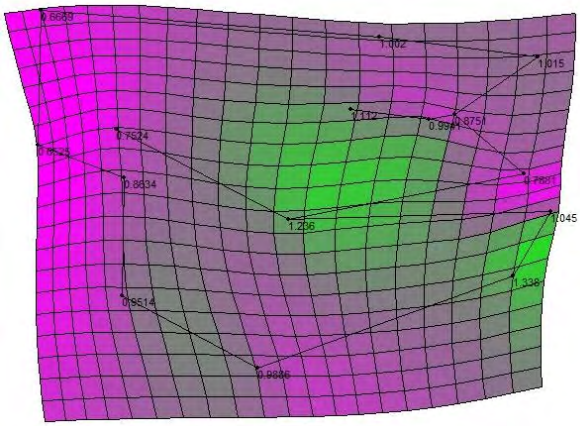

Age Class 10

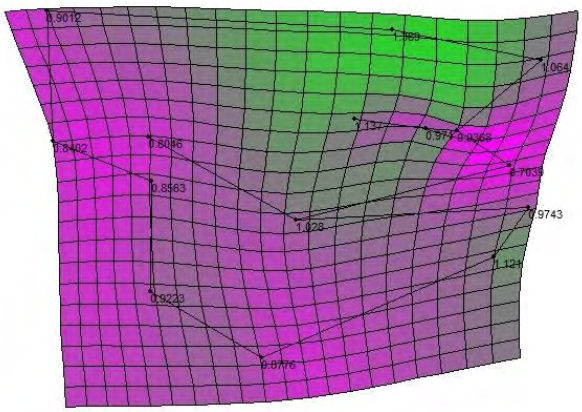

Age Class 11

Figure 4-16. Thin-plate splines depicting shape transformations in *D. bicornis*. Green areas indicate centers of expansion and purple areas indicate centers of contraction. Bright areas represent stronger expansion/contraction than dark areas..

the mandibular ramus, anterior mandible, and posterior facial region and anterior zygomatic arch. Two areas had strong contraction areas in Age Classes 5-6: the posterior occiput and the nasal incision.

In Age Classes 7-8, the anterior facial region had a stronger expansion factor while the mandibular ramus had a weaker expansion factor. The posterior occiput and nasal incision retained strong contraction factors. In Age Classes 8-11, the frontal and nasal regions displayed stronger expansion factors, and the mandibular ramus changed to a slight contraction factor. Also in Age Classes 8-11, the anterior mandible remained at a consistent expansion factor, and the occiput remained at a consistent contraction factor.

CHAPTER 5. DISCUSSION

5.1 FUNCTIONAL INFERENCES

Table 5-1 provides the functional character states for *T. major* and the extant rhinos. Functional inferences regarding the characters are discussed below. Refer to Table 2-3 for explanations regarding browsing and grazing character states of the functional characters.

5.1.1 Oral Cavity and Dentition

Three ratios were used to describe oral cavity morphology. For muzzle shape, DW to MXPPW and MXAPW to MXPPW were used. Statistical results for muzzle shape suggest that both ratios somewhat predict feeding ecologies in the extant rhinos. As expected, *C. simum* has the highest median ratios and *D. bicornis* has the lowest median ratios; both *D. sumatrensis* and *R. unicornis* have intermediate median ratios. Although *R. unicornis* was expected to have higher ratios than *D. sumatrensis* based on the higher percentage of grass in its diet, these species both have large maxillary incisors for honing with the mandibular tusks. *T. major*, also having maxillary incisors, has similar ratios to *D. sumatrensis* and *R. unicornis*. Both diet and large incisors likely contribute to muzzle shape in rhinos. Although *C. simum* and *D. bicornis* have the expected muzzle shape ratios related to feeding ecology, this character appears to be an ineffective feeding ecology distinguisher in species possessing maxillary incisors.

The third ratio of the oral cavity, premolar row length to molar row length, has also been used to distinguish grazers from browsers. Premolar row length to molar row length ratio does not significantly distinguish any of the extant rhinos as no differences in the maxillary or mandibular ratios were apparent. However, *T. major* was clearly distinguishable from extant rhinos, having significantly lower ratios. This difference in premolar row length to molar row length between *T. major* and the extant rhinos is likely related to premolar developmental

Table 5-1. Summary of functional character states in *T. major* and the extant rhinos.

Character	**Number**	***T. major***	***R. unicornis***	***D. sumatrensis***	***C. simum***	***D. bicornis***
Premaxilla width / palate width	1	Intermediate	Intermediate	Intermediate	High	Low
Anterior maxilla	2	Shallow	Deep	Deep	Deep	Deep
Posterior maxilla and jugal	3	Broad	Broad	Narrow	Intermediate	Narrow
Anterior jugal extension	4	Anterior	Posterior	Posterior	Anterior	Posterior
Orbit location	5	Anterior	Anterior	Medial	Posterior	Medial
Braincase length	6	Short	Long	Long	Short	Long
Occipital height	7	Low	High	Intermediate	Low	Intermediate
Mandibular condyle height	8	Intermediate	High	Low	Intermediate	Low
Premolar row / molar row length	9	Low	High	High	High	High
Mandibular body	10	Deep	Shallow	Shallow	Deep	Intermediate
Mandibular angle	11	Very convex	Very convex	Convex	Slightly convex	Convex
Mandibular ramus	12	Large	Large	Intermediate	Intermediate	Small

differences. In *T. major*, the mandibular p1 is absent throughout all of ontogeny, and the mandibular p2 is commonly shed in adulthood. This degree of premolar shortening is not found in the extant rhinos, as the p2 was present in all adult specimens, and often the p1 was present into late adulthood.

As all functional premolars were included in the measurements for all adult specimens, a possible reason for the lack of distinguishable ratios among the extant rhinos is the differences in p1 shedding. All *C. simum* specimens Age Class 8 and older were missing the mandibular p1, but in *D. bicornis*, the p1 was sometimes present through Age Class 11; both *R. unicornis* and *D. sumatrensis* lost the p1 by Age Class 10. Thus, the adult samples for *R. unicornis*, *D. sumatrensis*, and *D. bicornis* did not have equal amounts of premolars measured, which likely affected the ratios. Differences in dental ratios may exist among the extant rhinos, but differences were not discernable in these samples based on the variation of premolars present.

Premolar row length to molar row length ratio is not an accurate feeding ecology predictor in this study because there are no discernable differences among species from the Kruskal-Wallis comparisons. However, in a similar comparison of the dental ratios in the extant rhinos, Mead and Wall (1998b) found more distinction among species. *Dicerorhinus sumatrensis* and *D. bicornis* were found to have relatively longer premolar rows, while *R. unicornis* and *C. simum* had shorter premolar rows. This finding indicates that extant rhinos appear to follow the artiodactyl dental patterns of grazers having shorter premolar rows compared to browsers. With distinction found among extant rhinos (Mead and Wall 1998b), the shortened premolar row in *T. major* is suggestive of a grazing feeding ecology. However, this suggestion requires a reexamination of extant rhino samples with more comparable measurements in the future.

5.1.2 Anterior Skull

Three anterior skull characters, mandibular body depth, orbit location, and anterior maxilla depth, have been correlated with feeding ecology in ungulates. Mandibular body depth mostly predicts the feeding ecologies of the extant rhinos, as *C. simum* has the deepest mandibular body while *R. unicornis* and *D. sumatrensis* have the shallowest mandibular bodies. *Diceros bicornis* has medium body depth, which is deeper than expected for a browser, but it may be related to dry habitats in which it resides. In dry habitats, vegetation is coarse and grit is commonly consumed during feeding (Sanson 2006). *Diceros bicornis* has a more abrasive diet than the tropical browser *D. sumatrensis*, so a deeper mandibular body could be related to slightly higher-crowned dentition in *D. bicornis*. As the mandibular body seems to be an accurate feeding ecology predictor, the very deep mandibular body of *T. major* is suggestive of a grazing feeding ecology, likely in dry habitats, which is similar to *C. simum*.

Orbit location anteriorly-posteriorly predicts the feeding ecology of three extant species, as *C. simum* has a posterior orbit location and *D. sumatrensis* and *D. bicornis* have more anterior locations. *Rhinoceros unicornis*, however, has the most anterior orbit location, which is contrary to expectations of a medial orbit location for a mixed feeder with sub-hypsodont dentition. Similar to *R. unicornis*, *T. major* also has an anterior orbit location. *Rhinoceros unicornis* and *T. major* share similar character states, so the anterior orbit locations may be an indication of similar feeding ecologies, as mixed feeding conditions do not necessarily fall between browsers and grazers (Janis 1995).

The depth and size of the anterior maxilla does not accurately predict the feeding ecologies of the extant rhinos, as all the species have deep anterior maxillae. *T. major* has a shallow and small anterior maxilla not similar to any of the extant rhinos. This noticeable

difference in the anterior maxillae appears to be related to horn size and support. The extant rhinos have large, strongly curved nasal bones supported by deep and broad maxillae around the infraorbital foramen. The thin, straight nasals of *T. major* are connected to the maxillae with less structural support. As there are no noticeable anterior maxilla differences among the extant rhinos, no feeding ecology inferences for *T. major* are made based on this character.

The character states of the anterior orbit and anterior maxilla among the species are likely linked functionally. The graph of ontogenetic maxilla expansion for each species (Appendix 3) shows that in adulthood, *C. simum* has the broadest maxilla, *D. sumatrensis* and *D. bicornis* have intermediately broad maxillae, and *R. unicornis* and *T. major* have the most contracted maxillae. The extensive facial contraction in *R. unicornis* and *T. major* could be related to similarities in feeding ecology or weapon use. In *R. unicornis*, intraspecific combat is primarily mediated with tusks (Laurie 1982, Dinerstein 1991), and the same has been suggested for *T. major* based on similarities in tusk dimorphism (Mihlbachler 2005). Perhaps an anteriorly located orbit would aid vision during tusk combat. However, regardless of the shared anterior maxilla contraction in *R. unicornis* and *T. major*, the known functional influences of these characters in perissodactyls do not confidently infer the feeding ecology of *T. major*.

5.1.3 Masseter Muscle

Five characters, the posterior maxilla and jugal, the anterior jugal, the mandibular angle, the mandibular ramus, and mandibular condyle height, are related to the function and size of the masseter muscle. A broader posterior maxilla and jugal reflect a greater attachment area for the deep masseter, and these characters are accurate ecological predictors for the extant species. Both *D. sumatrensis* and *D. bicornis* have narrow areas while *R. unicornis* and *C. simum* have broad areas. Somewhat contrary to expectations is *R. unicornis*, with the broadest area, broader

than *C. simum*. Bales (1996) proposed that the smaller masseter and exaggerated temporalis in *C. simum* are related to its strongly inclined occiput. Bales (1996) suggested that the temporalis is so exaggerated in order to support a large mandible while feeding with a downward head orientation. In this orientation, the masseter does not have as much work in the vertical component compared to rhinos with a horizontal feeding orientation, so the masseter of *C. simum* is not large for a grazer. The very broad jugal in *T. major* is suggestive of grazing or mixed feeding and seems to be an accurate predictor for the extant rhinos with close to horizontal head orientations

A further anterior extension of the jugal reflects a greater attachment area for the superficial masseter, and this character also accurately predicts the feeding ecologies for the extant rhinos. *Ceratotherium simum* has the furthest anterior jugal extension relative to the orbit, and *D. sumatrensis* and *D. bicornis* have the most posterior jugal extensions; *R. unicornis* falls in between *C. simum* and the browsers as expected. *Teleoceras major* has an anterior jugal extension slightly further than *C. simum*, past the anterior orbit. As the anterior jugal extension accurately predicts the feeding ecologies for the extant rhinos, *T. major* has a character state suggestive of a grazer.

A strong curvature of the mandibular angle and a large size of the mandibular ramus reflect a greater attachment area for the deep and superficial masseter, and these characters seems to be accurate predictors of feeding ecology for the extant rhinos. *Rhinoceros unicornis* has a large and strongly convex angle and a large ramus, and *D. sumatrensis* and *D. bicornis* have somewhat small and convex angles and small rami as expected. *Ceratotherium simum* has a small and weakly convex angle and a small ramus, but again Bales (1996) explained the small masseter size in *C. simum*. As the mandibular angle seems to be an accurate predictor, the

character states of a strongly convex angle and large ramus for *T. major* indicate a grazing or mixed feeding condition similar to *R. unicornis*.

An increased distance of the mandibular condyle from the cheek teeth results in a greater moment arm and mechanical advantage of the masseter muscle (Radinsky 1984, Homberger and Walker 2004). When a visual height of the condyle from the occlusal plane is used as an estimator of this moment arm, this character seems to be an accurate feeding ecology predictor for extant rhinos. *Ceratotherium simum* has an intermediate condyle height, higher than the browsers *D. sumatrensis* and *D. bicornis* as expected. *Rhinoceros unicornis* has a higher condyle than all other extant species, again demonstrating its overall large masseter as a mixed feeder. *Teleoceras major* has an intermediate condyle height, similar to the grazer *C. simum*, which is suggestive of a grazing feeding ecology.

Overall, the masseter characters accurately predict feeding ecology in the extant rhinos with horizontal head orientations. The skull morphology of *C. simum* is divergent, with smaller attachment areas for the masseter due to its proposed decreased functional requirements for mastication. As *T. major* has a horizontal head orientation, the estimated masseter size and attachment areas suggest the feeding ecology of a grazer or mixed feeder.

5.1.4 Temporalis Muscle

Two characters, braincase length and occipital height, are related to the size and function of the temporalis muscle. A greater braincase length, which was estimated using the PCL measurement, reflects a larger temporalis muscle, and this character accurately predicts the feeding ecologies of the extant rhinos. *Ceratotherium simum* has a short PCL, while *R. unicornis, D. sumatrensis*, and *D. bicornis* have a long PCL. The short PCL for *T. major* was most similar to *C. simum*, which is suggestive of a grazing feeding ecology.

A greater occipital height also reflects a larger temporalis muscle, and this character is an accurate predictor for three of the extant species. *Ceratotherium simum* has the lowest occiput while *D. sumatrensis* and *D. bicornis* have higher occiputs. *Rhinoceros unicornis* has the highest occiput, which is contrary to expectations of a mixed feeder having an intermediate occipital height. Functional character states indicate that *R. unicornis* has large temporalis and masseter muscles, which may be indicative of a mixed feeder. Perhaps in rhinos, mixed feeders need large temporalis and masseter muscles to meet the functional requirements of a grazer and a browser. Keeping the results for *R. unicornis* in mind, *T. major* has a low occipital height similar to *C. simum*, which is suggestive of a grazing feeding ecology.

The results of *C. simum* having a small temporalis muscle seem contradictory in light of the visually apparent large temporal fossa. A few reasons could explain the statistical results for the temporalis muscle. First, the measurements that were used may not truly reflect actual temporalis size. For example, the PCL posterior landmark was the opisthion, not the temporalis origination area along the occipital crest. The PCL anterior landmark was the glenoid fossa, which is close to, but not along, the temporalis insertion area of the coronoid process. Another possibility is that *C. simum* does in fact have a small temporalis muscle relative to overall body size. The functional measurements were normalized to total skull length to prevent significant size differences among the species from biasing the results. For example, the maximum skull lengths for each species used in this study were: *T. major* 497.5 mm, *R. unicornis* 527 mm, *D. sumatrensis* 416 mm, *C. simum* 640.5 mm, *D. bicornis* 548.5 mm. Although *C. simum* does have a large occiput in appearance, *C. simum* also has the largest overall skull.

With the results suggesting that *C. simum* does in fact have the large temporalis conditions of grazers, the masseter of *C. simum* appears to be small. Despite the small masseter

size in *C. simum*, the extant species with horizontal head orientations have functional character states coinciding with feeding ecologies. *Teleoceras major* has a considerable amount of grazer characters, so the suggested feeding ecology for *T. major* is a grazer.

5.2 ONTOGENETIC INFERENCES

5.2.1 Horns and Tusks

Differences in the timing of nasal horn development were found among the rhino species. The appearance of the dorsal nasal pronouncement occurred earliest in African rhinos (Age Class 1), slightly later in *R. unicornis* (Age Class 3), and latest in *T. major* (Age Class 5). Nasal rugosity appeared in Age Class 8 in extant rhinos and in Age Class 10 in *T. major*. These differences in nasal horn development are likely related to differences in nasal horn size and use. The African rhinos have significantly longer nasal horns than *R. unicornis*; the nasal horn of *T. major* is likely the smallest based on nasal rugosity size. Horns are the sole weapons in African rhinos, and nasal horn development begins earliest in these species.

In the three rhino species with tusks, di_2 shedding and tusk eruption occurs in similar age classes. All Age Class 6 specimens had di_2 present, and all Age Class 8 specimens but one (*T. major*, UNSM 52230) had erupted tusks. Further, the only Age Class 7 specimen in the samples (*D. sumatrensis*, AMNH 173576) had empty i_2 alveoli. Altogether, tusk eruption in *T. major*, *R. unicornis*, and *D. sumatrensis* seems to occur in Age Classes 7-8.

Comparable timings of tusk eruption (Age Classes 7-8) and horn rugosity development (Age Class 8 in the extant rhinos) suggest similar importance in function and maturity. The estimated chronological age for Age Classes 7-8 in *D. bicornis* is 5-8 years old (Hitchins 1978). This age estimate for tusk eruption and horn rugosity development coincides with the age of maturity in males and the age of first parturition in females, between 5-8 years (Owen-Smith

1988). Dinerstein (1991) also noted the coincidence of tusk eruption with attainment of breeding age in *R. unicornis* males. Although nasal development in *T. major* occurred later and was possibly of secondary importance in competition and defense, tusk development did coincide with breeding age, as in *R. unicornis* and *D. sumatrensis*. These age estimates suggest a relationship between weapons and sexual maturity in rhinos, as males require weapons to compete for mating rights, and females require weapons for defense of their young.

The importance of weapon development for combat and defense is especially evident given the mortality profiles Mihlbachler (2003) reported for *T. proterum* from Florida localities. Comparing *T. proterum* bone accumulations with those previously reported for *D. bicornis*, Mihlbachler (2003) showed similar mortality spikes for each species. The first mortality spike occurred around 3-5 years old (approximately Age Classes 5-6), which was estimated to correspond with mother-calf separation before maturation. Full body size is not yet achieved during this time of susceptibility to predation (Mihlbachler 2003), and significant horn and tusk development has not yet occurred. The second mortality spike occurred around 6-15 years old (approximately Age Classes 6-12), which corresponded with the attainment of maturation in young adults but not necessarily breeding rights in males. This is a time of aggression and competition for reproduction (Mihlbachler 2003); the development of weapons for combat and defense coincides with this age.

5.2.2 Sexual Dimorphism

Sexual dimorphism in extant rhino specimens was not apparent. First, there were no apparent qualitative differences in morphological development. Second, although the tusks were not measured, tusk size was not visually dimorphic and there were no perceptible developmental differences in tusk eruption. Third, only one skull dimension, TCL in *R. unicornis*, was found to

be dimorphic, with the females being significantly larger than the males. Dimorphism documented in *R. unicornis* indicates that males often have significantly larger skull, tusk, and postcranial dimensions than females (Groves 1982, Dinerstein 1991). The curious dimorphism find in *R. unicornis* in this study is likely related to a small sample size, as only 4 male and 3 female adult specimens were included.

In the *T. major* sample, only two adult males were included, which are identifiable based on visually apparent tusk size dimorphism (Voorhies and Stover 1978). Several adults from this sample were included in the sexual dimorphism study by Mead (2000), who found adult males to be significantly larger than females in several cranial, mandibular, postcranial, and tusk dimensions; males also had prolonged limb growth. Further differences in tusk development between sexes have been identified in *Teleoceras*. Mihlbachler (2005) found that *Teleoceras proterum* male tusks erupted later in life than in females, and male tusks also had prolonged growth. Comparable dimorphic tusk development has not been found in *R. unicornis* or *D. sumatrensis*, and Mihlbachler (2005) attributed this degree of dimorphism in *T. proterum* to higher levels of competition relative to extant rhinos.

Although development of dimorphism in rhinos was not elucidated in this study, previous work by Groves (1975) on *C. simum* and by Dinerstein (1991) on *R. unicornis*, give indications of the timing of dimorphism. Cranial dimension dimorphisms in *C. simum* and body size dimorphisms in *R. unicornis* were found to appear around four to five years of age, beginning slightly before the onset of maturity. Future sexual dimorphism research in the extant rhinos and *Teleoceras* may show similar developmental patterns coinciding with horn and tusk development and maturity.

5.2.3 Non-Molariform Dentition

For mandibular dentition, p1 is shed early in *C. simum* (Age Class 8) and late in *R. unicornis, D. sumatrensis,* and *D. bicornis* (Age Class 10). The p2 is also shed in Age Class 10 in *T. major*. For maxillary dentition, P1 is shed early in *C. simum* and *D. sumatrensis* (Age Class 8) and late in *T. major, R. unicornis,* and *D. bicornis* (Age Classes 10-11). Premolar shedding is associated with eruption of adult teeth, as in Age Class 8 specimens the p2, p3, and m2 were recently erupted, and in Age Class 10 specimens, m3 was recently erupted. Anterior premolar shedding in rhinos therefore makes room for new molariform teeth that are important in mastication.

The lower i2 tusk and upper I1 honing incisor combination is the synapomorphy for Rhinocerotidae, and matching I2 and i1 become reduced or nonexistent (Radinsky 1966). Although *C. simum* and *D. bicornis* do not possess this functional incisor combination in adulthood, these incisors are occasionally present in ontogeny. *Diceros bicornis* commonly possesses small, nub-like upper and lower incisors in all ages, in the same locations as in Asian rhinos and *T. major*. Hitchins (1978) noted the common appearance of up to two pairs of mandibular and maxillary incisors in *D. bicornis*, most common early in ontogeny. Some *C. simum* specimens have questionable incisor presence based on shallow incisor alveoli. In both *T. major* and *R. unicornis* specimens, small, lower incisors medial of i2 are present in all ages, which are interpreted as rudimentary i1. *R. unicornis* specimens also have small upper incisors located lateral of I1 early in ontogeny, interpreted as rudimentary I2. With *D. bicornis*, *T. major*, *R. unicornis,* and possibly *C. simum* all possessing rudimentary incisors, incisors may have a function such as in scratching, mating, or feeding in infancy, or they could be vestigial incisors that are non-functional.

5.2.4 Skull Development

Extant rhinos and *T. major* have similar ontogenetic patterns in dorsal cranial developmental changes. In Age Classes 1-2, all species have rounded crania except for *C. simum*, which has a lengthened and angular cranium. All species undergo distinct cranial lengthening in Age Classes 3-5, making crania easily distinguishable to species. Co-occurring with cranial lengthening is occipital crest pronouncement and temporal line appearance. The temporal lines become visible early in *T. major* and *R. unicornis* (Age Classes 3-4) and late in *C. simum* and *D. bicornis* (Age Class 6).

In Age Class 5, the occiput and frontal plate begin to widen and develop angularly into adult morphologies, and different developmental patterns follow. The Asian rhino crania widen more proportionately, while African rhino crania widen with continued lengthening. Through Age Classes 3-6, *T. major* has morphological similarities with both Asian rhinos (rounded occiput) and African rhinos (frontal plate). *Teleoceras major* also has distinct characters early in ontogeny that are not found in extant rhinos, such as laterally flared zygomatic arches and short, pointed nasals; these characters are present in *T. major* through ontogeny.

In all species, nasals, frontal plate, and occiput continue to change in Age Classes 7-9, and in Age Class 10 adult morphology is reached with little change afterward. Morphological changes in Age Classes 10-15 are slight exaggerations to the nasals, zygomatic arches, frontal plate, and occiput. The occipital and temporal crests also become more pronounced through Age Classes 10-15.

Cranial suture development is similar across rhino species. Parietal-occipital and frontal-parietal sutures close in Age Classes 6-8. Facial sutures close in Age Classes 10-12. Nasal-frontal and jugal-zygoma sutures disappear in Age Classes 10-12 in extant rhinos, but these

sutures were not closed in *T. major* specimens. This apparent lack of suture closure is likely due to fracturing of peripheral fossil bones common in *T. major* specimens.

Dorsal cranial ontogenetic changes in extant rhinos and *T. major* are similar to those described in *Chilotherium wimani* by Deng (2001). Deng (2001) described similar occipital and parietal shape changes, occipital and temporal crest pronouncement timings, and suture closings in *C. wimani*. Unfortunately, descriptions and depictions of the lateral skull were not provided for a comparison of characters related to feeding ecology used in this study.

Comparisons of the lateral skull suggest that development of primary muscle attachment areas (mandibular angle, zygomatic arch, and occiput) and dentition area (mandibular body) are distinct among species. Early in ontogeny, *T. major* stands out with its enlarged mandibular angle and zygomatic arch. These masseter attachment sites in *T. major* continually expand through ontogeny, remaining significantly larger than in other species. All species appear to have considerable increases in jugal broadness in Age Classes 5-7, and the mandibular angle appears to change consistently across species. Although *R. unicornis* reaches mandibular angle morphology similar to *T. major* in adulthood, *T. major* has the most developed angle and zygomatic arch earliest in ontogeny.

Ceratotherium simum also stands out with its enlarged and posteriorly oriented occiput early in ontogeny. The occiput in *C. simum* expands through ontogeny, remaining larger and more posteriorly oriented than the other species. *Rhinoceros unicornis* and *D. bicornis* have changes in occipital height and angle beginning in Age Class 3. In *T. major*, the occipital angle does not begin to change until Age Classes 4-5, and occipital height does not noticeably change until after Age Class 5.

The deep mandibular bodies of *C. simum* and *T. major* appear to follow different developmental patterns compared to the shallower mandibular bodies of *R. unicornis, D. sumatrensis,* and *D. bicornis*. In *C. simum*, the mandibular body is deep early in ontogeny, but other species including *T. major* have thin mandibular bodies at similar ages. *Ceratotherium simum* and other extant rhinos have consistent increases in body depth through ontogeny, but *T. major* reaches the deep body proportions of *C. simum* around Age Class 10, which suggests different mandibular body developmental patterns in *T. major* and *C. simum*.

Despite early developmental differences in the mandibular angle, zygomatic arch, occiput, and mandibular body, all species show similar exaggerations in robustness in Age Classes 10-15. Adulthood is thus characterized by increases to species-specific morphologies achieved earlier in ontogeny. Perhaps having larger attachment areas and more developed muscles early in ontogeny are a selective advantage for the mastication of coarse vegetation.

5.2.5 Thin-Plate Splines

The thin-plate splines depicted developmental shape differences related to muscle attachment areas, dentition, and horns. The most similar ontogenetic change across all species is consistent posterior and ventral occipital contraction. Similar contraction seems counterintuitive as species develop large occiputs with differing morphologies and orientations. However, braincase develops with negative allometry in mammals (Emerson and Bramble 1993), which is thus demonstrated in the thin-plate splines. Another similarity is consistent mandibular ramus expansion in all species. *Rhinoceros unicornis,* however, does have stronger expansion, which is explained by its small ramus early in ontogeny and its large ramus in adulthood. All species demonstrate zygomatic arch expansion through ontogeny except for *C. simum*. *Ceratotherium*

simum has zygomatic expansion only in adulthood as *C. simum* has a long zygomatic throughout ontogeny.

Nasal, maxilla, and mandibular body developments exhibit the greatest differences among species. Nasal expansion is consistent through ontogeny in the species, but the degree of expansion varies among rhinos. African rhinos have weak nasal expansion, and Asian rhinos and *T. major* have strong nasal expansion. Weaker nasal expansion in the African rhinos is likely related to their large nasal size early in ontogeny. Maxilla and mandibular body expansion through ontogeny also is present in all species, but *C. simum* and *T. major* have weaker and stronger expansions, respectively. These maxilla and mandibular body differences in *C. simum* and *T. major* are related to the areas for dental housing, being deep in *C. simum* throughout ontogeny and becoming deep in *T. major* in adulthood.

5.2.6 Principal Component Analysis of Landmarks

PC1 for each species explained the most variation in four characters: the occiput, zygomatic arch, mandibular angle, and nasals. These areas undergo the most morphological change among species, but the zygomatic arch in *D. sumatrensis* and *C. simum* and the mandibular angle in *C. simum* were not primary areas for PC1. Little ontogenetic change occurs in these areas for these species, which is displayed by the consistently weak mandibular angle and long zygomatic arch in *C. simum*, and by the consistently thin zygomatic arch in *D. sumatrensis*. The occiput and nasals, as well as the zygomatic arch and mandibular angle, are viewed as areas that develop the most in rhinos.

PC2 explained variation, and therefore considerable ontogenetic change, in mandibular body depth for *T. major*, *R. unicornis*, and *D. bicornis*, and occipital height for *T. major*, *R. unicornis*, and *D. sumatrensis*. For the mandibular body, *C. simum* and *D. sumatrensis* showed

less ontogenetic change in depth, retaining deep and shallow bodies, respectively, throughout ontogeny. For the occiput, *C. simum* and *D. bicornis* showed less ontogenetic change in occipital height throughout ontogeny, which is somewhat unexpected for *D. bicornis*. However, PC3 is a significant component for *D. bicornis* that explained significant occipital height change, so *D. bicornis* has slightly less occipital changes compared to *T. major*, *R. unicornis*, and *D. sumatrensis*. One further character with significant ontogenetic variation is anterior cranial depth. *Teleoceras major* had considerable anterior cranial depth variation in PC2, as did *C. simum* in PC3, which could be related to increased maxillary depth for high-crowned upper dentition.

5.2.7 Canonical Variate Analysis of Landmarks

CV1 appears to group species based on developments in length of the entire skull. The primary CVs depicted skull areas with the most variation among species' ontogenies as a whole, not just in infancy or adulthood. Occipital orientation, mandibular angle curvature, and facial length were the primary distinguishing characters among species for CV1. Overlapping intermediate CV1 scores for *D. sumatrensis* and *D. bicornis* indicate similar ontogenetic paths, as do high CV1 scores for *T. major* and *R. unicornis*.

CV2 appears to group species based on feeding ecology. In CV2, the primary distinguishing characters were mandibular body depth, occipital height, and jugal length, which are related to differences between grazers and browsers. The low CV2 score for *C. simum* and *T. major* are indicative of grazing conditions, and the high and intermediate scores in *D. bicornis*, *R. unicornis*, and *D. sumatrensis* are indicative of browsing and mixed feeding conditions.

In CV3, two of the characters with the most variation, mandibular angle size and mandibular condyle height, were related to feeding ecology. Although there is less separation

among species, the similarities in *C. simum* and *R. unicornis*, and in *D. bicornis* and *D. sumatrensis*, indicate that CV3 groups the extant species based on feeding ecology. *Ceratotherium simum* and *R. unicornis* have grazing character states for the mandibular angle and mandibular condyle, while *D. bicornis* and *D. sumatrensis* have browsing character states. CV3 has little interpretative ability because no other species have intermediate scores and the mixed feeder, *R. unicornis*, has high scores.

5.2.8 Skull Allometry

Allometric coefficients for cranial, mandibular, and dental variables indicate several growth patterns among the extant rhinos and *T. major* that can be explained by functional morphology and feeding ecology. *T. major* and *C. simum*, with likely grazing ecologies, have similar growth allometries for MCL and TCL. As MCL estimates anterior zygomatic arch size, isometric MCL growth in both species suggests that both species may retain consistent growth of a masseter attachment area for feeding on coarse vegetation. Likewise, negative allometric MCL growth in the browsers and mixed feeder suggests that continued expansion of the anterior zygomatic arch is not necessary because large masseter muscles are not required for mastication of softer vegetation. *Ceratotherium simum* and *T. major* also have isometric TCL growth while the browsers and mixed feeder have negative allometric TCL growth. As grazers tend to have lengthened skulls, perhaps consistent overall skull growth in *C. simum* and *T. major* is to retain functionally efficient grazing proportions.

Similarities in occipital growth allometry also provide comparisons in feeding ecology between grazers and browsers. *Ceratotherium simum* and *T. major* have negative allometric growth for OH, which indicates less vertical adult occipital growth. In comparison, positive allometric OH growth in the browsers and mixed feeder suggests increased adult occipital

growth to develop a large temporalis muscle for browsing. PCL provides further occipital developmental trends that are both shared and distinct among species. This character is likely related to brain size, as all species have negative PCL allometry. The mammalian brain develops early in ontogeny, resulting in negative allometric growth postnatally compared to the rest of the skull (Emerson and Bramble 1993). Differences in the degree of negative PCL allometry exist among species, and morphological occipital developmental differences are verified by assessing vertical and horizontal allometric components together. *Ceratotherium simum* and *D. sumatrensis* have the highest negative PCL allometry, *R. unicornis* and *D. bicornis* have the lowest negative PCL allometry, and *T. major* has intermediate negative PCL allometry. Skull allometries for *C. simum* indicate more posterior than vertical occipital development. The opposite conditions are found in *R. unicornis* and *D. bicornis*, with more vertical than posterior occipital development. High scores in both directions for *D. sumatrensis*, and low scores in both directions for *T. major*, indicate intermediate occipital conditions. The occipital allometry scores confirm occipital morphological changes in the rhino species.

Similarities in ZW allometries group the species geographically with *T. major* being more similar to Asian rhinos. Asian rhinos and *T. major* have isometric ZW growth and African rhinos have negative allometric ZW growth. Asian rhinos and *T. major* have broad posteriorly flared arches that increase through adulthood, but African rhinos have slightly flared arches with less noticeable developmental changes. Although Joeckel (1990) found correlations between occiput size and zygomatic width suggesting a relationship with the temporalis muscle, these differences in ZW morphology and development may instead be related to masseter size. Morphological assessments reveal that *T. major* and *R. unicornis* have large masseter muscles that pass through laterally flared arches. Another reason for zygomatic arch differences between

Asian and African rhinos is related to weapon display. African rhinos possess two large horns that are visually apparent, sometimes over 1000 mm in length. Asian rhinos fight primarily in tusks, which are not as visually apparent as large nasal and frontal horns, so perhaps flared zygomatic arches are related to threat display in rhino species with large tusks.

ACL allometries reflect differences in nasal horn development and structural support between extant rhinos and *T. major*. The most positive ACL allometry in *T. major* suggests later structural nasal development from a weak anterior face early in ontogeny. Extant rhinos have less positive allometry compared to *T. major*, which suggests stronger nasal horn support early in ontogeny. Conversely, similarities in SW allometries for all species except *C. simum* indicate that SW is not necessarily related to the presence or absence of the frontal horn. There are no score differences between species possessing a frontal horn (*D. sumatrensis* and *D. bicornis*) and those without a frontal horn (*T. major* and *R. unicornis*). *Ceratotherium simum* does not have a noticeably narrower frontal region compared to other species early in ontogeny, but *C. simum* does have a very wide frontal region in adulthood. Positive SW allometry in *C. simum* indicates that the frontal region develops more in *C. simum* than in other species.

Most allometric similarities among species were of the mandible and dentition. Both MXDL and MNDL had positive allometry for all species, which is consistent with large adult teeth steadily added to the dental rows. Isometric ML growth for all species is likely a combination of positive allometry in MXDL and MNDL and negative allometry in RL. The ramus is likely negatively allometric because it must be large early in ontogeny for efficient mastication regardless of feeding ecology. Low negative RL allometries in *C. simum* and *T. major* verify little morphological change of the mandibular ramus in these species.

The dental variable with the most variation among species was MNAPW, which is related to muzzle shape. Negative MNAPW allometry in *C. simum* indicates that its mouth opening is very broad early in ontogeny. Positive MNAPW allometry in *D. bicornis* suggests that early in ontogeny its mouth opening is narrow, and positive allometry is needed to reach adult proportions. MNAPW isometry in *T. major* and *R. unicornis* suggests little ontogenetic shape change to maintain the function of deciduous and adult lower incisors. MNPPW is also related to muzzle shape, which is negatively allometric with few differences among the species. Shape differences in the oral cavity among species are therefore a result of ontogenetic changes to the anterior muzzle.

CHAPTER 6. CONCLUSIONS AND DIRECTIONS FOR FUTURE RESEARCH

The present study reveals that several functional characters found in perissodactyl grazers and browsers are accurate feeding ecology predictors in extant rhinos. *Teleoceras major* is proposed to be a grazer based on its high number of grazing characters, such as a deep mandibular body, a large posterior maxilla and jugal, an anterior jugal extension, a large and strongly curved mandibular angle, and a low and short occiput. *Teleoceras* has previously been hypothesized as a grazer based on its high-crowned dentition and shortened limbs for low-grass grazing, and the results of this study support this hypothesis.

A few functional character states did not coincide with feeding ecology in extant rhinos, bringing to light the complexities of morphological assessments. The premolar row length to molar row length ratio, a variable often used for examining feeding ecology affinities, yielded no differences among extant rhinos. Character states of the mandibular ramus and occiput produced results contrary to feeding ecology expectations for *C. simum* and *R. unicornis*. *Ceratotherium simum* was found to have small masseter attachment areas and large temporalis attachment areas, which is likely related to its strongly inclined head orientation. In *R. unicornis*, the combination of a high, browsing occiput and a large, grazing mandibular ramus demonstrates its mixed feeding ecology.

Functional characters that were accurate predictors in extant rhinos can be useful for investigating feeding ecology of other extinct rhinos. Tracking functional characters across the nine *Teleoceras* species may reveal changes or specializations in feeding ecology temporally as well as geographically. Similar functional assessments can be completed for Eurasian teleoceratins, which have a range of proposed feeding ecologies with differing skull morphologies and body types. In further feeding ecology assessments, dental row lengths and

masseter and temporalis attachment areas could be measured differently to more accurately reflect functional dimensions.

Ontogenetic comparisons in the extant rhinos and *T. major* reveal both shared and distinct patterns in rhino weapon development. Tusk eruption and nasal horn rugosity appearance occur with the onset of sexual maturity, indicating the importance of weapons in male competition and female defense of offspring. In *T. major*, late nasal horn rugosity development and negative allometry of the anterior face suggest a more important role of the tusks. In the extant rhinos, thin-plate spline nasal expansions and nasal horn pronouncement timing indicate early nasal development in the African rhinos, likely related to the nasal horn being the primary weapon used in combat and defense. Flared zygomatic arches in the Asian rhinos and *T. major* as adults are proposed as a display in tusk fighting rhinos.

Rhino species share several morphological skull developments in ontogeny, such as early cranial lengthening followed by occipital and frontal widening. Cranial sutures close in similar age classes, and pronouncement of the temporal and occipital crests occurs synchronously across all species regardless of cranial morphology. Each species' adulthood is characterized by exaggeration of the nasals and the temporalis and masseter attachment areas.

Species' ontogenies are primarily distinguished by changes in the occiput, zygomatic arch, mandibular angle, and mandibular body, which are all characters related to feeding ecology. The ontogenetic PCA of shape variables displayed the greatest overall changes in the occiput, zygomatic arch, and mandibular angle for each ontogeny. The ontogenetic CVA of shape variables grouped species according to feeding ecology with the most variation in mandibular body depth, occipital height, and jugal length. Skull allometries further link

developmental morphology to feeding ecology, as *C. simum* and *T. major* share similar zygomatic arch and occiput allometries, as do *R. unicornis, D. sumatrensis,* and *D. bicornis.*

Morphological descriptions and thin-plate splines further reveal developmental differences in muscle attachment areas and dental housing areas, especially in grazers. The occiput, mandibular body, maxilla, and zygomatic arch all develop early with less ontogenetic change in *C. simum*. The mandibular ramus and zygomatic arch also develop early in *T. major*, but the maxilla and mandibular body develop significantly more in adulthood than in other species. Early developments of areas related to masseter and temporalis muscle attachment and dental housing are interpreted as adaptations for grazing in *C. simum* and *T. major*.

The comparative methods used in this study can be applied to a range of extinct rhino species to assess development and feeding ecology. The partially complete ontogenetic skull sequence of the Miocene *Chilotherium wimani*, which has a similar morphology and proposed feeding ecology as *Teleoceras*, may elucidate further developmental patterns related to grazing rhinos. Other extinct rhino species with only a few immature specimens may contribute to developmental trends shared among extant rhinos and distantly related lineages. Inferences from this study regarding weapon development and maturity, and cranial and mandibular changes and feeding ecology highlight the potential of ontogenetic comparisons. Ontogenetic investigations provide an innovative approach to understanding the evolution and development of the Rhinocerotidae.

BIBLIOGRAPHY

Bales, G. S. 1996. Skull evolution in the Rhinocerotidae (Mammalia, Perissodactyla): Cartesian transformations and functional interpretations. *Journal of Mammalian Evolution* 3: 261-279.

Berger, J. 1994. Science, conservation and black rhinos. *Journal of Mammalogy* 75: 298-308.

Cerdeño, E. 1995. Cladistic analysis of the family Rhinocerotidae (Perissodactyla). *American Museum Novitates* 3143: 1-25.

Deng, T. 2001. Cranial ontogenesis of *Chilotherium wimani* (Perissodactyla, Rhinocerotidae). *Proceedings of the Eighth Annual Meeting of the Chinese Society of Vertebrate Paleontology* 8: 101-112.

Dinerstein, E. 1991. Sexual dimorphism in the greater one-horned rhinoceros (*Rhinoceros unicornis*). *Journal of Mammalogy* 72: 450-457.

Emerson, S. B. and D. M. Bramble. 1993. Scaling, allometry, and skull design. *The Skull, Volume 3: Functional and Evolutionary Mechanisms*. B. K. Hall and J. Hanken. Chicago, The University of Chicago Press: 384-421.

Geraads, D. 2005. Pliocene Rhinocerotidae (Mammalia) from Hadar and Dikika (Lower Awash, Ethiopia), and a revision of the origin of modern African rhinos. *Journal of Vertebrate Paleontology* 25: 451-461.

German, R. Z. and L. L. Meyers. 1989. The role of time and size in ontogenetic allometry: I. Review. *Growth, Development & Aging* 53: 101-106.

Giannini, N. P., F. Abdala, and D. A. Flores. 2004. Comparative postnatal ontogeny of the skull in *Dromiciops gliroides* (Marsupialia: Microbiotheriidae). *American Museum Novitates* 3460: 1-17.

Goddard, J. 1970. Age criteria and vital statistics of a black rhinoceros population. *East African Wildlife Journal* 8: 105-121.

Goto, R. and C. G. N. Mascie-Taylor. 2007. Precision of measurement as a component of human variation. *Journal of Physiological Anthropology* 26: 253-256.

Gould, S. J. 1966. Allometry and size in ontogeny and phylogeny. *Biological Reviews of the Cambridge Philosophical Society* 41: 587-640.

Groves, C. P. 1965. Description of a new subspecies of rhinoceros, from Borneo, *Didermocerus sumatrensis harrissoni*. *Säugetierkundliche Mitteilungen* 13: 128-131.

Groves, C. P. 1967. On the rhinoceroses of South-East Asia. *Säugetierkundliche Mitteilungen* 15: 221-237.

Groves, C. P. and F. Kurt. 1972. *Dicerorhinus sumatrensis*. *Mammalian Species* 21: 1-6.

Groves, C. P. 1972. *Ceratotherium simum*. *Mammalian Species* 8: 1-6.

Groves, C. P. 1975. Taxonomic notes on the white rhinoceros *Ceratotherium simum* (Burchell, 1817). *Säugetierkundliche Mitteilungen* 23: 200-212.

Groves, C. P. 1982. The skulls of Asian rhinoceroses: wild and captive. *Zoo Biology* 1: 251-261.

Groves, C. P. 1983. Phylogeny of the living species of rhinoceros. *Zeitschrift für Zoologische Systematik und Evolutionsforschung* 21: 293-313.

Hammer, Ø. (2002). Morphometrics. Text presented at a morphometrics meeting in Zürich.

Hammer, Ø., D. A. T. Harper, and P. D. Ryan. 2009. PAST – PAlaeontological STatistics, ver. 1.89. University of Oslo, Oslo, Norway.

Heissig, K. 1989. The Rhinocerotidae. *The Evolution of Perissodactyls*. D. R. Prothero and R. M. Schoch. New York, Oxford University Press: 399-417.

Heissig, K. 1999. Family Rhinocerotidae. *The Miocene Land Mammals of Europe*. G. E. Rössner and K. Heissig. München, Verlag Dr. Friedrich Pfeil: 175-188.

Hillman-Smith, A. K. K., N. Owen-Smith, J. L. Anderson, A. J. Hall-Martin, and J.P. Selaladi. 1986. Age estimation of the white rhinoceros (*Ceratotherium simum*). *Journal of Zoology, London* 210: 355-379.

Hillman-Smith, A. K. K. and C. P. Groves. 1994. *Diceros bicornis*. *Mammalian Species* 455: 1-8.

Hitchins, P. M. 1978. Age determinism of the black rhinoceros (*Diceros bicornis* Linn.) in Zululand. *South African Journal of Wildlife Research* 8: 71-80.

Homberger, D. G. and W. F. Walker, Jr. 2004. *Vertebrate Dissection, Ninth Edition.* Belmont, California, Brooks/Cole.

Hofmann, R. R. and D. R. M. Stewart. 1972. Grazer or browser: a classification based on the stomach-structure and feeding habits of East African ruminants. *Mammalia* 36: 226-240.

Hofmann, R. R. 1973. The ruminant stomach. *East African Monographs in Biology, No. 2*. Nairobi, East African Literature Bureau.

Huxley, J. S. 1932. *Problems of relative growth*. New York, Lincoln Mac Veagh - The Dial Press.

Janis, C. M. and D. Ehrhardt. 1988. Correlation of relative muzzle width and relative incisor width with dietary preference in ungulates. *Zoological Journal of the Linnean Society* 92: 267-284.

Janis, C. M. 1990. Correlation of cranial and dental variables with dietary preferences: a comparison of macropodoid and ungulate mammals. *Memoirs of the Queensland Museum* 28: 349-366.

Janis, C. M. 1995. Correlations between craniodental morphology and feeding behavior in ungulates: reciprocal illumination between living and fossil taxa. *Functional Morphology in Vertebrate Paleontology*. J. J. Thomason. Cambridge, Cambridge University Press: 76-98.

Joeckel, R. M. 1990. A functional interpretation of the masticatory system and paleoecology of entelodonts. *Paleobiology* 16: 459-482.

Jolicoeur, P. 1963. The multivariate generalization of the allometry equation. *Biometrics* 19: 497-499.

Klingenberg, C. P. 1998. Heterochrony and allometry: the analysis of evolutionary change in ontogeny. *Biological Reviews of the Cambridge Philosophical Society* 73: 79-123.

Klingenberg, C.P. 2008. MorphoJ. Faculty of Life Sciences, University of Manchester, UK. http://www.flywings.org.uk/MorphoJ_page.htm.

Laurie, A. 1982. Behavioural ecology of the greater one-horned rhinoceros (*Rhinoceros unicornis*). *Journal of Zoology, London* 196: 307-341.

Laurie, W. A., E. M. Lang, and C. P. Groves. 1983. *Rhinoceros unicornis*. *Mammalian Species* 211: 1-6.

MacFadden, B. J. 1998. Tale of two rhinos: isotopic ecology, paleodiet, and niche differentiation of *Aphelops* and *Teleoceras* from the Florida Neogene. *Paleobiology* 24: 274-286.

Matthew, W. D. 1932. A review of the rhinoceroses with a description of *Aphelops* material from the Pliocene of Texas. Bulletin of the University of California Department of Geological Science, 20: 411-480.

McKenna, M. C. and S. K. Bell. 1997. *Classification of Mammals Above the Species Level*. New York, Columbia University Press.

McKinney, M. L. and R. M. Schoch. 1985. Titanothere allometry, heterochrony, and biomechanics: revising an evolutionary classic. *Evolution* 39: 1352-1363.

Mead, A. J. and W. P. Wall. 1998a. Dietary implications of jaw biomechanics in the rhinocerotoids *Hyracodon* and *Subhyracodon* from Badlands National Park, South

Dakota. National Park Service Paleontological Research Volume 3 Technical Report NPS/NRGRD/GRDTR-98/1: 23-28

Mead, A. J. and W. P. Wall. 1998b. Paleoecological implications of the craniodental and premaxilla morphologies of two rhinocerotoids (Perissodactyla) from Badlands National Park, South Dakota. National Park Service Paleontological Research Volume 3 Technical Report NPS/NRGRD/GRDTR-98/1: 18-22.

Mead, A. J. 2000. Sexual dimorphism and paleoecology in *Teleoceras*, a North American Miocene rhinoceros. *Paleobiology* 26: 689-706.

Mendoza, M., C. M. Janis, and P. Palmqvist. 2002. Characterizing complex craniodental patterns related to feeding behaviour in ungulates: a multivariate approach. *Journal of Zoology, London* 258: 223-246.

Mihlbachler, M.C. 2001 Aspects of the paleobiology of the Neogene rhinoceroses of Florida. Master's Thesis. University of Florida, Gainesville.

Mihlbachler, M. C. 2003. Demography of late Miocene rhinoceroses (*Teleoceras proterum* and *Aphelops malacorhinus*) from Florida: linking mortality and sociality in fossil assemblages. *Paleobiology* 29: 412-428.

Mihlbachler, M. C., S. G. Lucas, R. J. Emry, and B. Bayshashov. 2004. A new brontothere (Brontotheriidae, Perissodactyla, Mammalia) from the Eocene of the Ily Basin of Kazakstan and a phylogeny of Asian "horned" brontotheres. *American Museum Novitates* 3439: 1-43.

Mihlbachler, M. C. 2005. Linking sexual dimorphism and sociality in rhinoceroses: insights from *Teleoceras proterum* and *Aphelops malacorhinus* from the Late Miocene of Florida. *Bulletin of the Florida Museum of Natural History* 45: 495-520.

Osborn, H. F. 1898. A complete skeleton of *Teleoceras fossiger*. Notes upon the growth and sexual characters of this species. *Bulletin of the American Museum of Natural History* 10: 51-59.

Owen-Smith, R. N. 1988. *Megaherbivores: The Influence of Very Large Body Size on Ecology*. Cambridge, Cambridge University Press.

Pérez-Barbería, F. J. and I. J. Gordon. 1999. The functional relationship between feeding type and jaw and cranial morphology in ungulates. *Oecologia* 118: 157-165.

Prothero, D. R., E. M. Manning, and C. B. Hanson. 1986. The phylogeny of the Rhinocerotoidea (Mammalia, Perissodactyla). *Zoological Journal of the Linnean Society of London* 87: 341-366.

Prothero, D. R. 2005. *The Evolution of North American Rhinoceroses*. Cambridge, Cambridge University Press.

Radinsky, L. B. 1966. The families of the Rhinocerotoidea (Mammalia, Perissodactyla). *Journal of Mammalogy* 47: 631-639.

Radinsky, L. B. 1981. Evolution of skull shape in carnivores. 1. Representative modern carnivores. *Biological Journal of the Linnean Society* 15: 369-388.

Radinsky, L.B. 1984. Ontogeny and phylogeny in horse skull evolution. *Evolution* 38: 1-15.

Rohlf, F. J. 2008. TPSDIG2. Version 2.12. Department of Ecology and Evolution, SUNY, Stony Brook, NY.

Rossi, M., E. Ribeiro, and R. Smith. 2003. Craniofacial asymmetry in development: an anatomical study. *Angle Orthodontist* 73: 381-385.

Sanson, G. 2006. The biomechanics of browsing and grazing. *American Journal of Botany* 93: 1531-1545.

Shea, B. T. 1985. Bivariate and multivariate growth allometry: statistical and biological considerations. *Journal of Zoology, London* 206: 367-390.

Smith, K. K. 1993. The form of the feeding apparatus in terrestrial vertebrates: studies of adaptation and constraint. *The Skull, Volume 3: Functional and Evolutionary Mechanisms*. B. K. Hall and J. Hanken. Chicago, The University of Chicago Press: 150-196.

Solounias, N. and B. Dawson-Saunders. 1988. Dietary adaptations and paleoecology of the Late Miocene ruminants from Pikermi and Samos in Greece. *Palaeogeography, Palaeoclimatology, Palaeoecology* 65: 149-172.

Voorhies, M. R. and S. G. Stover. 1978. An articulated fossil skeleton of a pregnant rhinoceros, *Teleoceras major* Hatcher. *Proceedings of the Nebraska Academy of Sciences* 88: 47-48.

Voorhies, M. R. and J. R. Thomasson. 1979. Fossil grass anthoecia within Miocene rhinoceros skeletons: diet in an extinct species. *Science* 206: 331-333.

Voorhies, M. R. 1985. A Miocene rhinoceros herd buried in volcanic ash. *Research Report, National Geographic Society* 159: 671-688.

Wayne, R. K. 1986. Cranial morphology of domestic and wild canids: the influence of development on morphological change. *Evolution* 40: 243-261.

Webb, S. D. 1969. The Burge and Minnechaduza Clarendonian mammalian faunas of north-central Nebraska. *University of California Publications in Geological Sciences* 78: 1-191.

Zelditch, M. L., D. L. Swiderski, H. D. Sheets, and W. L. Fink. 2004. *Geometric Morphometrics for Biologists: A Primer*. London, Elsevier Academic Press.

Zeuner, F. E. 1936. Palaeobiology and climate of the past. *Problems of Palaeontology* 1: 199-216.

Zeuner, F. E. 1945. New reconstructions of the woolly rhinoceros and Mereck's rhinoceros. *Proceedings of the Linnean Society of London* 156: 183-185.

Zschokke, S. and B. Baur 2002. Inbreeding, outbreeding, infant growth, and size dimorphism in captive Indian rhinoceros (*Rhinoceros unicornis*). *Canadian Journal of Zoology* 80: 2014-2023.

APPENDIX 1. MEASUREMENT STATISTICS FOR CALIPERS

Digital Calipers

Measurement	ACLR	ACLL	OH	DW	MXPLR	MXPLL	MXMLR	MXMLL
Minimum	117.65	117.2	146.09	48.84	119.93	113.77	140.23	142.63
Maximum	118.34	120.3	149.98	52.69	122.29	114.81	140.72	144.14
Mean	118.008	118.908	148.19	51.056	121.152	114.5	140.538	143.622
SD	0.24468	1.22204	1.45405	1.46555	0.96634	0.42556	0.20584	0.64732
CV	0.20734	1.02772	0.98121	2.87048	0.79763	0.37167	0.14647	0.45071

Measurement	MXAPW	MXPPW	MNPLR	MNPLL	MNMLR	MNMLL
Minimum	142.71	72.28	97.01	96.32	139.72	139.25
Maximum	144.96	73.44	99.01	97.51	140.56	140.81
Mean	143.56	72.862	97.87	96.74	140.218	140.154
SD	0.97080	0.48303	0.74354	0.49462	0.30963	0.56376
CV	0.67623	0.66294	0.75972	0.51129	0.22082	0.40225

Manual Calipers

Measurement	TCLR	TCLL	PCLR	PCLL	MCLR	MCLL	SW	ZW
Minimum	516	516	211	213	218	215	260	325
Maximum	523	518	215	218	219	218	262	327
Mean	518.2	517.2	212.8	215.2	218.2	216.6	260.8	325.8
SD	2.86356	0.83666	1.48324	1.92354	0.44721	1.14018	0.83666	0.83666
CV	0.55260	0.16177	0.69701	0.89384	0.20496	0.52640	0.32081	0.25680

Measurement	MLR	MLL	RLR	RLL	CW	MXDLR	MXDLL	MNDLR	MNDLL
Minimum	444	449	178	185	305	245	243	234	233
Maximum	448	453	182	186	306	247	245	237	235
Mean	446	450.8	179.6	185.2	305.6	246	244.4	235.2	234.2
SD	1.58114	1.64317	1.51658	0.44721	0.54772	1.0000	0.89443	1.09545	0.83666
CV	0.35452	0.36450	0.84442	0.24148	0.17923	0.40650	0.36597	0.46575	0.35724

APPENDIX 2. SPECIMEN COUNTS FOR STATISTICAL ANALYSES

Asymmetry Specimen Counts

Species	Group	TCL%	PCL%	MCL%	ACL%	ML%	RL%
T. major	Ages 0-4	4	5	6	5	4	5
	Ages 5-7	5	5	5	5	5	5
	Ages 8-9	3	3	3	3	3	3
	Ages 10-17	13	13	13	10	13	13
	Ages 0-17	25	26	27	23	25	26
R. unicornis	Ages 0-4	3	3	3	3	3	1
	Ages 5-7	2	2	2	2	2	2
	Ages 8-9	1	1	1	1	1	1
	Ages 10-17	8	8	9	9	8	8
	Ages 0-17	14	14	15	15	14	12
D. sumatrensis	Ages 0-4	1	1	1	1	1	0
	Ages 5-7	1	1	1	1	1	1
	Ages 8-9	1	1	1	1	1	1
	Ages 10-17	4	3	3	4	4	4
	Ages 0-17	7	6	6	7	7	6
C. simum	Ages 0-4	7	7	7	7	7	6
	Ages 5-7	2	3	3	3	3	3
	Ages 8-9	3	3	3	3	3	3
	Ages 10-17	5	5	7	7	7	7
	Ages 0-17	17	18	20	20	20	19
D. bicornis	Ages 0-4	6	6	7	7	7	6
	Ages 5-7	3	3	3	3	3	3
	Ages 8-9	3	3	3	3	3	3
	Ages 10-17	13	13	13	13	11	11
	Ages 0-17	25	25	26	26	24	23

Table continued

Species	Group	MXPL%	MXML%	MXDL%	MNPL%	MNML%	MNDL%
T. major	Ages 0-4	5	0	5	5	0	5
	Ages 5-7	5	4	5	5	5	5
	Ages 8-9	3	3	3	3	3	3
	Ages 10-17	13	13	13	13	13	13
	Ages 0-17	26	20	26	26	21	26
R. unicornis	Ages 0-4	1	0	1	1	0	1
	Ages 5-7	2	1	2	2	1	2
	Ages 8-9	1	1	1	1	1	1
	Ages 10-17	9	9	8	9	9	9
	Ages 0-17	13	11	12	13	11	13
D. sumatrensis	Ages 0-4	0	0	0	0	0	0
	Ages 5-7	1	1	1	1	1	1
	Ages 8-9	1	1	1	1	1	1
	Ages 10-17	4	4	4	4	4	4
	Ages 0-17	6	6	6	6	6	6
C. simum	Ages 0-4	7	0	7	7	0	7
	Ages 5-7	3	3	3	3	3	3
	Ages 8-9	3	3	2	3	3	3
	Ages 10-17	6	7	6	7	7	7
	Ages 0-17	19	13	18	20	13	20
D. bicornis	Ages 0-4	6	0	6	6	0	6
	Ages 5-7	3	2	3	3	3	3
	Ages 8-9	3	3	3	3	3	3
	Ages 10-17	13	13	12	13	13	13
	Ages 0-17	25	18	24	25	19	25

Sexual Dimorphism Permutation T-Tests Specimen Counts

Species	Sex	TCL	PCL	MCL	ACL	SW	OH	ZW	ML	RL	CW
R. unicornis	Male	4	4	4	4	4	4	4	4	4	3
	Female	3	3	3	3	3	3	3	3	3	3
C. simum	Male	3	3	3	3	3	3	3	3	3	3
	Female	3	3	3	3	3	3	3	3	3	3
D. bicornis	Male	4	4	4	4	4	4	4	4	4	4
	Female	4	4	4	4	4	4	4	4	4	3

Sexual and Subspecific Shapiro-Wilk Specimen Counts

Species	TCL	PCL	MCL	ACL	SW	OH	ZW	ML	RL	CW
R. unicornis	7	7	8	8	8	7	8	8	8	7
C. simum	6	6	7	7	7	6	7	7	7	7
D. bicornis	13	13	13	13	13	13	13	13	13	12

Functional Characters Specimen Counts

Species	PCL	OH	RL	MXPL/MXML	MNPL/MNML	DW/PPW	APW/PPW
T. major	14	14	14	14	14	12	14
R. unicornis	8	8	8	9	9	8	9
D. sumatrensis	4	4	4	4	4	4	4
C. simum	8	8	8	9	9	7	8
D. bicornis	14	14	14	14	14	7	14

Cranial PCA Missing Specimen Counts

Species	Specimens	TCL	PCL	MCL	ACL	SW	OH	ZW
T. major	26	0	0	0	0	3	0	0
R. unicornis	14	0	0	0	0	0	2	0
D. sumatrensis	7	0	0	0	0	0	0	1
C. simum	19	0	0	0	0	0	2	0
D. bicornis	25	0	0	0	0	0	0	0

Mandibular and Dental PCA Missing Specimen Counts

Species	Specimens	ML	RL	CW	MXDL	MNDL	MNAPW	MNPPW
T. major	25	0	0	1	0	0	0	0
R. unicornis	12	0	0	1	0	0	0	0
D. sumatrensis	6	0	0	0	0	0	0	0
C. simum	19	0	1	0	0	0	1	0
D. bicornis	24	0	0	2	0	0	0	0

Geometric Morphometric Specimen Counts

Species	Specimens
T. major	13
R. unicornis	11
D. sumatrensis	6
C. simum	11
D. bicornis	12

APPENDIX 3. MAXILLA EXPANSION IN ONTOGENY

Maxilla Expansion of the Anterior Orbit (A) and Nasal Incision (N) in *T. major* Ontogeny

Age Class	M2	M1	P4	P3	P2	P1
2				A	N	
3				A	N	
4				A	N	
5			A		N	
6						
7						
8			A	N		
9			A	N		
10		A		N		
11		A	N			
12		A		N		
13						
14		A		N		
15		A		N		

Maxilla Expansion of the Anterior Orbit (A) and Nasal Incision (N) in *R. unicornis* Ontogeny

Age Class	M2	M1	P4	P3	P2	P1
1				A	N	
2						
3				A		N
4						
5				A		N
6			A			N
7						
8			A		N	
9						
10						
11			A		N	
12			A		N	
13			A		N	

Maxilla Expansion of the Anterior Orbit (A) and Nasal Incision (N) in *D. sumatrensis* Ontogeny

Age Class	M2	M1	P4	P3	P2	P1
2				A	N	
3						
4						
5						
6						
7			A		N	
8		A			N	
9						
10		A			N	
11		A			N	
12						
13		A			N	

Maxilla Expansion of the Anterior Orbit (A) and Nasal Incision (N) in *C. simum* Ontogeny

Age Class	M2	M1	P4	P3	P2	P1
1				A	N	
2			A		N	
3			A		N	
4			A		N	
5			A		N	
6			A		N	
7		A			N	
8		A			N	
9		A			N	
10		A			N	
11	A			N		
12	A			N		
13						
14	A			N		

Maxilla Expansion of the Anterior Orbit (A) and Nasal Incision (N) in *D. bicornis* Ontogeny

Age Class	M2	M1	P4	P3	P2	P1
1				A	N	
2						
3			A		N	
4			A		N	
5			A		N	
6			A		N	
7			A		N	
8		A			N	
9						
10		A			N	
11		A			N	
12		A		N		
13		A		N		
14		A		N		
15		A				
16						
17		A		N		

APPENDIX 4. ONTOGENETIC SEQUENCES OF SPECIES' SPECIMENS

* indicates captive specimens with no dental inconsistencies. ** indicates captive specimens with dental inconsistencies, resulting in exclusion from the ontogenetic sequence.

***T. major* Ontogenetic Sequence**

Age Class	Specimen
2	UNSM 27817 UNSM 52245 UNSM 27814
3	UNSM 27810
4	UNSM 52279 UNSM 51101
5	UNSM 52231 UNSM 52374 UNSM 52222 UNSM 52234 UNSM 52219
8	UNSM 52230 UNSM 52232
9	UNSM PI136
10	UNSM 52223 UNSM 52238
11	UNSM 52228 UNSM 52273 UNSM 27808 UNSM 52272 UNSM 52283
12	UNSM 52286 UNSM 27807 UNSM 52289
14	UNSM 52373 UNSM 52288
15	UNSM 52218

***R. unicornis* Ontogenetic Sequence**

Age Class	Specimen
1	AMNH 274636 USNM 574963
3	AMNH 70445
5	AMNH 119475
6	USNM 464963
8	AMNH 54456
10	UNSM ZM13844**
11	FMNH 140883** USNM 336953 AMNH 35759
12	AMNH 54454 FMNH 57822 FMNH 25708
13	FMNH 57639* FMNH 25707

***D. sumatrensis* Ontogenetic Sequence**

Age Class	Specimen
2	AMNH 54764
7	AMNH 173576
8	FMNH 63878
10	USNM A49561 USNM 269392
11	AMNH 54763
13	AMNH 81892

***C. simum* Ontogenetic Sequence**

Age Class	Specimen
1	AMNH 51918
2	AMNH 51927 AMNH 51882
3	USNM 164588 AMNH 51916 AMNH 51881
4	AMNH 51872
5	AMNH 51870
6	AMNH 51862
7	AMNH 51930
8	AMNH 51931
9	AMNH 54125 AMNH 51865
10	AMNH 125413
11	AMNH 29174 AMNH 51890
12	FMNH 51471 AMNH 51858 AMNH 51856
14	AMNH 51854

***D. bicornis* Ontogenetic Sequence**

Age Class	Specimen
0	USNM 182019 USNM A34717
1	USNM 182030
3	AMNH 113779 USNM 162932 USNM A34718
4	USNM A34720
5	USNM 240884
6	FMNH 33490
7	USNM 199708
8	USNM A34719 USNM 161925
9	FMNH 60784**
10	USNM 161924
11	FMNH 85429 FMNH 127848
12	FMNH P14823 FMNH 127849 FMNH 22366 FMNH 166520**
13	FMNH 34278 USNM 54004
14	FMNH 121646* FMNH 127851
15	FMNH 57809*
17	USNM 182195

APPENDIX 5. ASYMMETRY INDEX STATISTICS

Asymmetry Index Statistics for Right-Left Measurements

	Statistic	*T. major*	*R. unicornis*	*D. sumatrensis*	*C. simum*	*D. bicornis*
TCL	Min	-3.0303	-2.12766	-1.49626	-0.497512	-3.67347
	Max	3.125	2.91262	1.01523	1.2848	1.41129
	Mean	-0.68812	0.120832	-0.0691285	0.289925	-0.00580282
	Median	-0.697674	0	0	0.253787	0.191939
	Variance	1.98504	1.7727	0.689646	0.273296	0.896638
PCL	Min	-15.1713	-2.42424	-4.87805	-2.41546	-3.21101
	Max	8.02597	5.14019	0	2.39521	4.34333
	Mean	-2.78681	0.876003	-1.95119	-0.485316	0.339234
	Median	-2.5658	0.69483	-1.96263	-0.789843	0.578035
	Variance	34.5988	5.40117	2.91223	1.98528	4.18409
MCL	Min	-4.81283	-6.10329	-2.24719	-5.58688	-6.93069
	Max	10.1695	0.526316	4.25532	5.15873	5.40541
	Mean	2.48679	-2.16148	0.293258	0.179512	-0.529476
	Median	1.93548	-2.39044	-0.588256	0.324773	-0.708154
	Variance	10.1802	3.39832	5.87656	7.82958	10.0289
ACL	Min	-13.5532	-6.14971	-5.70932	-3.65854	-8.12875
	Max	12.2378	5.20559	5.74454	3.48837	5.50247
	Mean	3.18556	0.90299	-0.108535	-0.622138	0.335315
	Median	3.68346	0.809429	0.00954381	-1.27133	0.275401
	Variance	29.9907	7.17365	13.4613	4.29886	9.28965
ML	Min	-5.62061	-2.29885	-1.02564	-1.83824	-2.7933
	Max	6.81319	0.980392	0.719424	2.27273	1.87793
	Mean	1.99066	-0.545578	-0.285794	0.389621	-0.328311
	Median	2.52874	-0.472831	0	0.289811	-0.218341
	Variance	8.10656	0.770573	0.410248	1.1827	1.43125
RL	Min	-3.52941	-4.5977	-0.549451	-4.82759	-4.2328
	Max	4.21053	2.80374	3.06748	3.63636	3.40909
	Mean	1.13424	-0.895739	1.19361	0.0677789	0.262883
	Median	1.88841	-1.18849	1.28051	0.460829	0.370206
	Variance	4.85426	4.55778	2.67677	3.81537	4.03767

Table continued

	Statistic	*T. major*	*R. unicornis*	*D. sumatrensis*	*C. simum*	*D. bicornis*
MXPL	Min	-7.2814	-6.85476	0.587927	-13.3291	-2.98258
	Max	6.77259	18.28	1.3539	0.931499	12.932
	Mean	0.3735	-0.123267	0.90447	-2.7231	0.438777
	Median	1.59684	-1.83541	0.838027	-0.963408	-0.583583
	Variance	16.4392	58.2001	0.111751	29.0524	17.9907
MXML	Min	-4.42139	-2.74582	-1.52629	-2.48447	-7.96046
	Max	3.52941	6.91824	2.67799	1.25	3.75
	Mean	-0.164108	1.21595	0.805335	-0.211822	-0.357123
	Median	-0.628931	0.474618	1.03482	0	-0.383489
	Variance	6.4306	9.09683	3.17612	2.3406	8.48145
MXDL	Min	-5.08475	-1.8315	-2.33645	-5.42636	-1.32743
	Max	39.1635	10.0358	0.606061	1.77305	4.58015
	Mean	3.01571	1.15068	-0.298907	-0.562686	0.674233
	Median	0.711744	0.380228	0.26738	0	0.544197
	Variance	125.097	12.2786	1.9183	7.1216	2.17192
MNPL	Min	-11.5817	-6.21081	-3.23657	-0.747178	-5.93928
	Max	16.9	3.54914	-0.232558	1.68861	2.15401
	Mean	0.882607	-1.06574	-1.92032	0.56683	-1.01271
	Median	0.123191	-0.341164	-2.10608	0.614191	-0.118671
	Variance	64.7067	8.01747	1.63187	0.831788	6.58746
MNML	Min	-4.04911	-2.61486	-0.0367647	-4.69175	-3.70871
	Max	4.54545	8.05934	4.45509	3.82166	2.02435
	Mean	-1.19857	1.2409	1.44699	-0.343354	0.138078
	Median	-1.91083	0.860872	0.684825	-0.47866	0.533483
	Variance	6.35046	11.0313	4.39221	8.72397	2.97467
MNDL	Min	-3.65854	-2.8	-1.87793	-2.18341	-1.14504
	Max	5.30612	2.54237	1.13636	1.40845	3.87931
	Mean	0.0827717	-0.110158	-0.611159	-0.115404	0.55928
	Median	0	-0.706714	-0.851533	0	0.398406
	Variance	6.67543	2.5601	1.69314	1.20163	1.64959

APPENDIX 6. FUNCTIONAL CHARACTER STATISTICS

	Statistic	*T. major*	*R. unicornis*	*D. sumatrensis*	*C. simum*	*D. bicornis*
PCL	Min	0.36760	0.41487	0.42308	0.39344	0.40058
	Max	0.42955	0.43653	0.45006	0.41256	0.43487
	Mean	0.39422	0.42246	0.44023	0.40348	0.41950
	Median	0.39381	0.42020	0.44389	0.40400	0.42110
	Variance	0.00039	0.00005	0.00015	0.00006	0.00011
OH	Min	0.21896	0.31177	0.24478	0.23581	0.24605
	Max	0.29762	0.39563	0.31314	0.27765	0.30184
	Mean	0.26147	0.34572	0.28350	0.25195	0.27728
	Median	0.26913	0.33937	0.28804	0.25011	0.27526
	Variance	0.00064	0.00059	0.00086	0.00022	0.00028
RL	Min	0.31194	0.33170	0.28695	0.31953	0.28259
	Max	0.41866	0.40830	0.42118	0.40000	0.37259
	Mean	0.37440	0.38173	0.35572	0.35502	0.32043
	Median	0.37458	0.39205	0.35738	0.34111	0.31240
	Variance	0.00059	0.00066	0.00464	0.00099	0.00091
MXPL / MXML	Min	0.56066	0.84710	0.71301	0.73000	0.66402
	Max	0.93339	1.01814	1.18504	1.24171	1.27592
	Mean	0.68123	0.92957	0.85068	0.93322	0.87953
	Median	0.66528	0.92194	0.75234	0.84701	0.87568
	Variance	0.00887	0.00319	0.05003	0.04400	0.01989
MNPL / MNML	Min	0.41338	0.67757	0.64340	0.76380	0.68656
	Max	0.75474	0.83565	1.16792	1.36092	0.88392
	Mean	0.50411	0.74019	0.84048	0.96107	0.76074
	Median	0.49525	0.74849	0.77531	0.80253	0.73746
	Variance	0.00748	0.00226	0.05152	0.06626	0.00417
DW / MXPPW	Min	0.25696	0.43529	0.60649	0.30940	0.17393
	Max	0.38808	1.03934	0.80513	0.74986	0.54500
	Mean	0.32602	0.58687	0.68066	0.60022	0.28049
	Median	0.32419	0.44977	0.65551	0.70281	0.24652
	Variance	0.00155	0.04871	0.00755	0.03260	0.01497
MXAPW / MXPPW	Min	0.32572	0.45175	1.07235	0.47940	0.36358
	Max	0.66785	1.48216	1.83275	1.95334	2.19009
	Mean	0.48248	0.79473	1.45223	1.22634	0.75185
	Median	0.48272	0.55864	1.45191	1.43219	0.43816
	Variance	0.00730	0.17364	0.10746	0.35507	0.41978

APPENDIX 7. CRANIAL PCA EIGENVALUES AND VARIANCE

***T. major*.** Joliffe cut-off value: 0.00514200

PC	Eigenvalue	% Variance	Cumulative %
1	0.04683190	91.078	91.078
2	0.00240805	4.683	95.761
3	0.00125502	2.441	98.202
4	0.00042267	0.822	99.024
5	0.00034768	0.676	99.700
6	0.00014346	0.279	99.979
7	0.00001105	0.021	100.000

***R. unicornis*.** Joliffe cut-off value: 0.01238800

PC	Eigenvalue	% Variance	Cumulative %
1	0.11961000	96.942	96.942
2	0.00224923	1.823	98.765
3	0.00093724	0.760	99.525
4	0.00034913	0.283	99.808
5	0.00015657	0.127	99.934
6	0.00007101	0.058	99.992
7	0.00001033	0.008	100.000

***D. sumatrensis*.** Joliffe cut-off value: 0.01218100

PC	Eigenvalue	% Variance	Cumulative %
1	0.11847300	97.258	97.258
2	0.00205474	1.687	98.945
3	0.00090612	0.744	99.689
4	0.00028504	0.234	99.923
5	0.00005964	0.049	99.972
6	0.00003441	0.028	100.000
7	0.00000000	0.000	100.000

***C. simum*.** Joliffe cut-off value: 0.00694960

PC	Eigenvalue	% Variance	Cumulative %
1	0.06426160	92.467	92.467
2	0.00429381	6.179	98.646
3	0.00046296	0.666	99.312
4	0.00026771	0.385	99.697
5	0.00017026	0.245	99.942
6	0.00002685	0.039	99.981
7	0.00001323	0.019	100.000

***D. bicornis*.** Joliffe cut-off value: 0.01902700

PC	Eigenvalue	% Variance	Cumulative %
1	0.18714200	98.357	98.357
2	0.00136083	0.715	99.072
3	0.00084489	0.444	99.516
4	0.00065493	0.344	99.860
5	0.00018387	0.097	99.957
6	0.00006403	0.034	99.991
7	0.00001743	0.009	100.000

APPENDIX 8. CRANIAL AND MANDIBULAR PCA VARIABLE LOADINGS

PC1. Negative mandibular and dental PC1 loadings in red for *D. sumatrensis* indicate its PCA does not reflect growth allometry.

	T.major	***R. unicornis***	***D. sumatrensis***	***C. simum***	***D. bicornis***
TCL	0.3716	0.3466	0.3269	0.3902	0.328
PCL	0.291	0.3066	0.3441	0.3416	0.2986
MCL	0.3792	0.3502	0.3452	0.3844	0.3417
ACL	0.5199	0.4078	0.4335	0.4399	0.3489
SW	0.3608	0.3621	0.3492	0.4166	0.3614
OH	0.3042	0.4944	0.4442	0.3302	0.5758
ZW	0.3746	0.3485	0.3851	0.3274	0.3204
ML	0.3542	0.3284	0.02091	0.3332	0.3712
RW	0.1782	0.03616	0.6663	0.1449	0.3189
CW	0.2879	0.2749	-0.05897	0.3143	0.269
MXDL	0.5236	0.5583	-0.4985	0.5739	0.4972
MNDL	0.5333	0.6054	-0.5241	0.586	0.3911
MNAPW	0.3654	0.3383	-0.133	0.1738	0.4804
MNPPW	0.2605	0.1504	-0.106	0.2575	0.2391

PC2

	T.major	***R. unicornis***	***D. sumatrensis***	***C. simum***	***D. bicornis***
TCL	-0.1236	-0.2869	-0.01982	-0.2139	-0.05074
PCL	0.1417	-0.1865	0.1344	-0.09998	-0.2292
MCL	0.03442	-0.2726	-0.316	-0.191	0.1788
ACL	-0.4227	0.2071	-0.2026	-0.2342	0.3385
SW	0.5842	-0.398	0.2655	0.02958	0.6399
OH	-0.5162	0.758	0.6532	0.9206	-0.6167
ZW	0.4208	-0.1809	-0.5861	-0.06805	0.09276
ML	-0.1493	-0.2959	-0.1171	-0.2297	-0.05385
RW	-0.037	-0.8951	-0.2096	-0.638	-0.6554
CW	0.687	-0.07362	-0.4104	-0.2601	0.4665
MXDL	-0.2922	0.1114	-0.1605	0.1024	0.2432
MNDL	-0.3996	0.251	0.1713	0.5278	0.4198
MNAPW	0.389	-0.1658	-0.8327	-0.3787	-0.3034
MNPPW	0.3287	-0.05511	-0.1594	-0.2002	-0.1498

APPENDIX 9. MANDIBULAR PCA EIGENVALUES AND VARIANCE

T. major. Joliffe cut-off value: 0.00640170

PC	Eigenvalue	% Variance	Cumulative %
1	0.05966970	93.210	93.210
2	0.00182768	2.855	96.065
3	0.00137833	2.153	98.218
4	0.00057679	0.901	99.119
5	0.00036009	0.562	99.682
6	0.00017446	0.273	99.954
7	0.00002953	0.046	100.000

R. unicornis. Joliffe cut-off value: 0.00325500

PC	Eigenvalue	% Variance	Cumulative %
1	0.02948480	90.584	90.584
2	0.00180839	5.556	96.140
3	0.00074949	2.303	98.442
4	0.00034658	1.065	99.507
5	0.00009940	0.305	99.813
6	0.00003920	0.120	99.933
7	0.00002169	0.067	100.000

D. sumatrensis. Joliffe cut-off value: 0.00163390

PC	Eigenvalue	% Variance	Cumulative %
1	0.01450560	88.776	88.776
2	0.00121731	7.450	96.226
3	0.00039887	2.441	98.667
4	0.00019945	1.221	99.888
5	0.00001822	0.112	100.000
6	0.00000000	0.000	100.000
7	0.00000000	0.000	100.000

***C. simum*.** Joliffe cut-off value: 0.00975020

PC	Eigenvalue	% Variance	Cumulative %
1	0.09032210	92.636	92.636
2	0.00445459	4.569	97.205
3	0.00117632	1.207	98.411
4	0.00101888	1.045	99.456
5	0.00033633	0.345	99.801
6	0.00013125	0.135	99.936
7	0.00006221	0.064	100.000

***D. bicornis*.** Joliffe cut-off value: 0.01069900

PC	Eigenvalue	% Variance	Cumulative %
1	0.09454580	88.369	88.369
2	0.00611472	5.715	94.084
3	0.00271645	2.539	96.623
4	0.00225911	2.112	98.735
5	0.00089615	0.838	99.572
6	0.00040590	0.379	99.952
7	0.00005139	0.048	100.000

APPENDIX 10. GEOMETRIC MORPHOMETRIC PCA STATISTICS

T. major

PC	Eigenvalue	% Variance	Cumulative %
1	0.00176201	42.024	42.024
2	0.00061199	14.596	56.620
3	0.00050295	11.995	68.615
4	0.00030804	7.347	75.962
5	0.00028094	6.700	82.662
6	0.00018798	4.483	87.146
7	0.00017410	4.152	91.298
8	0.00014901	3.554	94.852
9	0.00011787	2.811	97.663
10	0.00007094	1.692	99.355
11	0.00002705	0.645	100.000

R. unicornis

PC	Eigenvalue	% Variance	Cumulative %
1	0.00211281	50.429	50.429
2	0.00091369	21.808	72.237
3	0.00039925	9.529	81.766
4	0.00024816	5.923	87.689
5	0.00022628	5.401	93.090
6	0.00010747	2.565	95.655
7	0.00007753	1.851	97.505
8	0.00004508	1.076	98.581
9	0.00003657	0.873	99.454
10	0.00002287	0.546	100.000

D. sumatrensis

PC	Eigenvalue	% Variance	Cumulative %
1	0.00181273	53.356	53.356
2	0.00070081	20.628	73.983
3	0.00036294	10.683	84.666
4	0.00034407	10.127	94.793
5	0.00017689	5.207	100.000

C. simum

PC	Eigenvalue	% Variance	Cumulative %
1	0.00126222	48.556	48.556
2	0.00044791	17.230	65.786
3	0.00026220	10.087	75.872
4	0.00017113	6.583	82.455
5	0.00013942	5.363	87.818
6	0.00011767	4.527	92.345
7	0.00010131	3.897	96.242
8	0.00004345	1.671	97.914
9	0.00003744	1.440	99.354
10	0.00001680	0.646	100.000

D. bicornis

PC	Eigenvalue	% Variance	Cumulative %
1	0.00138682	34.086	34.086
2	0.00098458	24.200	58.286
3	0.00053790	13.221	71.507
4	0.00041537	10.209	81.716
5	0.00029670	7.292	89.009
6	0.00018158	4.463	93.472
7	0.00011284	2.773	96.245
8	0.00007617	1.872	98.117
9	0.00004498	1.105	99.223
10	0.00001999	0.491	99.714
11	0.00001164	0.286	100.000

VITA

Mark Daniel Hagge was born August 23, 1981, in Indianapolis, Indiana, to parents Michael and Lynne. Mark grew up in Green Bay, Wisconsin, and aside from fighting with Aaron, his older brother, Mark also became fascinated with dinosaurs. While attending the University of Wisconsin-Madison, Mark decided to pursue his long interest in extinct creatures. For three summers during his undergraduate studies, Mark worked at the Hagerman Fossil Beds National Monument in Hagerman, Idaho, collecting, preparing, and staring at fossils. It was during this time that Mark decided to pursue mammalian paleontology. Mark graduated from the University of Wisconsin-Madison in December 2004 with a Bachelor of Science degree in geology and zoology. Mark continued his paleontological pursuits at Louisiana State University in 2005. While working toward a Master of Science degree in geology in Baton Rouge, Louisiana, Mark met his future wife, Jen Booth.